FILM COOLING WITH FORWARD AND BACKWARD INJECTION FOR CYLINDRICAL AND FAN-SHAPED HOLES USING PSP MEASUREMENT TECHNIQUE

A Thesis

by

ANDREW F CHEN

Submitted to the Office of Graduate and Professional Studies of
Texas A&M University
in partial fulfillment of the requirements for the degree of

MASTER OF SCIENCE

Chair of Committee,	Je-Chin Han
Committee Members,	Devesh Ranjan
	Hamn-Ching Chen
Head of Department,	Andreas A. Polycarpou

December 2013

Major Subject: Mechanical Engineering

Copyright 2013 Andrew F Chen

ABSTRACT

A systematic study was performed to investigate the combined effects of hole geometry, blowing ratio, density ratio and free-stream turbulence intensity on flat plate film cooling with forward and backward injection. Detailed film cooling effectiveness distributions were obtained using the steady state pressure sensitive paint (PSP) technique. Four common film-hole geometries with forward injection were used in this study: simple angled cylindrical holes and fan-shaped holes, and compound angled (β = 45°) cylindrical holes and fan-shaped holes. Additional four film-hole geometries with backward injection were tested by reversing the injection direction from forward to backward to the mainstream. There are seven holes in a row on each plate and each hole is 4 mm in diameter. The blowing ratio effect is studied at 10 different blowing ratios ranging from M = 0.3 to M = 2.0. The coolant to main stream density ratio (DR) effect is studied by using foreign gases with DR = 1 (N_2), 1.5 (CO_2), and 2 (15% SF_6 + 85% Ar). The free stream turbulence intensity effect is tested at 0.5% and 6%. The results of the parametric effects to the film cooling effectiveness with forward injection agreed with open literatures. In general, the results show the film cooling effectiveness with backward injection is greatly reduced for shaped holes as compared with the forward injection. However, significant improvements can be seen in simple angled cylindrical hole at higher blowing ratios. Backward injection also shows improvements at near film-hole regions for compound angled cylindrical holes at higher blowing ratios.

Comparison was made between the experimental data and empirical correlation for simple angled fan-shaped holes.

ACKNOWLEDGEMENTS

I am genuinely grateful for my committee chair Dr. Han for his guidance and support throughout the course of this research. I would also like to thank Dr. Ranjan and Dr. Chen for their support and serving as my committee members.

I am also thankful for all my colleagues at the Turbine Heat Transfer Lab. at Texas A&M University, especially Dr. Li for her assistance. Finally, I would like to thank my parents for their encouragement.

NOMENCLATURE

α	Axial angle to the mainstream
β	Compound angle to the mainstream
η	Film cooling effectiveness
$\eta_{ave.}$	Span-wise averaged film cooling effectiveness
ρ	Density, kg/m^3
C	Mass fraction
D	Diameter of film cooling hole
DR	Coolant to mainstream density ratio
h	Heat transfer coefficient, $W/(m^2 \cdot K)$
M	Blowing ratio/ Mass flux ratio
q	Heat flux, W/m^2
T	Temperature
Tu	Turbulence intensity
v	Velocity
x	distance from the trailing edge of holes

Subscript

∞	Mainstream property
air	Property with air injection
aw	Adiabatic wall

blk	Black condition
c	Coolant
f	Film
fg	Property with foreign gas injection
m	Mainstream
ref	Reference condition
w	Wall

TABLE OF CONTENTS

Page

ABSTRACT ii

ACKNOWLEDGEMENTS iv

NOMENCLATURE v

TABLE OF CONTENTS vii

LIST OF FIGURES ix

LIST OF TABLES xi

CHAPTER I INTRODUCTION 1

CHAPTER II BACKGROUND 3

- Flat Plate Film Cooling 3
- Effects of Blowing Ratios 4
- Effects of Hole Configuration and Geometry 4
- Effects of Density Ratios 6
- Effects of Free-Stream Turbulence 7
- Backward Injection 8
- Correlation Development 9
- Objective of Current Study 9

CHAPTER III EXPERIMENTAL SETUP AND THEORY 11

- Instrumentation 11
- Pressure Sensitive Paint Technique 14
- Film Cooling Effectiveness and Measurement Theory 18

CHAPTER IV RESULTS 22

- Comparison with Open Literature 22
- Results of Forward Injection 27
  - Effects of Geometry and Blowing Ratio 27
  - Effects of Density Ratio 29
  - Effects of Free-Stream Turbulence 33
- Results of Backward Injection 38

Effects of Geometry and Blowing Ratio 39
Effects of Density Ratio 40
Backward Injection Comparison with Forward Injection 43
Backward Injection Comparison with Numerical Results 45
Comparison with Empirical Correlation 47
Uncertainty Analysis 50

CHAPTER V CONCLUSIONS 51

Forward Injection 51
Backward Injection 52

REFERENCES 53

APPENDIX 57

LIST OF FIGURES

Page

Fig. 1 Typical turbine rotor blade internal and external cooling system....2

Fig. 2 Various film cooling hole configurations 6

Fig. 3 Schematic diagram of the test facility....12

Fig. 4 Four different hole geometries used in this study. (a) simple angled cylindrical hole. (b) compound angled cylindrical hole. (c) simple angled fan-shaped hole. (d) compound angled fan-shaped hole 13

Fig. 5 Schematic diagram showing (a) the forward injection and (b) the backward injection....14

Fig. 6 Schematic diagram of PSP measurement....15

Fig. 7 Schematic diagram of the calibration setup for PSP 16

Fig. 8 PSP calibration fitting curves....17

Fig. 9 Film cooling two layer model schematic plot 18

Fig. 10 Heat transfer and mass transfer analogy in measuring the film cooling effectiveness. Here, z direction is normal to the surface and x is the stream-wise direction. The film temperature/mass fraction is a function of x,z, while wall temperatures/mass fraction are functions of x only 20

Fig. 11 Span-wise averaged effectiveness compared with Sinha *et al.* at a density ratio near to 1 23

Fig. 12 Span-wise averaged effectiveness compared with Sinha *et al.* at a density ratio near to 1.5 24

Fig. 13 Span-wise averaged effectiveness compared with Sinha *et al.* at DR = 2 24

Fig. 14 Span-wise averaged effectiveness comparison with Rallabandi *et al.*- simple angled cylindrical holes....26

Fig. 15 Span-wise averaged effectiveness comparison with Rallabandi *et al.*- compound angled cylindrical holes....26

Fig. 16 The effect of hole geometry and blowing ratio. Laterally averaged effectiveness at DR = 1 for four different geometries 29

Fig. 17 The density ratio effect. Laterally averaged effectiveness at DR = 1.5 and DR = 2 for simple angled and compound angled cylindrical holes.....30

Fig. 18 The density ratio effect. Laterally averaged effectiveness at DR = 1.5 and DR = 2 for simple angled and compound angled fan-shaped holes 31

Fig. 19 Cross-comparison of the density ratio effect at M = 0.3, 1, 2, DR = 1, 1.5 and 2, forward injection 32

Fig. 20 The free stream turbulence effect. Laterally averaged effectiveness at Tu = 6%, DR = 1 for four different geometries 34

Fig. 21 The free stream turbulence effect. Laterally averaged effectiveness at Tu = 6%, DR = 2 for four different geometries. 35

Fig. 22 Cross-comparison of the turbulence effect at M = 0.5, 1, and 2, DR = 1 36

Fig. 23 Cross-comparison of the turbulence effect at M = 0.5, 1, and 2, DR = 2 37

Fig. 24 Laterally averaged effectiveness with backward injection at DR = 1.....40

Fig. 25 Laterally averaged effectiveness with backward injection, simple angled cylindrical and compound angled cylindrical holes at DR = 1.5 and 2 41

Fig. 26 Laterally averaged effectiveness with backward injection, simple angled fan-shaped and compound angled fan-shaped holes at DR = 1.5 and 2.....42

Fig. 27 Cross-comparison of the density ratio effect at M = 0.3, 1, 2, DR = 1, 1.5 and 2, backward injection 43

Fig. 28 Cross-comparison between different geometries with forward and backward injection at M = 1, 2, and DR = 1, 2. (Abbreviations: SC- Simple Cylidrical; CC- Compound Cylindrical; SF- Simple Fan-shaped; CF- Compound Fan-shaped) 45

Fig. 29 Backward injection centerline effectiveness comparison between numerical and experimental results.....46

Fig. 30 Contour plot of backward injection. Left: experimental data at M = 0.7 and DR = 1.5. Right: numerical simulation at M = 0.67 and DR = 1.33.....47

Fig. 31 Comparison of experimental data using simple angled fan-shaped holes with empirical correlation developed by Colban *et al.* at DR = 2.0.....49

LIST OF TABLES

Page

Table 1 Summary of hole geometries used in this study.....13

Table 2 Experimental conditions of this study and Sinha *et al.* 23

Table 3 Experimental conditions of this study and Rallabandi *et al.* 25

Table 4 Test cases for forward injection 27

Table 5 Summary of higher free stream turbulence effect (at Tu = 6%) 38

Table 6 Test cases for backward injection 39

CHAPTER I

INTRODUCTION

Gas turbine cooling technology plays a critical role in the development of gas turbine engines. The operation efficiency and power output of gas turbines can be improved by increasing the rotor inlet temperature (RIT). The RIT of modern advanced gas turbines reach 1600 ˚C or above, while the RIT of land-based electric generators reaches 1200 ˚C or above. Under such high temperature which far exceeds the melting point of most metals, the structural materials of gas turbine components experience high thermal stress and can be easily damaged. Improving the cooling schemes of turbine blades can further increase the efficiency and power output, it also ensures the durability of turbine engines.

Turbine blade cooling can be achieved internally and externally, as shown in Fig. 1. Internal cooling such as impingement cooling, rib-turbulated cooling, and pin-fin cooling are used for heat transfer enhancement inside the blade internal cooling passages. External cooling is achieved by external cooling holes, which eject coolant from internal passages and create a layer of coolant that insulate the blade surface in the downstream portion. In this sense, external cooling is also known as film cooling. Film cooling effectiveness is used to quantify how good the coolant is covering the surface. In this study, detailed film cooling effectiveness distributions on a flat plate were obtained using the steady state Pressure Sensitive Paint (PSP) technique.

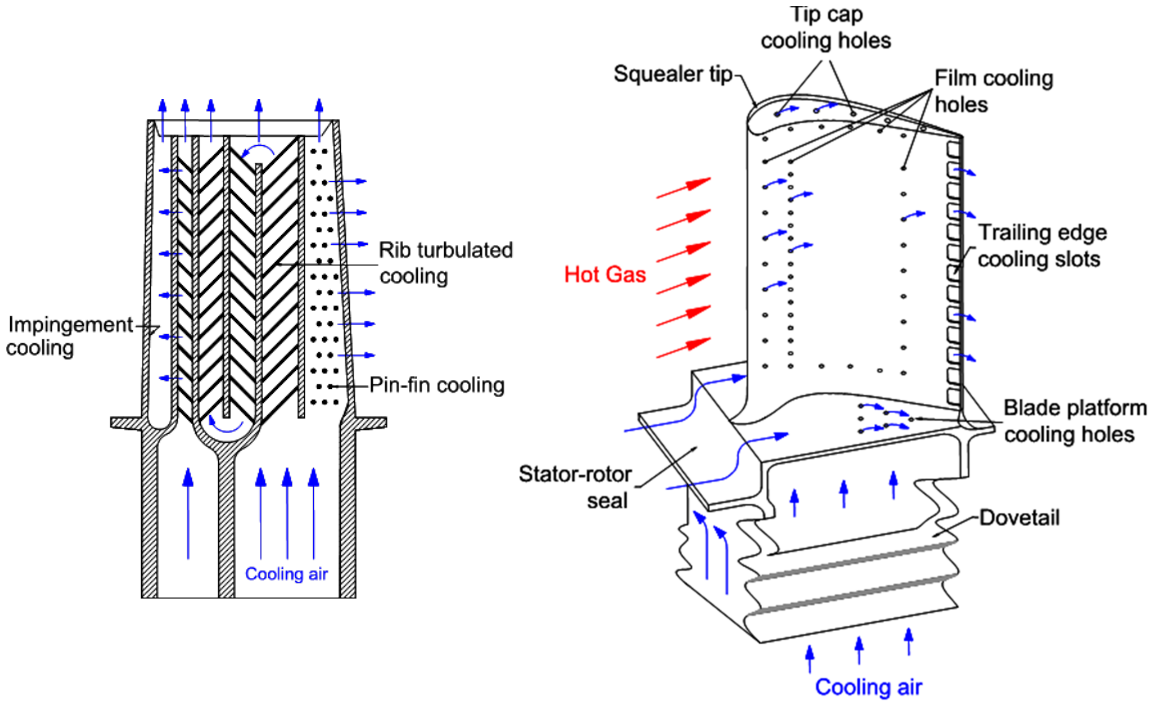

Fig. 1 Typical turbine rotor blade internal and external cooling system

Study of flat plate film cooling is a fundamental approach to understand the complex film cooling behavior in real gas turbines. In this study, a complete set of information was collected to depict various parametric effects on the flat plate film cooling effectiveness. These parameters include the hole geometry, blowing ratio, density ratio, free stream turbulence, and the novel backward injection approach. Experimental results are also compared with empirical correlations found in open literature.

CHAPTER II

BACKGROUND

Extensive researches on gas turbine film cooling in the past two decades have greatly improved the cooling of gas turbine components and hence increased the efficiency and power output of gas turbines. There are several parameters that affect the film cooling effectiveness, including the hole geometry, mass and momentum flux ratios, coolant density ratio, and mainstream turbulence intensity. Upstream wakes, passage/tip vortices, or surface curvature and roughness are also found to affect film cooling. Reviews of different parametric effects of film cooling can be found in Goldstein (1971) [1], Bunker (2005) [2], Bogard and Thole (2006) [3], and Han *et al.* (2013) [4].

Aside from getting experimental results of different geometries at different conditions, empirical correlations are developed to predict the performance of film cooling. Also, a new concept of backward injection is proposed and studied by numerical simulation.

Flat Plate Film Cooling

Fundamental study on flat plate film cooling gives an insight into the various parametric effects under real engine conditions. Experimental results on flat plates are used as a benchmark to compare and calibrate different experimental techniques in measuring heat transfer coefficient and film cooling effectiveness. Many flat plate film

cooling studies were carried out by researchers through the past ten years. These studies will be introduced in the following sections.

Effects of Blowing Ratios

Blowing ratio (M) is defined as below

$$M = \frac{\rho_c v_c}{\rho_m v_m} \tag{1}$$

where ρ_c is the coolant density and v_c is the coolant velocity; ρ_m is the mainstream density and v_m is the mainstream velocity. It is the mass flux ratio between coolant jets and the mainstream flow. Generally, film cooling effectiveness increases with increasing blowing ratio irrespective of the injection angle and hole exit shape. However, there is a turning point, where the film cooling effectiveness starts to decrease if further increase the blowing ratio. This phenomenon is due to strong coolant momentum that enable the coolant jet to penetrate into the mainstream flow. It is so called *coolant lift off* effect. It is witnessed in different hole configurations and geometries in vast studies such as Goldstein *et al.*[5], Pedersen *et al.* [6], Sinha *et al.* [7] and Rallabandi *et al.* [8].

Effects of Hole Configuration and Geometry

Film cooling holes are designed at an angle to the mainstream flow. Film cooling hole that is perpendicular to the surface results in very poor coverage while the film cooling slot that is parallel to the flow direction has the best coverage. However, the structural limitation and manufacturing cost constraint this kind of design. A film cooling hole at an axial angle (α) of 30° to 35° to the surface compromises between the

film cooling effectiveness, manufacturing cost and structural strength. This kind of hole direction is called simple angled injection direction if it is parallel to the mainstream flow direction when viewed from top of the surface. Simple angled hole configuration has poor lateral coverage. Moreover, the coolant jets tend to lift-off at higher coolant to mainstream blowing ratios. The lateral coverage of the coolant can be improved by injecting the coolant at a compound angle (β) to the mainstream, which found to increase the film cooling effectiveness and suppress the coolant lift-off (Ligrani *et al.* [9] and Ekkad *et al.* [10]). The axial angle (α) and compound angle (β) are shown schematically in Fig. 2

Aside from injection direction, hole exit geometry also influences the film cooling effectiveness. Goldstein *et al.* [5] pioneered in shaped hole research. Shaped holes that have an expanded exit reduce the coolant momentum, hence reduce the tendency of coolant lift-off (Schmidt *et al.* [11], Gritsch *et al.* [12] and Wright *et al.* [13]). Shaped holes also provide better lateral coverage than cylindrical holes due to superior lateral spread. Fig. 2 shows four common hole geometries with both simple angle injection and compound angle injection.

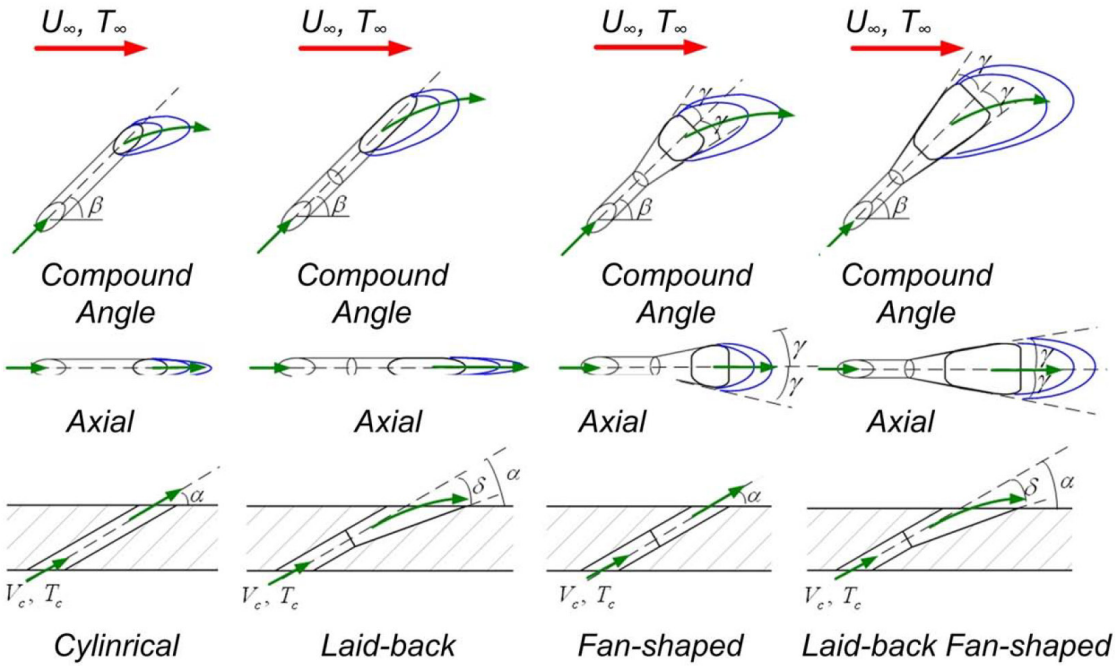

Fig. 2 Various film cooling hole configurations

Effects of Density Ratios

Coolant to mainstream density ratio (DR) has notable influences to the film cooling effectiveness. In a modern gas-turbine engine, the typical coolant to mainstream density ratio ranges from 1.7 to 2.0. The difference in density comes from the temperature difference between the coolant and mainstream air. Under a laboratory setting, a high density ratio can be achieved by a cryogenic heat transfer system (Pietrzyk *et al.* [14] and Sinha *et al.* [7]). The density ratio effect can also be studied with foreign gases of higher densities. Relevant work can be found in Goldstein *et al.* [5], Pedersen *et al.* [6], Wright *et al.* [13] and Narzary *et al.* [15]. Generally, at a given M, higher DR gives higher film cooling effectiveness. This is because the resulting

momentum of the coolant jet is lower, therefore, the mainstream can further push the coolant jets toward the surface. Similar to the effect of expanded hole geometry, lowering the coolant momentum (by increasing DR at a given M) results in a lower tendency of coolant lift-off.

Effects of Free-Stream Turbulence

In real engine condition, the mainstream flow in the gas turbine has high turbulence intensity (Tu). The turbulence intensity varies at different locations, typically ranging from 8% to 12% as shown in Saumweber *et al.* [16]. At the exit of the combustor, the turbulence intensity ranges from 7% to 20%. Consequently, the film cooling holes on the first stage stator vane experience the highest turbulence effect.

In a laboratory setting, free stream turbulence can be generated by a turbulence grid located upstream of the test section. The generated turbulence intensity at a given downstream location is related to the rod diameter, shape, and spacing. The turbulence intensity is found to be decreasing rapidly downstream of the turbulence grid, therefore, the distance between the turbulence grid and the film cooling holes is a sensitive parameter. Young *et al.* [17] studied the turbulence effect on a flat plate and provided an accurate correlation for estimating the turbulence intensity downstream of a turbulence grid.

Turbulence effect has been studied extensively. Consistent results were obtained by Kadotani and Goldstein [18], Bons *et al.* [19], Saumweber *et al.* [16], and Wright *et al.* [20]. For cylindrical holes at an inclined angle to the mainstream, higher Tu results in

a lower effectiveness at lower blowing ratios. For higher blowing ratios, higher Tu may slightly enhance the effectiveness due to enhanced turbulent mixing. Turbulent mixing reduces the coolant lift-off effect at higher blowing ratio so that the jets are less likely to penetrate into the mainstream. With higher Tu, the coolant traces are also found to be shorter and wider owing to accelerated spanwise diffusion and vortex formation.

On the other hand, for shaped holes, Saumweber *et al.* [16] found that higher Tu leads to a lower effectiveness even for large blowing ratios.

Backward Injection

Investigation on backward injection was carried out numerically by Li [21]. While the current design of coolant injection usually has a compound angle $\beta < 45°$ to the mainstream flow direction, film cooling with an injection direction against to the mainstream flow was studied on a simple cylindrical hole. The result shows that under a condition which has the same pressure loss as in the forward injection, numerical simulation showed enhanced film cooling effectiveness, a more uniform coverage and less coolant consumption. Improvements in the centerline film cooling effectiveness can also be seen in blowing ratios M = 1.33 and 1.67 and blowing angles 25°, 30°, and 35°. Backward injection can potentially increase the pressure loss, nevertheless, it can be reduced by reducing the coolant flow rate.

Correlation Development

Empirical correlations are used extensively in the design process of gas turbine components. An accurate and reliable prediction of thermal boundary conditions is essential for the finite element analysis. Since the turbine components are operating near the critical temperature, a small temperature difference (15 K) can reduce the component lifetime by half. Baldauf *et al.* [22] conducted a series of experiments to study the film cooling effectiveness by using Infrared Thermography. The results were used to develop a powerful correlation that can predict the film cooling effectiveness for simple angled cylindrical holes under different blowing ratios, density ratios, injection angles, hole spacing, or turbulence intensities. Colban *et al.* [23] developed a correlation specifically for simple angled shaped holes with better accuracy and broader ranges of parameters. While the existing correlations work at lower blowing ratios, the proposed correlation can predict effectiveness up to M=2.5 with reasonable accuracy.

Objective of Current Study

The primary objective of this research is to gather a comprehensive set of data on the combined effects of geometry, blowing ratio, density ratio, or free-stream turbulence intensity with forward and backward injection on a flat plate. Test will be done on four common hole geometries including simple angled cylindrical and fan-shaped holes, compound angled cylindrical and fan-shaped holes.

Accurate and detailed film cooling effectiveness distributions can be used for comparison with experimental results, computational results, or be used to develop empirical correlations.

Currently, there is no experimental results regarding backward injection. In numerical calculation, backward injection is found to be beneficial for the film cooling effectiveness. Experimental results will be provided and compared.

CHAPTER III

EXPERIMENTAL SETUP AND THEORY

In this chapter, the test facility and measurement technique will be introduced. Pressure sensitive paint measurement theory will also be explained.

Instrumentation

Experiments were taken in the test section of a low speed suction type wind tunnel at a mainstream velocity of 21.6 m/s. The entrance of the wind tunnel has a 4:1 contraction ratio in order to provide uniform flow. The cross-section of the test channel is 30.48 cm by 15.24 cm. A 5.6 kW axial blower was used to produce mainstream flow through the channel. The mainstream turbulence intensity at the test section was estimated to be 0.5%. The room temperature was kept at around 24 ˚C by the building's central air conditioning system.

The test section is located at the bottom surface of the wind tunnel. There is a cavity at the bottom of the wind tunnel and a plenum is connected below the cavity. A 15 mm thick film cooling plate can be fitted into the cavity. An O-ring was placed between the plenum and the test plate to ensure the air tightness.

Coolants are supplied by gas cylinders (N_2, CO_2, and mixture) or an air compressor to the plenum. The coolant flow rate was measured and controlled by Dwyer rotameters. The temperature of the mainstream flow and coolant flow were measured by thermocouples. The mainstream velocity was measured by a Pitot-static tube connected

to a micro-manometer. A turbulence grid was applied to the upstream of the test section to generate free stream turbulence for turbulence effect studies. Fig. 3 shows the test facility schematically.

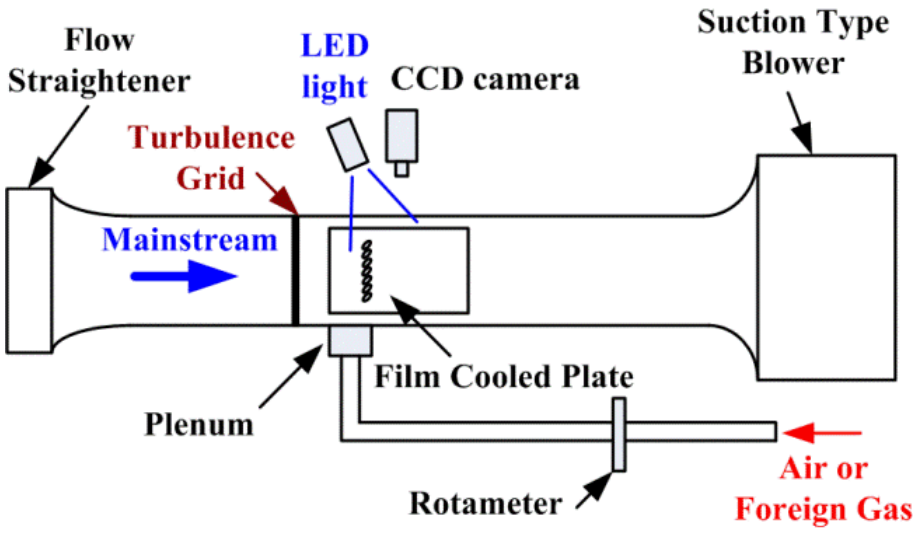

Fig. 3 Schematic diagram of the test facility

Four different hole geometries were used in this study. Fig. 4 shows the top view of the cooling holes. Table 1 summarizes the plate geometric parameters. The hole diameter D for all plates is 4mm. The plates with simple angled cylindrical holes and compound angled fan-shaped holes are fabricated using SLA process on Somos® stereolithography resins. The plates with compound angled cylindrical holes and simple angled fan-shaped holes are made using the EDM process on a stainless steel plate. All four geometries are frequently used in laboratory research and real engine conditions. Another plate with simple angled cylindrical holes at a α=35° to the main stream (plate

(e) in Table 1) was used to compare the results with Sinha *et al.* [7]. The L/D value for plate (e) is smaller than the previous four plates.

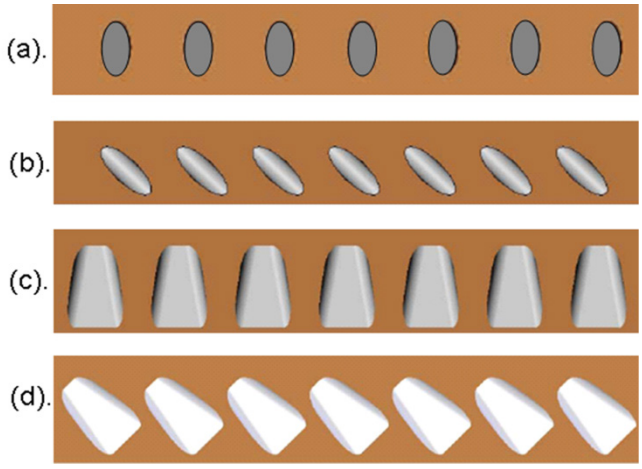

Fig. 4 Four different hole geometries used in this study. (a) simple angled cylindrical hole. (b) compound angled cylindrical hole. (c) simple angled fan-shaped hole. (d) compound angled fan-shaped hole

Table 1 Summary of hole geometries used in this study

#	α	β	Shape	Pitch	L/D
a	30°	0°	Cylindrical	3D (12mm)	7.5
b	22°	45°	Cylindrical	3D (12mm)	9.9
c	30°	0°	Laid Back Fan Shaped (Expansion angles: 10° stream-wise, 10° span-wise)	3.75D (15mm)	7.5
d	30°	45°	Laid Back Fan Shaped (Expansion angles: 10° stream-wise, 10° span-wise)	3.75D (15mm)	7.5
e	35°	0°	Cylindrical	3D (12mm)	3.5

To test the backward injection effect, the test plates were rotated 180 degrees. The injection directions were reversed from forward to backward to the mainstream as shown schematically in Fig. 5.

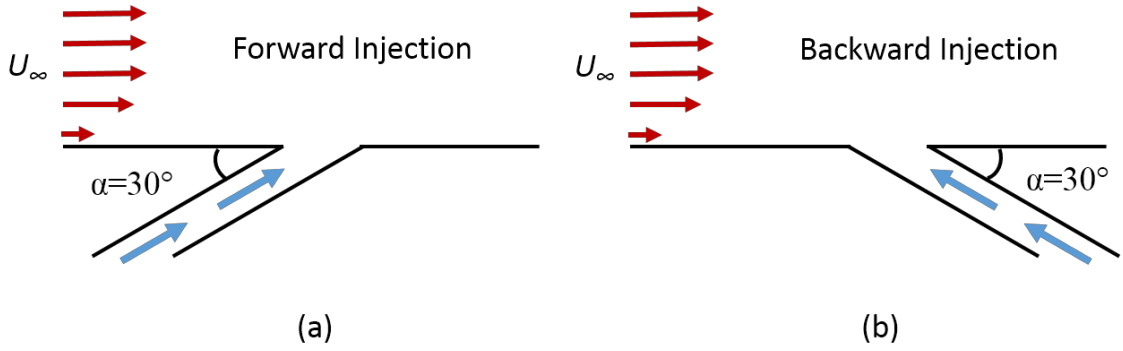

Fig. 5 Schematic diagram showing (a) the forward injection and (b) the backward injection

Pressure Sensitive Paint Technique

Film cooling effectiveness distributions were measured using pressure sensitive paint (PSP) technique through a mass analogy method. It is widely used in many aerodynamic applications where detailed surface pressure distribution is needed. It provides non-intrusive measurement and high spatial resolution compared to conventional methods. It is first used by Zhang and Jaiswal [24] in measuring the surface film cooling effectiveness. This technique has been used by Han *et al.* in various turbine film cooling studies [8, 20, 25]. PSP is comprised of fluorescent molecules and oxygen-permeable polymer binder. As shown in Fig. 6, a 397±10 nm LED lamp (Innovative Scientific Solutions, Inc. ISSI LM2X LED array) is used to excite the fluorescent

molecules in the polymer binder. The fluorescent molecules then emit fluorescent light at a wavelength > 590 nm when it relax from the excited state to the ground state. A CCD camera (SensiCam QE, The COOKE Corp., with 640*480 spatial resolution, 12bit RGB or grey level) with a long pass filter was used to capture the emission intensity of the painted surface.

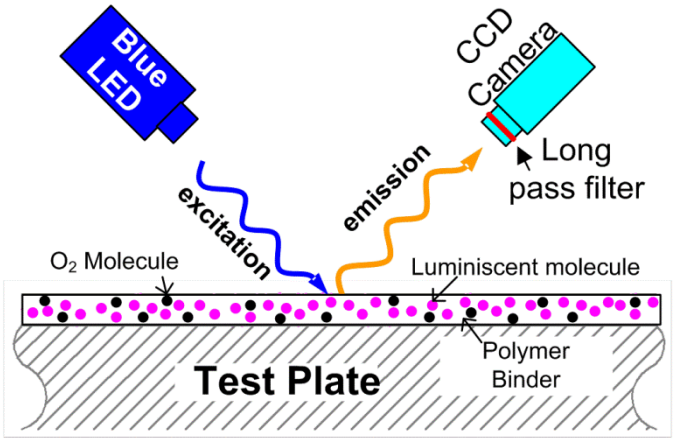

Fig. 6 Schematic diagram of PSP measurement

With the existence of oxygen molecules, the fluorescent molecules will go through another emission-free path to the ground state. As a result, the surface emission intensity will be smaller. This is known as the oxygen-quenching effect. With careful calibration, the oxygen partial pressure in close proximity to the painted surface can be deduced from the surface emission intensity.

A vacuum chamber (Fig. 7) with a transparent Plexiglas window was used to calibrate the partial pressure of oxygen (also the partial pressure of air since there is a

constant concentration of oxygen in the ambient air) and the emission intensity of a calibration sample. The LED array and the CCD camera were placed at the same distance and angle to the calibration sample as they were to the test plates in the test section. A calibration sample painted with Uni-FIB PSP (UF-470) from Innovative Scientific Solutions, Inc. (ISSI) was placed in the air tight calibration chamber.

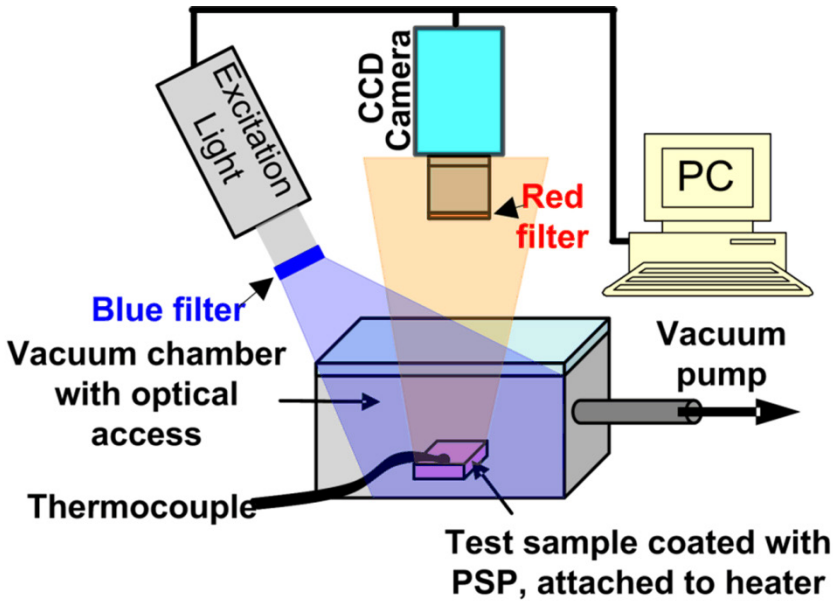

Fig. 7 Schematic diagram of the calibration setup for PSP

As shown in Fig. 8. The emission intensity of the PSP was recorded at a 2 inHg interval from 0 inHg (gauge pressure, which is equivalent to 1 atm, 1atm = 29.92 inHg) to -26 inHg (gauge pressure). The recording CCD camera was set to take 200 gray-scale images at each pressure. The intensity at a certain pressure was obtained by averaging the 200 images so as to cancel out the noise. The ambient pressure was used as the

reference pressure P_{ref}. And the intensity measured at the reference pressure was used as the reference intensity I_{ref}. The intensity obtained at lower pressures is denoted as I. The intensity obtained under completely black condition is the background noise of the camera I_{blk}, and will be subtracted from I and I_{ref}. The result was plotted as intensity ratio versus pressure ratio which can be expressed as:

$$\left(\frac{I - I_{blk}}{I_{ref} - I_{blk}}\right) = f\left(\frac{P_{O_2}}{\left(P_{O_2}\right)_{ref}}\right) \tag{2}$$

A power fitting curve was used to fit the data points as shown in Fig. 8. The data can be fitted with Eq. (3):

$$\frac{I}{I_{ref}} = 1.2311\left(\frac{P}{P_{ref}}\right)^{-0.69547} - 0.20937 \tag{3}$$

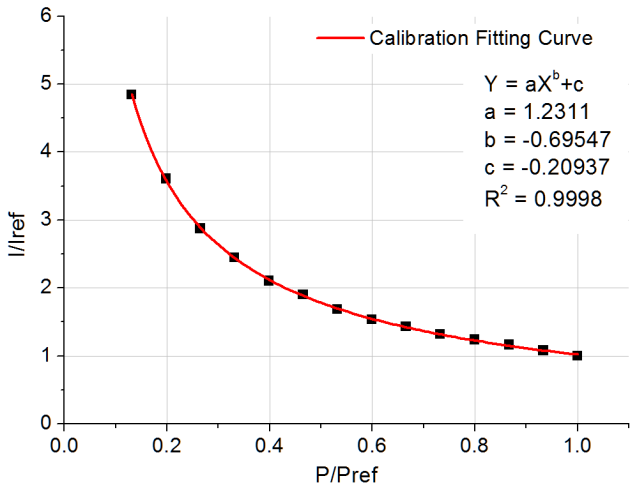

Fig. 8 PSP calibration fitting curves

Film Cooling Effectiveness and Measurement Theory

The heat load of an un-insulated surface can be calculated by the 1-D convective heat transfer equation:

$$q_o'' = h_o(T_\infty - T_w) \tag{4}$$

where h_o is the heat transfer coefficient without film cooling, T_∞ is the mainstream temperature, and T_w is the wall temperature. With film cooling, the heat transfer on the blade surface can be treated as a two layer model as shown in Fig. 9.

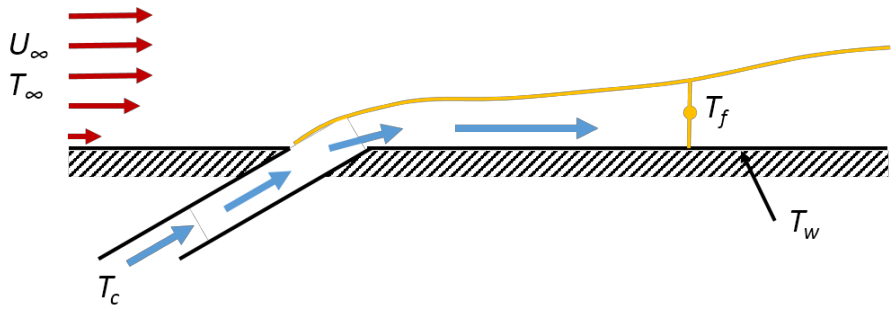

Fig. 9 Film cooling two layer model schematic plot

Cooling air at temperature T_c ejecting from the film cooling holes forms an insulating layer at temperature T_f on the blade surface. The heat load becomes:

$$q'' = h\left(T_f - T_w\right) \tag{5}$$

where h is the heat transfer coefficient with film cooling. At steady state, the film temperature T_f increases gradually downstream of the hole due to the mixing with hot turbulent mainstream air. A dimensionless parameter, the film cooling effectiveness η

$$\eta = \frac{T_\infty - T_f}{T_\infty - T_c} \tag{6}$$

is used to describe the effectiveness of film cooling effect. Higher effectiveness means lower T_f, which implies better coverage of the coolant air.

Measuring the film cooling effectiveness with PSP is a mass transfer method rather than a conventional heat transfer method. There will be no conduction effect, hence reduce the uncertainty at high temperature gradient regions. A detailed description of heat transfer and mass transfer analogy can be found in Han and Rallabandi [26]. To obtain the film cooling effectiveness with mass transfer method, a foreign gas is injected from the cooling holes into the mainstream. Foreign gas such as nitrogen forms an insulating layer above the surface, lowering down the oxygen concentration near the surface. This deficit of oxygen near the surface can be detected by the PSP. The oxygen partial pressure on the surface can be obtained. Fig. 10 shows the heat transfer and mass transfer analogy schematically. The heat and mass transfer analogy in measuring film cooling effectiveness can be related by the following equation:

$$\eta = \frac{T_f - T_\infty}{T_c - T_\infty} \approx \frac{T_{aw} - T_\infty}{T_c - T_\infty} \approx \frac{C_w - C_\infty}{C_c - C_\infty} = 1 - \frac{C_w}{C_\infty} \tag{7}$$

where T_{aw} is the adiabatic wall temperature. C represents the tracer mass fraction, which in this case is oxygen. C_w is the oxygen mass fraction on the wall surface, C_c is the oxygen mass fraction of the coolant gas (which can be taken as 0), and C_∞ is the oxygen mass fraction of the mainstream air.

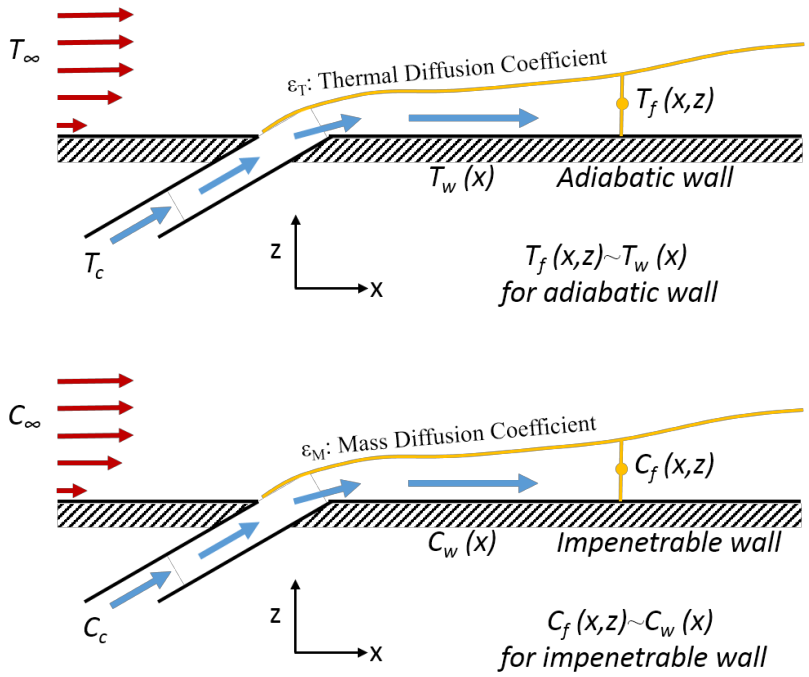

Fig. 10 Heat transfer and mass transfer analogy in measuring the film cooling effectiveness. Here, z direction is normal to the surface and x is the stream-wise direction. The film temperature/mass fraction is a function of x,z, while wall temperatures/mass fraction are functions of x only

Four tests are required to determine the film cooling effectiveness: the black test, the reference test, the air injection and the foreign gas injection tests. In each test, 200 images are taken and averaged to cancel out the noise. The black image intensity (I_{blk}) is acquired under completely black condition. This background intensity I_{blk} will be subtracted from other images. The reference image intensity (I_{ref}) is acquired with LED light illumination. Both I_{blk} and I_{ref} are taken while there is no mainstream and coolant flows. The air injection image intensity (I_{air}) is taken with mainstream flow and LED light illumination. Compressed air is injected as coolant. The corresponding oxygen

concentration and partial pressure are $C_{O2,air}$ and $P_{O2,air}$. The foreign gas image intensity (I_{fg}) is also taken with mainstream flow and LED light illumination. A foreign gas is injected through the cooling holes as coolant. The corresponding oxygen concentration and partial pressure are $C_{O2,fg}$ and $P_{O2,fg}$.

When the molecular weight of the foreign gas is close to that of air (e.g. nitrogen), the film cooling effectiveness can be calculated as:

$$\begin{aligned}\eta &\approx 1-\frac{C_w}{C_\infty}=1-\frac{C_{O_2,fg}}{C_{O_2,air}}=1-\frac{P_{O_2,fg}}{P_{O_2,air}}\\ &=1-\frac{P_{O_2,fg}/P_{O_2,ref}}{P_{O_2,air}/P_{O_2,ref}}\end{aligned} \tag{8}$$

When the molecular weight of the foreign gas is different from that of air, the equation needs to be modified in order to account for the variation of the effective molecular weight of the mixed gas in the cooling film. The film cooling effectiveness can be obtained by the following equation:

$$\eta=1-\frac{1}{\left(1+\left(\frac{P_{O_2,air}/P_{O_2,ref}}{P_{O_2,fg}/P_{O_2,ref}}-1\right)\frac{W_{fg}}{W_{air}}\right)} \tag{9}$$

where W_{air} is the molecular weight of ambient air and W_{fg} is the molecular weight of the foreign gas coolant.

CHAPTER IV

RESULTS

Span-wise (laterally) averaged data will be presented throughout this chapter. All span-wise averaged data in the current study consider the middle three holes only in order to avoid the edge effect. All span-wise averaged effectiveness plots and corresponding contour plots for all different test cases are documented in the Appendix (Fig. A 1 to Fig. A 32).

Comparison with Open Literature

Span-wise averaged effectiveness values obtained by using plate (e) (Table 1) are compared with Sinha *et al.* [7]. The test conditions are summarized in Table 2.

The comparison of span-wise averaged film cooing effectiveness at different density ratios are shown in Fig. 11, Fig. 12 and Fig. 13. The dashed lines are fitting curves for the data points. For DR ≈ 1 and DR ≈ 1.5, most cases are comparable or have minor deviation to each other except for the case at M = 0.8 and DR = 1.5, which the current data is overall lower than the reference value. For DR = 2, all values for $x/D < 7$ are higher than the reference values. This may be caused by the different L/D ratio. Generally, a larger L/D ratio yields a higher effectiveness.

Table 2 Experimental conditions of this study and Sinha *et al.*

	This study	Sinha *et al.*
Blowing Ratios (M)	0.25, 0.5, 0.6, 0.78 (DR=1) 0.57, 0.8, 0.9, 1.0 (DR=1.5) 0.5, 0.8, 1.0 (DR=2)	0.25, 0.5, 0.6, 0.78 (DR=1.2) 0.57, 0.8, 0.9, 1.0 (DR=1.6) 0.5, 0.8, 1.0 (DR=2)
Density Ratios (DR)	1, 1.5, 2 (Foreign gases)	1.2, 1.6, 2 (Temperature difference)
Mainstream Velocity	21.6 m/s	20 m/s
Measurement Method	PSP	Thermal couple
Turbulence Intensity	0.5%	0.2%
Hole Geometry and Material	D = 4 mm Pitch = 3D L/D = 3.5 α = 35°, β = 0° Made by SLA	D = 12.7 mm Pitch = 3D L/D = 1.75 α = 35°, β = 0° Made of Styrofoam

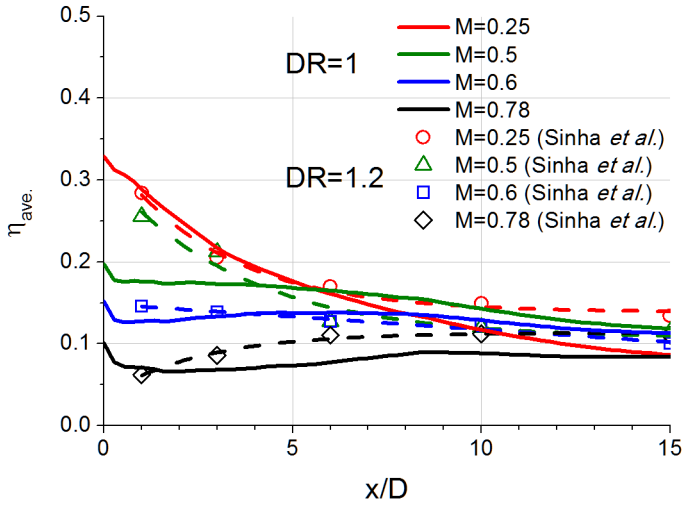

Fig. 11 Span-wise averaged effectiveness compared with Sinha *et al.* at a density ratio near to 1

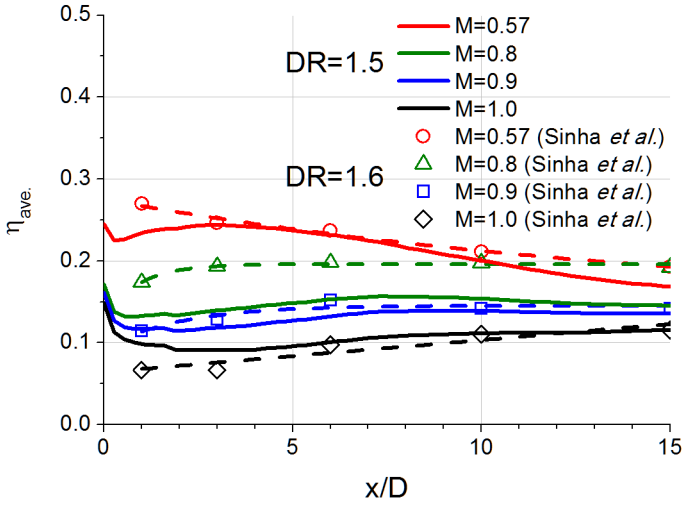

Fig. 12 Span-wise averaged effectiveness compared with Sinha *et al.* at a density ratio near to 1.5

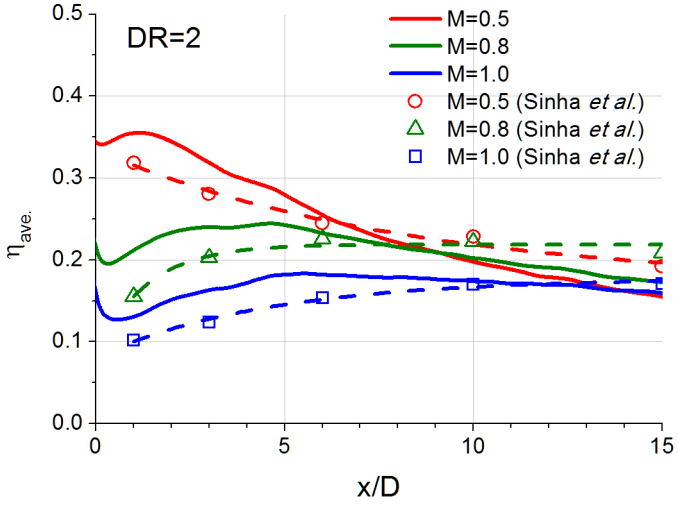

Fig. 13 Span-wise averaged effectiveness compared with Sinha *et al.* at DR = 2

Comparison was also made with data obtained by Rallabandi *et al.* [8]. The geometries used to compare were simple angled cylindrical and compound angled cylindrical holes. Test was performed with the same test facility, hole geometries, and the same measurement technique. The test conditions between Rallabandi *et al.* and this study are different in the main stream velocity and the plate material (Table 3).

Table 3 Experimental conditions of this study and Rallabandi *et al.*

	This study	Rallabandi *et al.*
Blowing Ratios (M)	0.3, 0.6, 1.0, 1.5	0.3, 0.6, 1.0, 1.5
Density Ratios (DR)	1 (Nitrogen)	1 (Nitrogen)
Mainstream Velocity	21.6 m/s	25 m/s
Measurement Method	PSP	PSP
Turbulence Intensity	0.5%	0.5%
Hole Geometry and Material	Plate (a) Made by SLA	Same geometry as plate (a) Made of polyurethane foam
	Plate (b) Made by SLA	Same geometry as plate (b) Made of Plexiglas

The comparison of span-wise averaged film cooling effectiveness of two different plates are shown in Fig. 14 and Fig. 15. The comparison shows consistent trend with each other although there is some deviation in effectiveness, which may be caused by different plate materials.

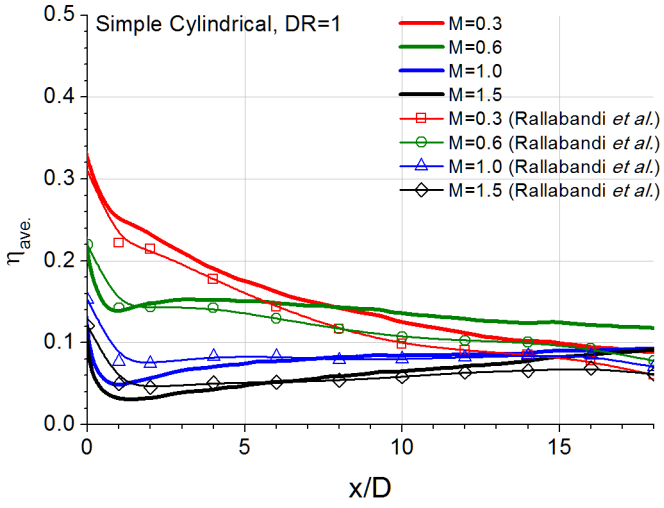

Fig. 14 Span-wise averaged effectiveness comparison with Rallabandi *et al.*- simple angled cylindrical holes

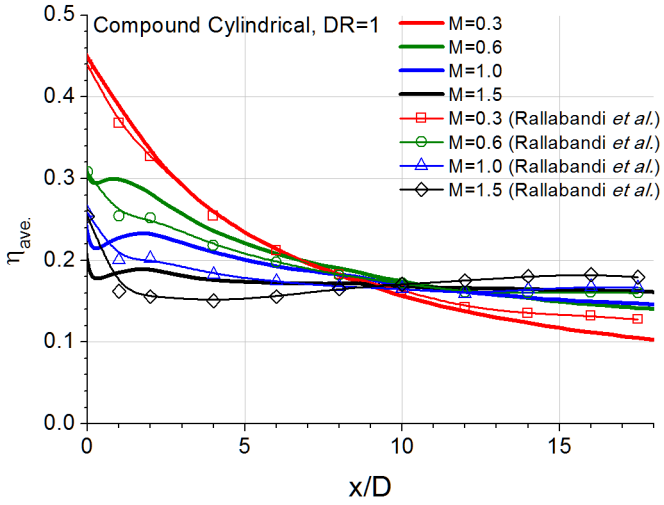

Fig. 15 Span-wise averaged effectiveness comparison with Rallabandi *et al.*- compound angled cylindrical holes

Results of Forward Injection

The test cases for forward injection in the current study is listed in Table 4. Test plates (a) to (d) (in Table 1) were tested in both forward injection and backward injection. All test cases have 10 different blowing ratios ranging from 0.3 to 2.0. In the forward injection, high free stream turbulence study (Tu = 6%), only DR=1 and DR=2 were tested.

Table 4 Test cases for forward injection

Mainstream and Coolant Temperature	T_m, T_c	297 K
Blowing Ratio (M)	$\rho_c V_c/\rho_m V_m$	0.3, 0.4, 0.5, 0.6, 0.7, 0.8, 1.0, 1.2, 1.5, 2.0
Density Ratio (DR) Free-stream Turbulence Intensity	ρ_c/ρ_m T_u	1 (N_2), 1.5 (CO_2), and 2 (15% SF_6 + 85% Ar) 0.5%
Density Ratio (DR) Free-stream Turbulence Intensity	ρ_c/ρ_m T_u	1 (N_2) and 2 (15% SF_6 + 85% Ar) 6%

Effects of Geometry and Blowing Ratio

For the four test geometries considered in this study, the blowing ratio effects are clearly shown in Fig. 16. The blowing ratio effect on simple angled cylindrical holes shows coolant lift off at higher blowing ratios. This is because the jets that have higher momentum can easily penetrate into the mainstream, while it may reattach to the surface at a downstream location. Coolant lift off results in low film cooling effectiveness near hole with a gradually increasing effectiveness downstream (reattachment). The

effectiveness near the hole exit decreases with increasing blowing ratio. The optimum blowing ratio for simple angled cylindrical hole is around M = 0.5 to 0.6 which agreed to open literature.

The compound angled cylindrical holes provide better coverage than the simple angled holes (Fig. A 1 and Fig. A 4). Lateral spread of coolant near the hole exit yields a higher effectiveness. However, coolant lift off also reduces the near hole effectiveness with increasing blowing ratio. Notably, the coolant reattachment occurs earlier (at smaller x/D) than the simple angled cylindrical holes.

The simple angled and compound angled fan-shaped holes show similar trend for varying blowing ratios. Since the expanded hole exit reduces the coolant momentum and increases lateral diffusion, the coolant jets have a low tendency to lift off. The results show higher film cooling effectiveness when compared to cylindrical holes, especially at higher blowing ratios. Without coolant lift off, the effectiveness increases with increasing blowing ratio up to some point ($M \approx 1.0$). Coolant partial lift off (not completely detaches from the surface, but remains within certain distance above the surface, almost parallel to the mainstream flow) then occurs if further increases the blowing ratio beyond the turning point, which results in a lower effectiveness.

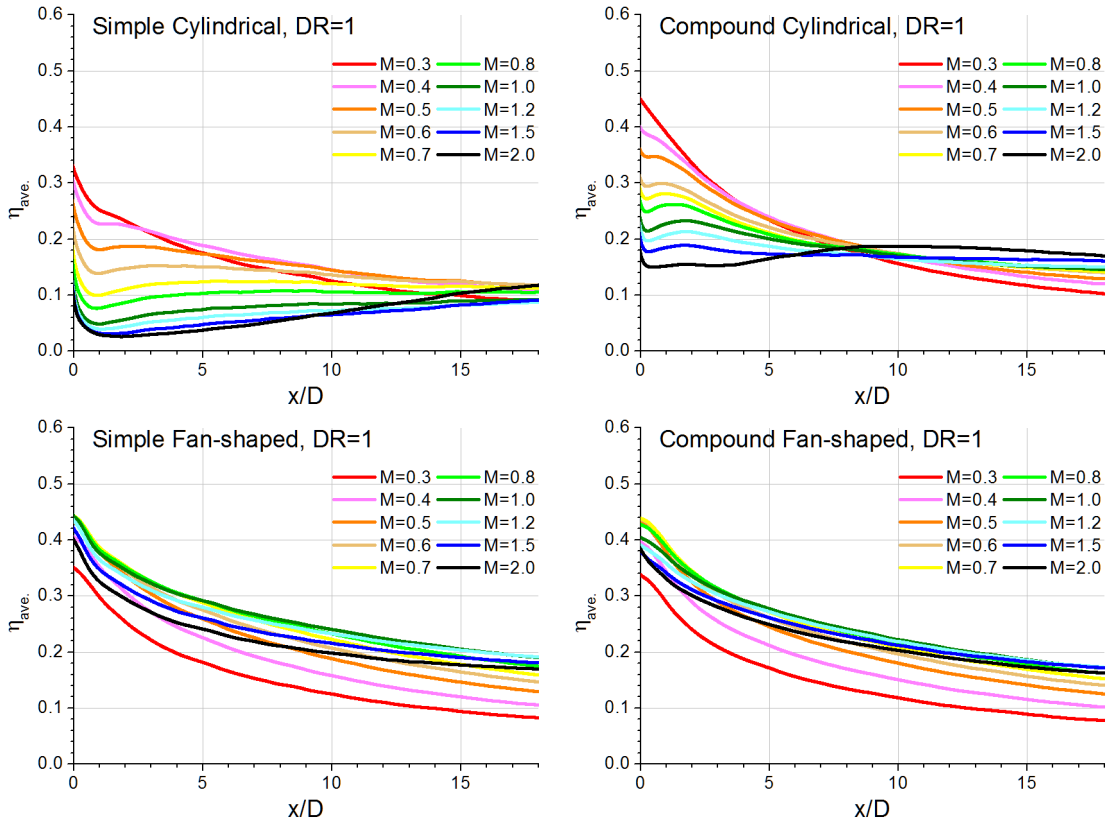

Fig. 16 The effect of hole geometry and blowing ratio. Laterally averaged effectiveness at DR = 1 for four different geometries

Effects of Density Ratio

Fig. 17 and Fig. 18 show the laterally averaged effectiveness at DR = 1.5 and DR = 2 for cylindrical holes and fan-shaped holes respectively. Readers can compare density ratio DR = 1 to DR = 1.5 and 2 from Fig. 16 to Fig. 18. Density ratio effect is more apparent for simple angled cylindrical and compound angled cylindrical holes. It seems to have a monotonic positive effect on effectiveness. The effectiveness has been enhanced by injecting heavier coolant at all blowing ratios. And the density ratio effect seems to have more influence at smaller x/D regions. The enhancement is due to reduced

coolant jet momentum at a higher density ratio at a given blowing ratio. As a result, at certain blowing ratio, coolant jets with heavier foreign gas has less tendency to lift off.

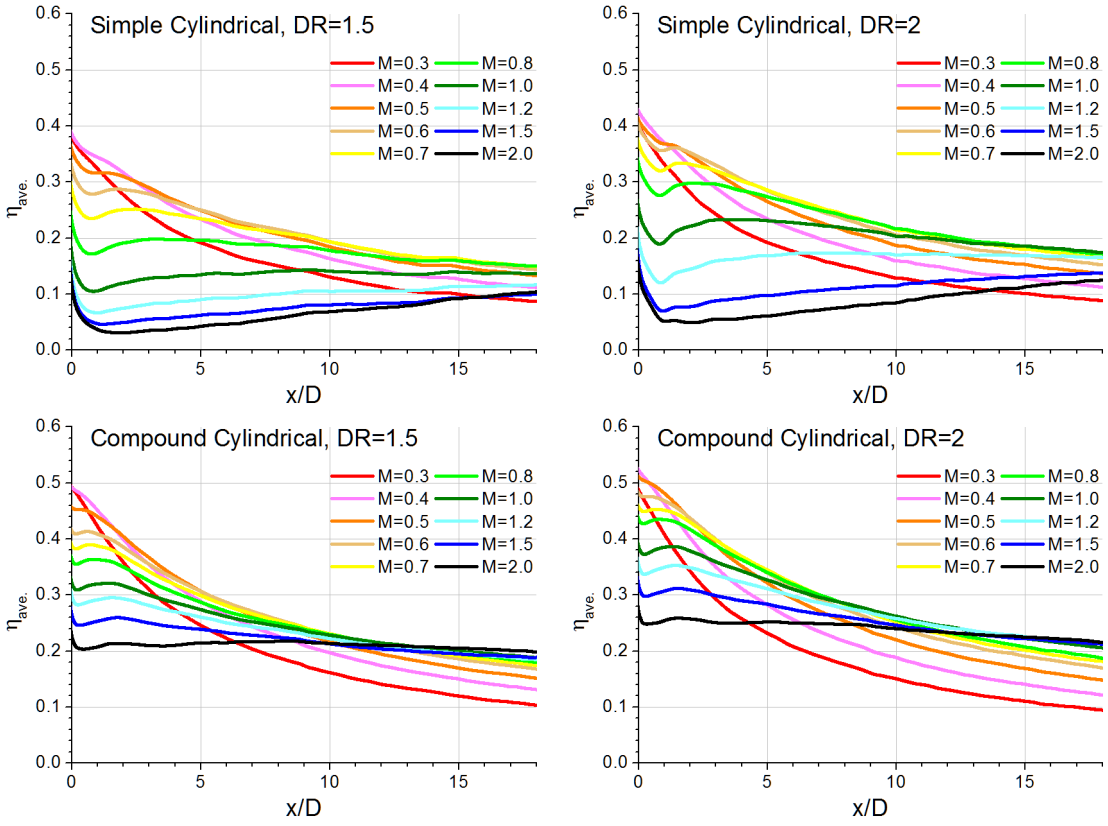

Fig. 17 The density ratio effect. Laterally averaged effectiveness at DR = 1.5 and DR = 2 for simple angled and compound angled cylindrical holes

Density ratio effect on fan-shaped holes can be detrimental at lower blowing ratios. The result shows no or negative effect on the effectiveness at small blowing ratios. It is due to lower coolant volume flow rate at higher density ratios at a given M. Which means there is less coolant to cover the surface, causing the effectiveness to drop

a little bit. However, it has positive effect at higher blowing ratios. At higher blowing ratios, owing to the reduced tendency of coolant lift off, the effectiveness can be increased. On the other hand, the optimal blowing ratio increases with increasing density ratio. For example, the blowing ratio that has the highest effectiveness for simple fan-shaped holes is about M = 1.2 at DR = 1.5, but it becomes M = 1.5 for DR = 2. Which means higher density ratio requires higher blowing ratio to reach the transition point.

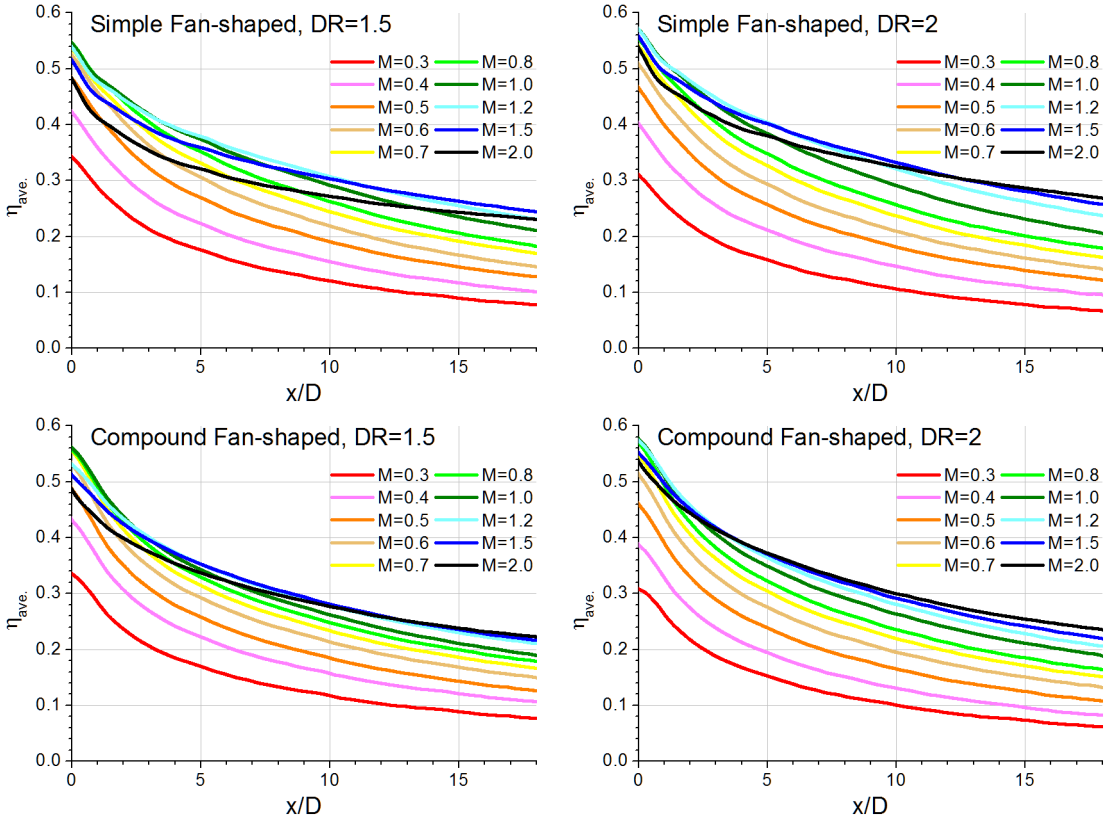

Fig. 18 The density ratio effect. Laterally averaged effectiveness at DR = 1.5 and DR = 2 for simple angled and compound angled fan-shaped holes

Cross-comparison was made to exhibit the density ratio effect at M = 0.3, 1, and 2. As shown in Fig. 19, higher density ratio gives higher effectiveness at a given blowing ratio, except for the compound angled cylindrical and fan-shaped holes at low blowing ratio.

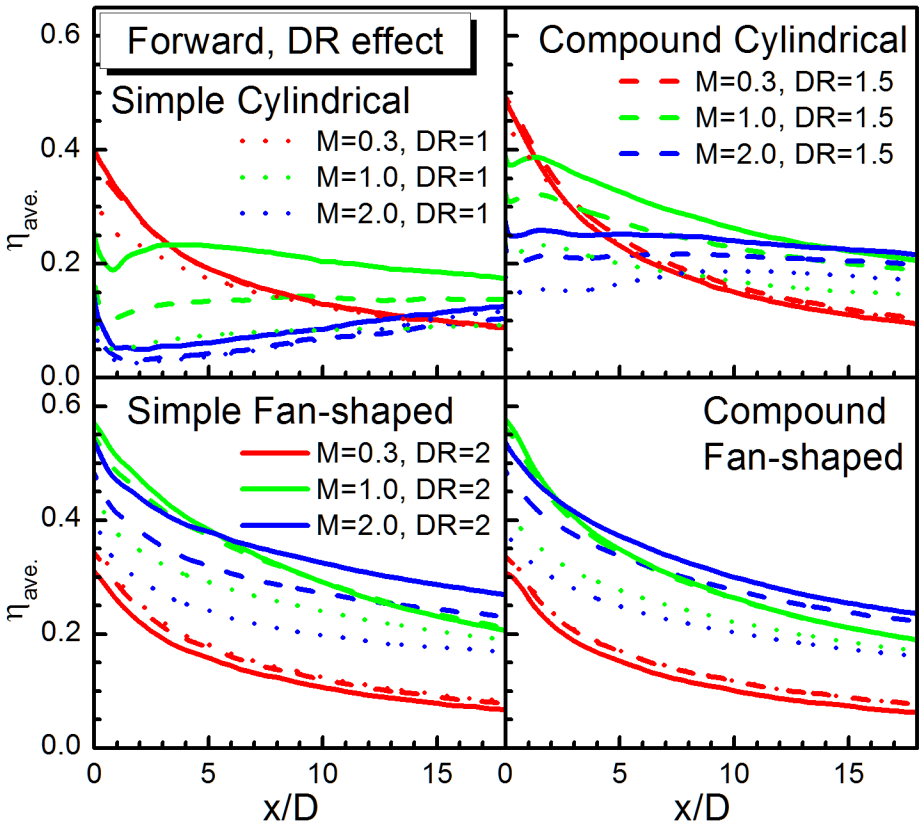

Fig. 19 Cross-comparison of the density ratio effect at M = 0.3, 1, 2, DR = 1, 1.5 and 2, forward injection

Effects of Free-Stream Turbulence

Turbulence in the mainstream promotes the mixing between coolant jet and the mainstream, consequently, the effectiveness will be reduced. Nevertheless, under certain conditions that the coolant jets lift off in the low turbulence cases, film cooling effectiveness can be enhanced with enhanced turbulence. This is because the enhanced mixing that brings the coolant from the lifted off coolant jets to the surface. As can be seen in the simple angled cylindrical holes at DR = 1 (Fig. 16 and Fig. 20). For simple fan-shaped holes at DR = 1 (Fig. 16 and Fig. 20) and compound cylindrical holes at DR = 2 (Fig. 17, Fig. 18 and Fig. 21), the laterally averaged effectiveness reduces at lower blowing ratios, but increases at higher blowing ratios. For all other cases where there is no or minimal coolant lift off, the effectiveness becomes lower under higher free stream turbulence, particularly for lower blowing ratios.

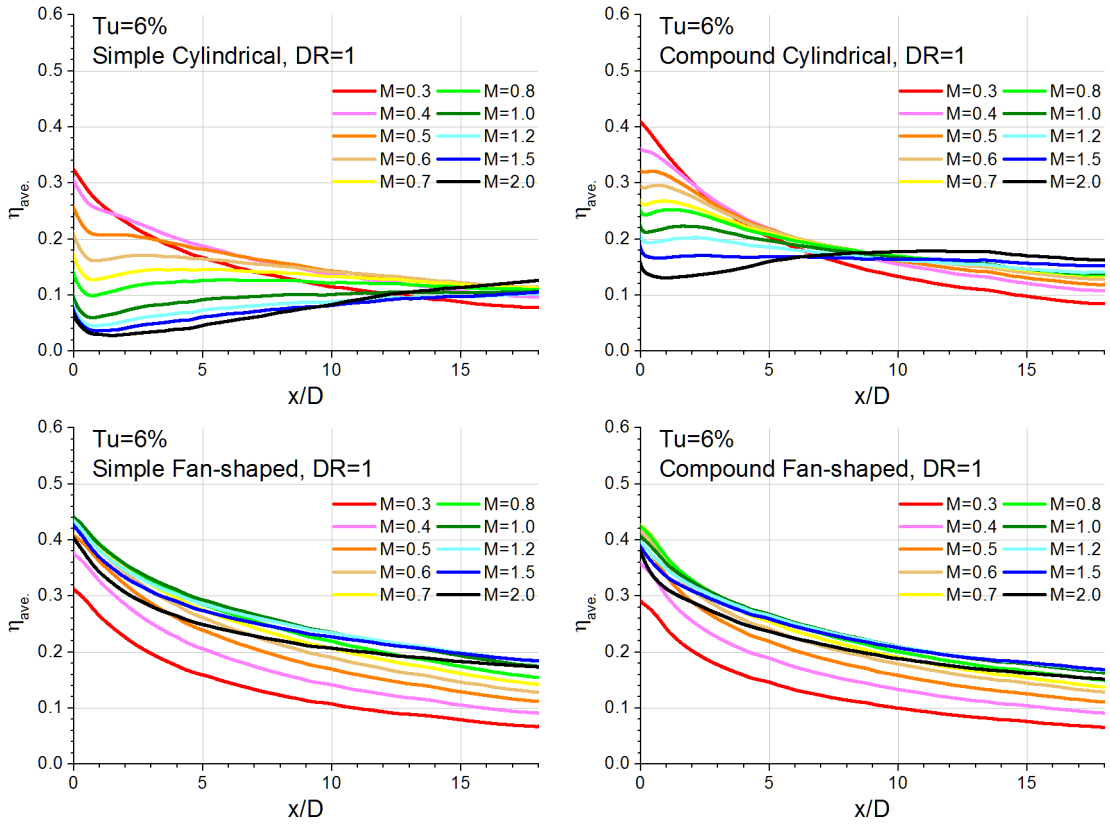

Fig. 20 The free stream turbulence effect. Laterally averaged effectiveness at Tu = 6%, DR = 1 for four different geometries

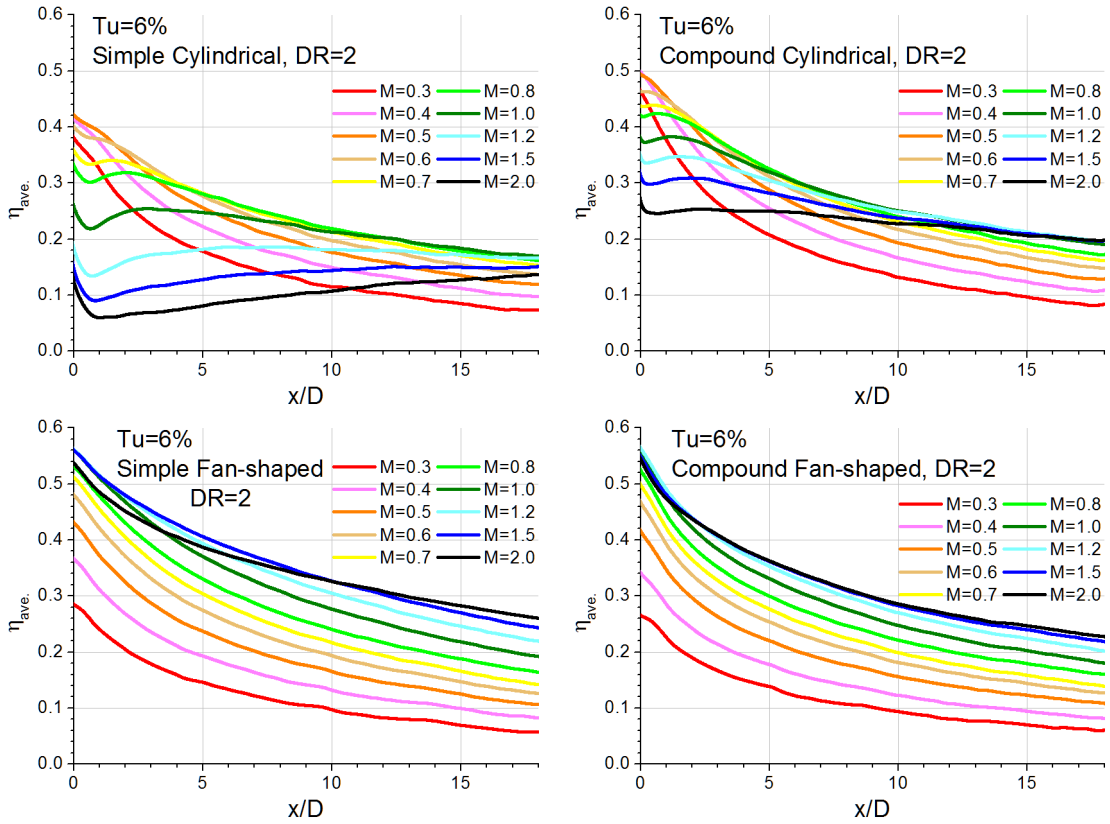

Fig. 21 The free stream turbulence effect. Laterally averaged effectiveness at Tu = 6%, DR = 2 for four different geometries.

Cross-comparison of the turbulence effect at M = 0.5, 1, and 2 at both density ratios 1 and 2 is shown in Fig. 22 and Fig. 23. In most cases, higher free stream turbulence reduces the effectiveness except for simple angled cylindrical and simple angled fan-shaped holes at higher blowing ratios.

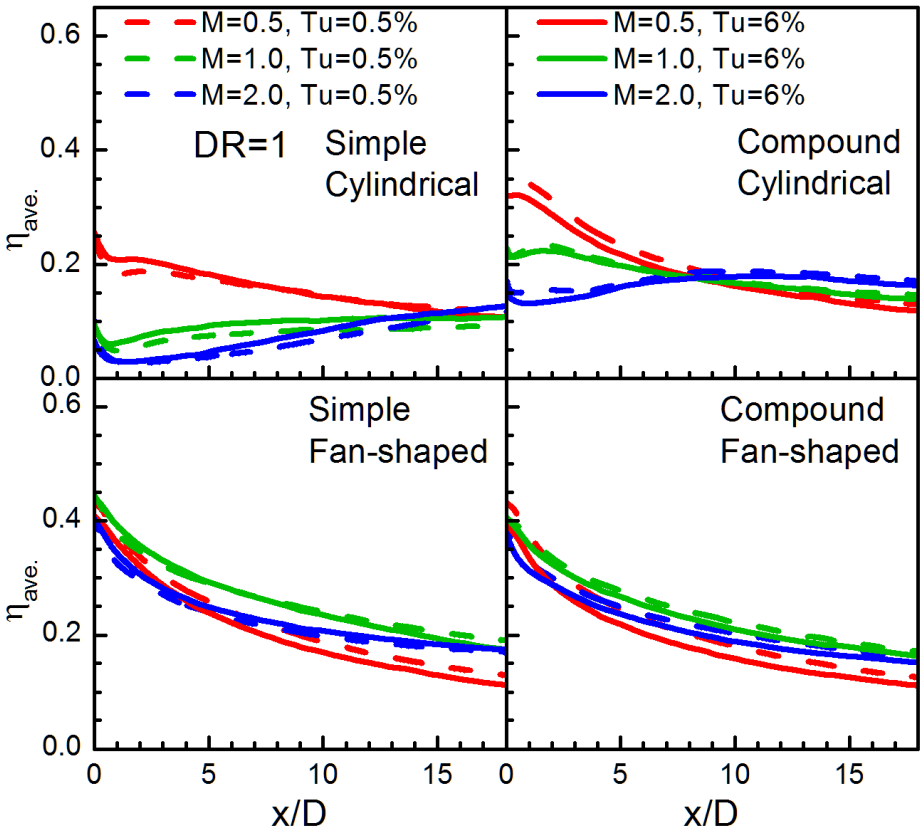

Fig. 22 Cross-comparison of the turbulence effect at M = 0.5, 1, and 2, DR = 1

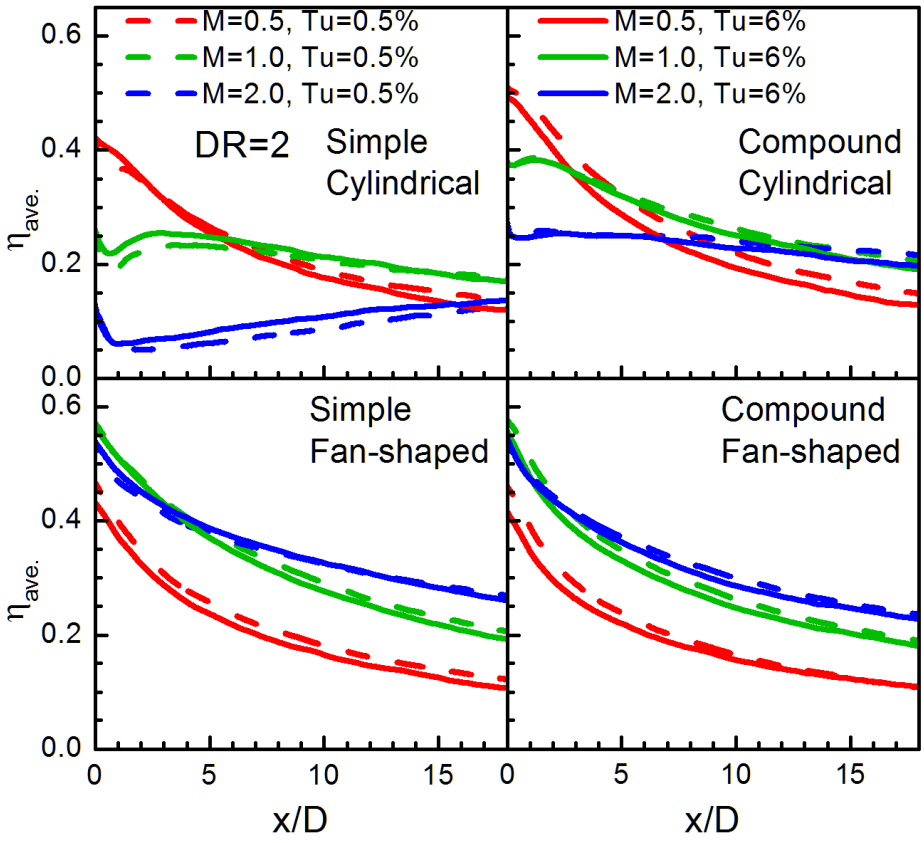

Fig. 23 Cross-comparison of the turbulence effect at M = 0.5, 1, and 2, DR = 2

Free stream turbulence effects on laterally averaged effectiveness for all different cases are summarized in Table 5.

Table 5 Summary of higher free stream turbulence effect (at Tu = 6%)

Effect to $\eta_{ave.}$ at Tu = 6%	DR = 1	DR = 2
Simple Cylindrical	Overall higher	Decreases at lower blowing ratios but increases at higher blowing ratios
Compound Cylindrical	Overall lower especially at lower blowing ratios	Overall lower especially at lower blowing ratios
Simple Fan-shaped	Decreases at lower blowing ratios but slightly increases at higher blowing ratios	Overall lower especially at lower blowing ratios
Compound Fan-shaped	Overall lower especially at lower blowing ratios	Overall lower especially at lower blowing ratios

In terms of the contour plots (Fig. A 13 to Fig. A 20), higher free stream turbulence intensity augments the mixing of coolant jets and the mainstream air, thereby ameliorate the lateral spreading of coolant jets. The contour of the coolant jet traces are shorter and wider than in the low turbulence intensity cases.

Results of Backward Injection

The test cases for backward injection in the current study is listed in Table 6.

Table 6 Test cases for backward injection

Mainstream and Coolant Temperature	T_m, T_c	297 K
Blowing Ratio (M)	$\rho_c V_c/\rho_m V_m$	0.3, 0.4, 0.5, 0.6, 0.7, 0.8, 1.0, 1.2, 1.5, 2.0
Density Ratio (DR)	ρ_c/ρ_m	1 (N_2), 1.5 (CO_2), and 2 (15% SF_6 + 85% Ar)
Free-stream Turbulence Intensity	T_u	0.5%

Effects of Geometry and Blowing Ratio

The film cooling effectiveness in most backward injection cases falls within $\eta_{ave.}$ = 0 ~ 0.4. The blowing ratio effect is not as influential as in the forward injection cases. The effectiveness only varies in a small range for all blowing ratios considered. Generally, the effectiveness increases with increasing blowing ratio up to some point, and then decreases due to coolant penetration into the main stream (as shown in Fig. 24). Compound angled cylindrical hole seems to have the highest effectiveness under backward injection condition, whereas simple angled fan-shaped hole has the lowest effectiveness. Coolant penetration effect can be seen in all four different configurations at higher blowing ratios. The coolant jets do not lift off from the surface under backward injection condition. Higher coolant momentum results in stronger penetration into the mainstream, thus enhances the mixing between coolant jets and the mainstream, resulting in a more uniform but thicker (less concentration of coolant) cooling film above the surface. The improved film coverage and uniformity because of the enhanced lateral and vertical spread and mixing can be seen in Fig. A 21 to Fig. A 32.

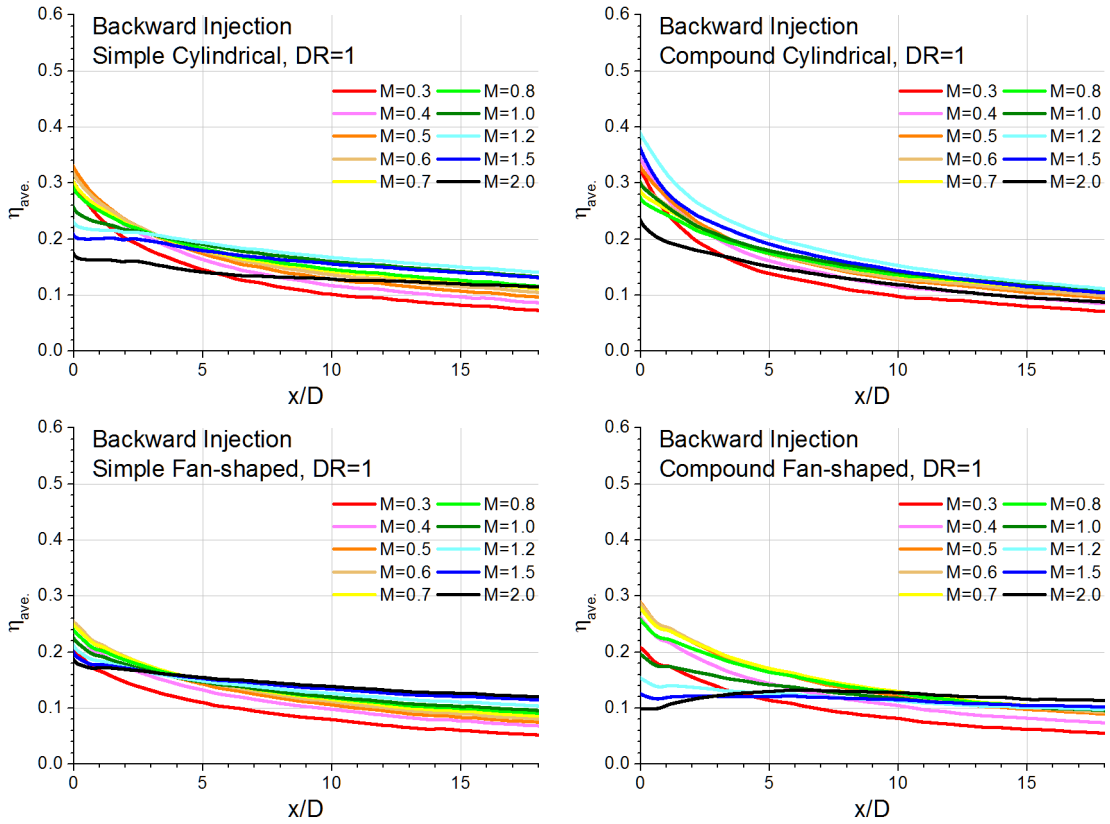

Fig. 24 Laterally averaged effectiveness with backward injection at DR = 1

Effects of Density Ratio

Detailed film cooling effectiveness at DR = 1.5 and 2 were plotted in Fig. 25 and Fig. 26. Density ratio also has a small influence to the effectiveness under backward injection condition. Although the influence to the effectiveness, whether positive or negative, is small, higher density ratios can postpone the occurrence of transition to higher blowing ratios.

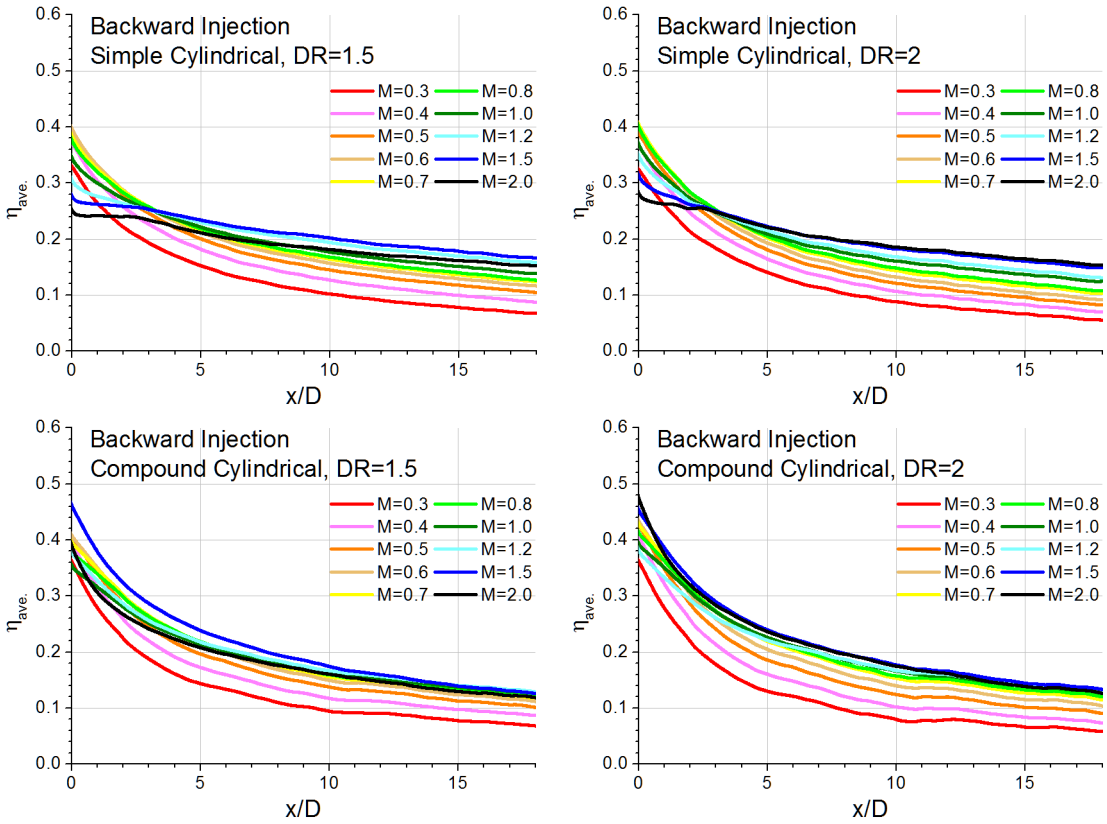

Fig. 25 Laterally averaged effectiveness with backward injection, simple angled cylindrical and compound angled cylindrical holes at DR = 1.5 and 2

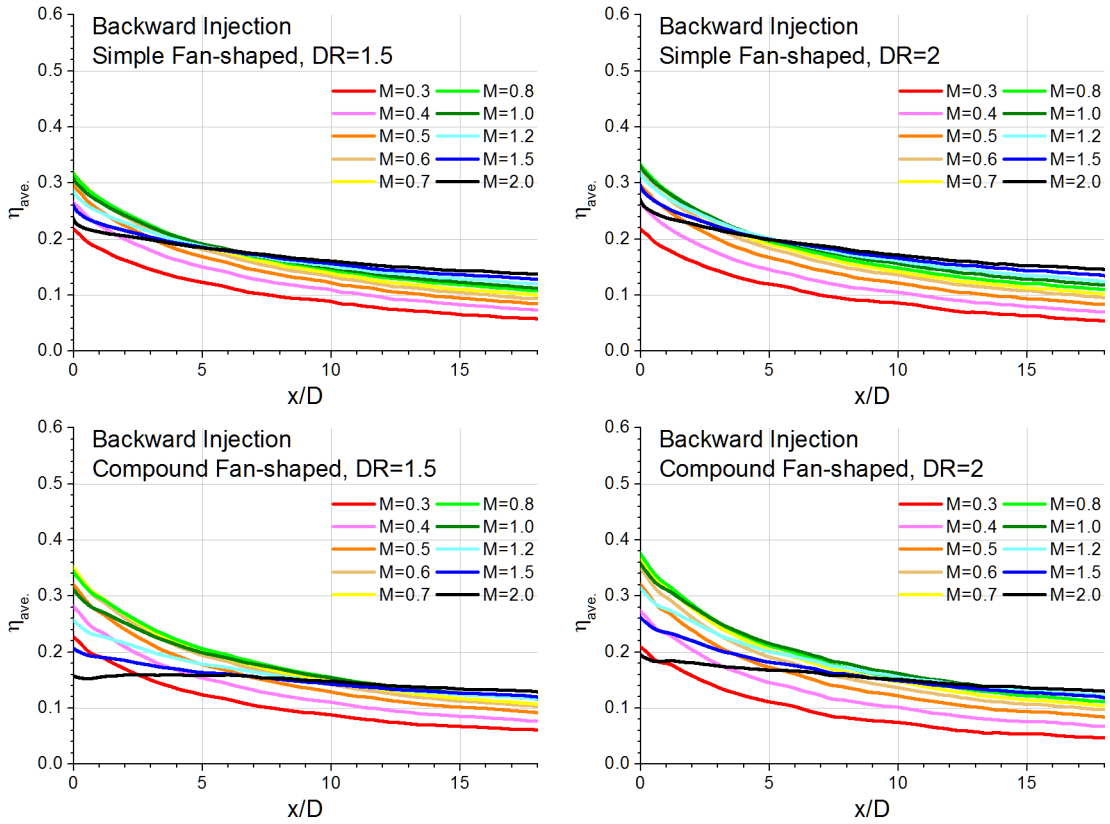

Fig. 26 Laterally averaged effectiveness with backward injection, simple angled fan-shaped and compound angled fan-shaped holes at DR = 1.5 and 2

Density ratio effect for backward injection is compared at M = 0.3, 1.0, 2.0 at density ratios DR = 1, 1.5 and 2 (Fig. 27). The density effect is not very strong in the backward injection cases. At lower blowing ratios, higher density ratio has no or negative effect to the effectiveness, whereas there is a small positive effect at higher blowing ratios.

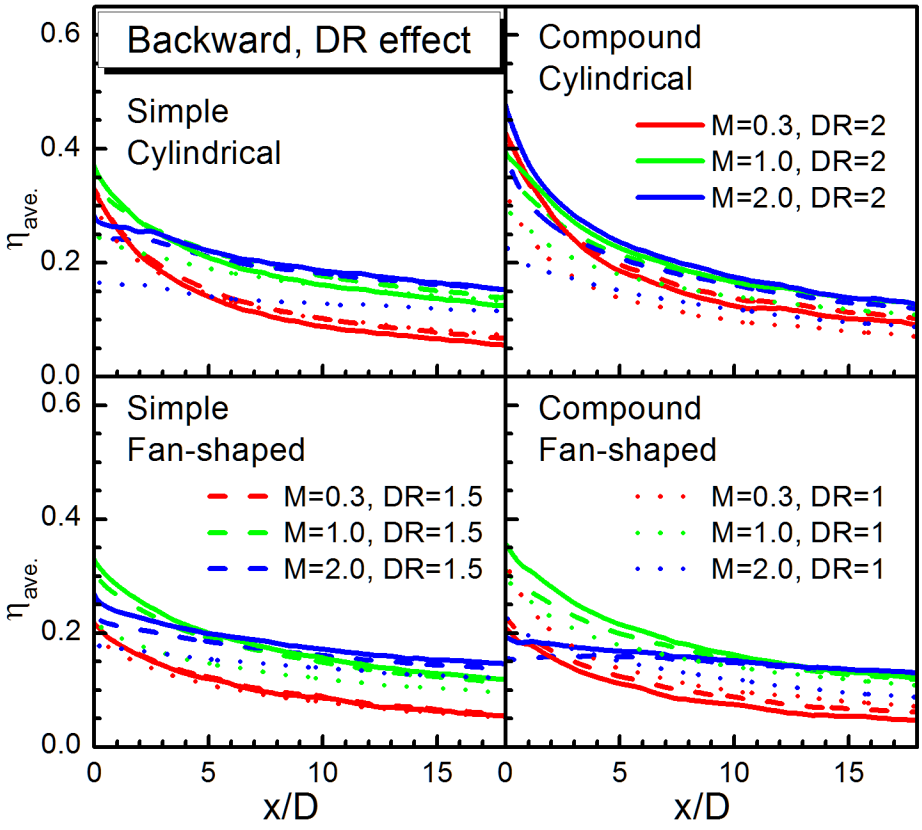

Fig. 27 Cross-comparison of the density ratio effect at M = 0.3, 1, 2, DR = 1, 1.5 and 2, backward injection

Backward Injection Comparison with Forward Injection

Experimental evidence demonstrates some improvements to the span-wise averaged effectiveness for cylindrical holes by using backward injection than forward injection (Fig. 16 and Fig. 24). For the simple angled cylindrical holes, backward injection reduces the effectiveness at lower blowing ratios, but has significant improvement at higher blowing ratios, particularly at near hole regions. For the compound angled cylindrical holes, effectiveness at near hole regions has been reduced

at lower blowing ratios. At higher blowing ratios, the effectiveness has been increased at only small x/D (near hole) regions. Similar results were obtained at higher density ratios (DR = 1.5 and DR = 2).

On the other hand, backward injection has no benefit for fan-shaped holes. The $\eta_{ave.}$ is greatly reduced at all blowing ratios for both simple angled and compound angled fan-shaped holes. This may be caused by the strong mixing of coolant jets and mainstream air at the expanded hole exits.

For all cases, backward injection has a more uniform film coverage, although the averaged effectiveness may be lower (See Appendix for detail).

Comparison between four geometries with forward and backward injection was made at blowing ratio 1 and 2, density ratio 1 and 2 as shown in Fig. 28. In all conditions considered in this figure, both simple angled and compound angled fan-shaped holes with forward injection give the highest effectiveness. Hence, backward injection for fan-shaped holes is detrimental.

For simple angled cylindrical hole, the effectiveness with backward injection at M = 1, DR = 2 and M = 2, DR = 1, 2 is higher than the forward injection cases at all x/D considered. For M = 1 and DR = 2, improvement can be seen at near hole region (x/D < 4).

For compound angled cylindrical hole, different levels of improvement can be seen at near hole region. The improvement is most evident at high blowing ratio and high density ratio condition (M = 2, DR = 2).

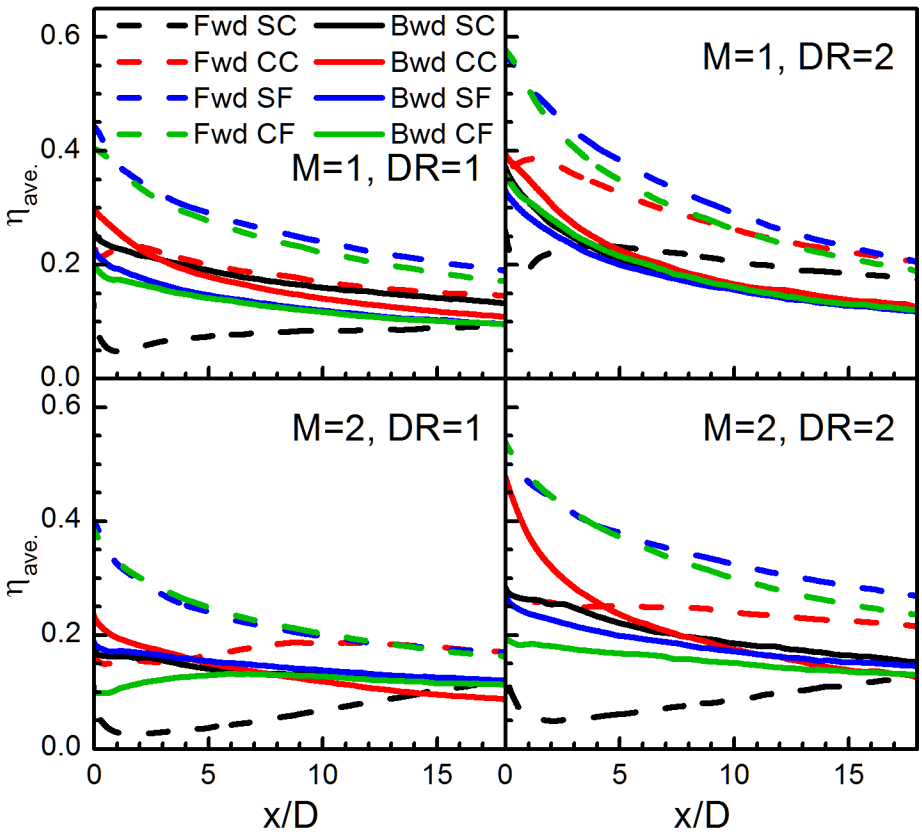

Fig. 28 Cross-comparison between different geometries with forward and backward injection at M = 1, 2, and DR = 1, 2. (Abbreviations: SC- Simple Cylidrical; CC- Compound Cylindrical; SF- Simple Fan-shaped; CF- Compound Fan-shaped)

Backward Injection Comparison with Numerical Results

Comparison was also made between numerical results [21] and experimental results with backward injection using simple angled cylindrical holes. As shown in Fig. 29, experimental results show lower effectiveness than the numerical results. Numerical and experimental results demonstrate similar trend at blowing ratios ~ 0.7 and 1.5, and density ratio ~ 1.5. It is important to note that the numerical simulation only considered a

single film hole while there were seven holes under the experimental condition. Which means there is no hole to hole interaction in the simulation. The lack of hole to hole interaction may be accounted for the difference in the comparison.

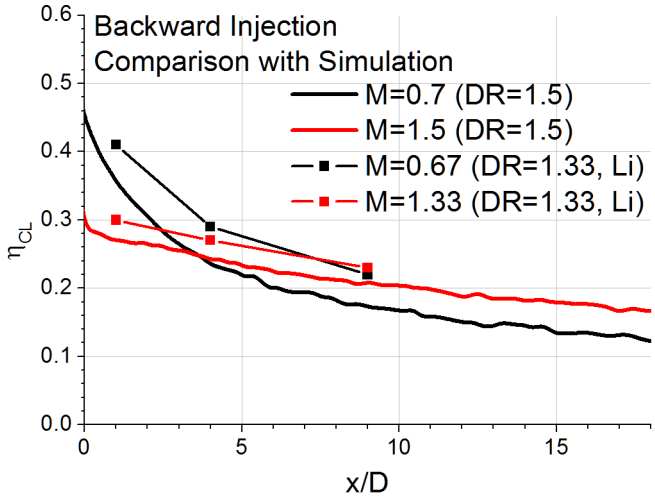

Fig. 29 Backward injection centerline effectiveness comparison between numerical and experimental results

The numerical simulation predicts a stronger flow in the lateral direction or z-direction (perpendicular to the flat surface). And there is also a reverse flow region immediate downstream of the cooling holes, where the velocity components are opposite to the mainstream flow direction. This is also witnessed in the experimental investigation as shown in Fig. 30.

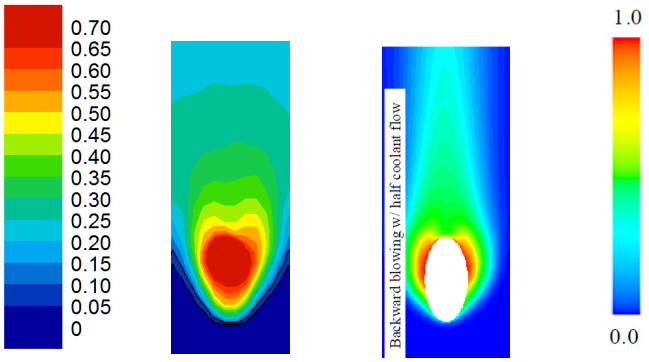

Fig. 30 Contour plot of backward injection. Left: experimental data at M = 0.7 and DR = 1.5. Right: numerical simulation at M = 0.67 and DR = 1.33

Although both data show the reverse flow pattern at the trailing edge of the cooling hole, the film cooling effectiveness distributions downstream of the hole are quite different. Experimental result shows an expanding pattern while the numerical simulation shows a narrowing or converging pattern. Again, this difference may arise from the lack of hole to hole interactions.

Comparison with Empirical Correlation

Fig. 31 shows the comparison between experimental data using simple angled fan-shaped holes at DR = 2 and the empirical correlation developed by Colban *et al.* [23]. The physics-based correlation equation is shown in Eq. (10), where P is the pitch between holes, t is the width of the hole at trailing edge, ξ is the film cooling scaling parameter defined in Eq. (11), and C_1 to C_3 are coefficients for the correlation. The correlation coefficients in the final form are determined as $C_1 = 0.1721$, $C_2 = -0.2664$ and $C_3 = 0.8749$.

$$\eta_{ave.} = \frac{1}{P/t + C_1 M^{C_2} \xi^{C_3}} \tag{10}$$

The film cooling scaling parameter ξ can be expressed by non-dimensional parameters as shown in Eq. (11):

$$\xi = \frac{4}{\pi} \frac{\frac{x}{D}\frac{P}{D}}{M \cdot AR} \tag{11}$$

and the area ratio AR is defined by Eq. (12):

$$AR = \frac{A_{exit}}{A_{in}} \tag{12}$$

where A_{exit} is the cross-sectional area at the hole exit and A_{in} is the cross-sectional area of the hole at the inlet.

The result shows that the correlation offers a convenient and express way to predict the averaged effectiveness of simple angled fan-shaped holes at various blowing ratios with adequate accuracy. However, this correlation gives the same effectiveness value at x/D = 0 for all different blowing ratios (in this case, the P/t = 2, and the effectiveness at x/D = 0 is 0.5 for all blowing ratios), therefore, in some cases, it has poor prediction capability at near hole regions.

In general, the overall prediction is good in terms of the current experimental data. Further modification of the correlation equation may be needed to take into account of the deviation at the near hole regions.

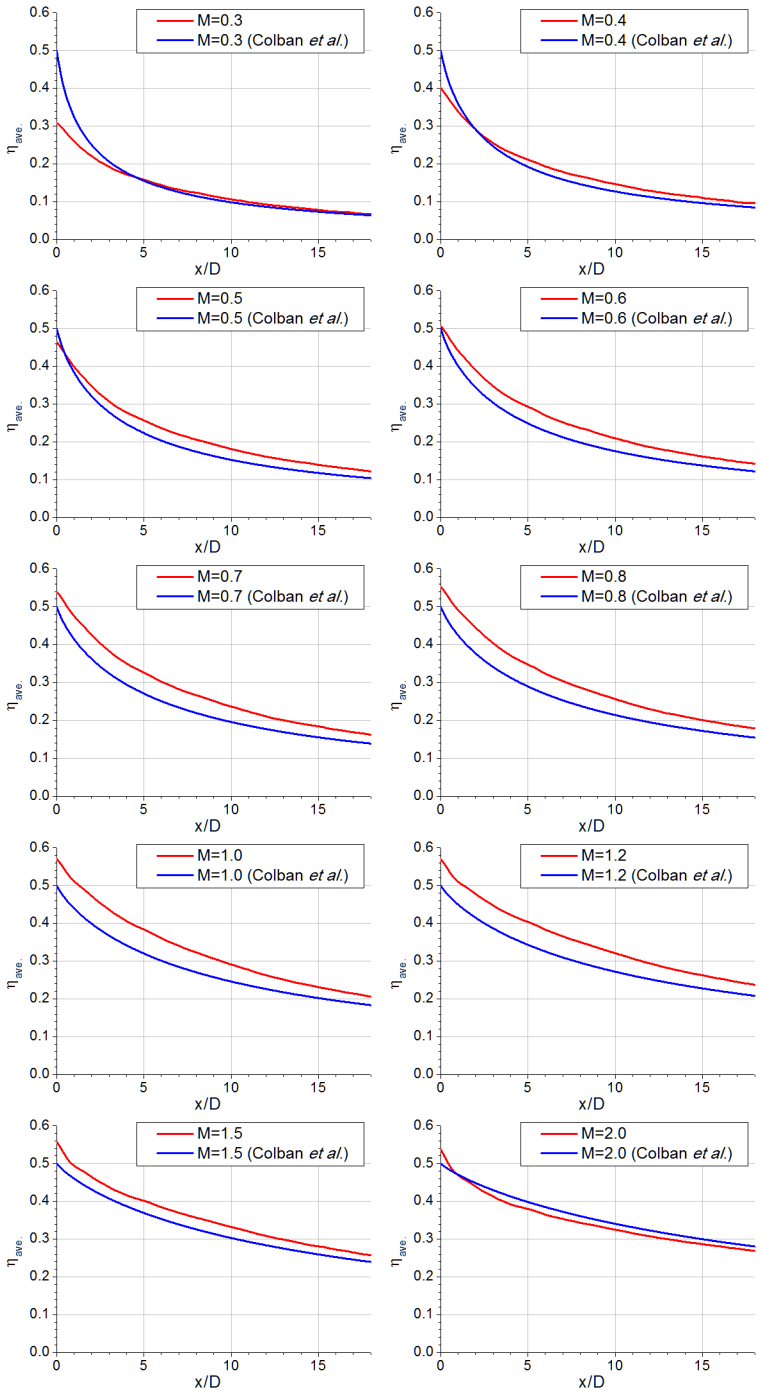

Fig. 31 Comparison of experimental data using simple angled fan-shaped holes with empirical correlation developed by Colban *et al.* at DR = 2.0

Uncertainty Analysis

The uncertainty analysis follows the Kline and McClintock approach [27]. Based on Eq. (8), the uncertainty in the derived effectiveness is affected by the pressure ratios $P_{O2,fg}/P_{O2,ref}$ and $P_{O2,air}/P_{O2,ref}$. These two values are derived directly from the calibration curve Eq. (3). When performing the calibration, there are some factors that may contribute to the uncertainty of the calibration curve. These factors include the uncertainty in pressure measurement (± 0.1 inHg), the potential bias error of the pressure transducer (± 0.1 inHg), the stability of imaging system, or some other minor effects such as small variation of temperature or the LED illumination intensity/uniformity. When conducting the experiment, the variation in the mainstream flow velocity (± 2%) and coolant flow rate (± 1 SCFH) may also contribute to the uncertainty of the result.

Generally, the uncertainty of the intensity acquired by the CCD camera is lower at higher effectiveness, where the emission intensity of the paint is higher. On the contrary, when the emission intensity of the paint decreases, the uncertainty increases. When the effectiveness is 0.3, the estimated uncertainty in pressure measurement is about 1%, and the uncertainty in the acquired intensity ratio is about 1% (estimated from multiple data taken under specific condition). These uncertainties gives the $P_{O2,fg}/P_{O2,ref}$ in Eq. (8) an uncertainty level of 3.3 %. And the overall uncertainty in effectiveness is around 8% ($\eta = 0.3 \pm 0.024$).

CHAPTER V

CONCLUSIONS

Comprehensive tests were performed on a flat plate characterizing the effects over a wide range of different parameters: blowing ratio (M = 0.3 – M = 2.0), density ratio (DR = 1, 1.5 and 2), free stream turbulence (Tu = 0.5% and 6%), and backward injection. Results were obtained using the steady state pressure sensitive paint (PSP) technique.

Forward Injection

- Shaped holes with expanded hole area have higher effectiveness than the cylindrical holes. Compound angled cylindrical holes have higher effectiveness than simple angled cylindrical holes.
- For cylindrical holes, coolant lift off reduces the effectiveness. For fan-shaped holes at high blowing ratios, coolant partial lift off also reduces the effectiveness.
- Higher coolant to mainstream density ratio increases the effectiveness for cylindrical holes, particularly at smaller x/D region.
- For fan-shaped holes, higher coolant to mainstream density ratio reduces the effectiveness at low blowing ratios, but increases the effectiveness at higher blowing ratios.
- Higher density ratio postpones the occurrence of coolant lift off.

- Higher free stream turbulence intensity enhances the mixing of coolant and mainstream air, resulting in lower effectiveness. Nevertheless, in some cases that the coolant lift off tends to occur, the effectiveness may be higher.

Backward Injection

- The film cooling effectiveness for most cases falls within $\eta_{ave.} = 0 \sim 0.4$. Compound angled cylindrical holes give the highest effectiveness in backward injection whereas simple angled fan-shaped holes give the lowest effectiveness.
- The blowing ratio effect and density ratio effect are not as influential as in the forward injection, but has similar effect to the effectiveness. Effectiveness increases with increasing blowing ratio up to some point, and then decreases due to stronger penetration and mixing with the mainstream. Higher density ratio generally results in higher effectiveness.
- Film coverage and uniformity was improved due to lateral spread and mixing.
- Compared to forward injection, substantial improvement in effectiveness can be seen in simple angled cylindrical holes. For compound angled cylindrical holes, higher effectiveness was obtained at near hole region ($x/D < 5$).
- For fan-shaped holes, backward injection is not beneficial in terms of effectiveness.

REFERENCES

[1] Goldstein, R. J., 1971, "Film Cooling," Advances in Heat Transfer, Vol. 7, Irvine, T. F., Jr and Hartnett, J. P., eds., Academic Press, New York, pp. 321-379.

[2] Bunker, R. S., 2005, "A Review of Shaped Hole Turbine Film-Cooling Technology," Journal of Heat Transfer-Transactions of the Asme, 127, pp. 441-453.

[3] Bogard, D. G., and Thole, K. A., 2006, "Gas Turbine Film Cooling," Journal of Propulsion and Power, 22, pp. 249-270.

[4] Han, J.-C., Dutta, S., and Ekkad, S., 2013, *Gas Turbine Heat Transfer and Cooling Technology*, CRC Press, Taylor & Francis Group, Florida.

[5] Goldstein, R. J., Eckert, E. R. G., and Burggraf, F., 1974, "Effects of Hole Geometry and Density on 3-Dimensional Film Cooling," International Journal of Heat and Mass Transfer, 17, pp. 595-607.

[6] Pedersen, D. R., Eckert, E. R. G., and Goldstein, R. J., 1977, "Film Cooling with Large Density Differences between Mainstream and Secondary Fluid Measured by Heat-Mass Transfer Analogy," Journal of Heat Transfer-Transactions of the Asme, 99, pp. 620-627.

[7] Sinha, A. K., Bogard, D. G., and Crawford, M. E., 1991, "Film-Cooling Effectiveness Downstream of a Single Row of Holes with Variable Density Ratio," Journal of Turbomachinery, 113, pp. 442-449.

[8] Rallabandi, A. P., Grizzle, J., and Han, J.-C., 2011, "Effect of Upstream Step on Flat Plate Film-Cooling Effectiveness Using Psp," Journal of Turbomachinery, 133, pp. 041024.

[9] Ligrani, P. M., Wigle, J. M., and Jackson, S. W., 1994, "Film-Cooling from Holes with Compound Angle Orientations .2. Results Downstream of a Single Row of Holes with 6d Spanwise Spacing," Journal of Heat Transfer-Transactions of the Asme, 116, pp. 353-362.

[10] Ekkad, S. V., Zapata, D., and Han, J. C., 1997, "Film Effectiveness over a Flat Surface with Air and Co2 Injection through Compound Angle Holes Using a Transient Liquid Crystal Image Method," Journal of Turbomachinery-Transactions of the Asme, 119, pp. 587-593.

[11] Schmidt, D. L., Sen, B., and Bogard, D. G., 1996, "Film Cooling with Compound Angle Holes: Adiabatic Effectiveness," Journal of Turbomachinery-Transactions of the Asme, 118, pp. 807-813.

[12] Gritsch, M., Schulz, A., and Wittig, S., 1998, "Adiabatic Wall Effectiveness Measurements of Film-Cooling Holes with Expanded Exits," Journal of Turbomachinery-Transactions of the Asme, 120, pp. 549-556.

[13] Wright, L. M., Mcclain, S. T., and Clemenson, M. D., 2011, "Effect of Density Ratio on Flat Plate Film Cooling with Shaped Holes Using Psp," Journal of Turbomachinery-Transactions of the Asme, 133, pp. 041011.

[14] Pietrzyk, J. R., Bogard, D. G., and Crawford, M. E., 1990, "Effects of Density Ratio on the Hydrodynamics of Film Cooling," Journal of Turbomachinery, 112, pp. 437-443.

[15] Narzary, D. P., Liu, K.-C., Rallabandi, A. P., and Han, J.-C., 2012, "Influence of Coolant Density on Turbine Blade Film-Cooling Using Pressure Sensitive Paint Technique," Journal of Turbomachinery, 134, pp. 031006.

[16] Saumweber, C., Schulz, A., and Wittig, S., 2003, "Free-Stream Turbulence Effects on Film Cooling with Shaped Holes," Journal of Turbomachinery-Transactions of the Asme, 125, pp. 65-73.

[17] Young, C. D., Han, J. C., Huang, Y., and Rivir, R. B., 1992, "Influence of Jet-Grid Turbulence on Flat-Plate Turbulent Boundary-Layer Flow and Heat-Transfer," Journal of Heat Transfer-Transactions of the Asme, 114, pp. 65-72.

[18] Kadotani, K., and Goldstein, R. J., 1979, "Nature of Jets Entering a Turbulent-Flow .B. Film Cooling Performance," Journal of Engineering for Power-Transactions of the Asme, 101, pp. 466-470.

[19] Bons, J. P., Macarthur, C. D., and Rivir, R. B., 1996, "The Effect of High Free-Stream Turbulence on Film Cooling Effectiveness," Journal of Turbomachinery-Transactions of the Asme, 118, pp. 814-825.

[20] Wright, L. M., Gao, Z. H., Varvel, T. A., and Han, J. C., 2005, "Assessment of Steady State Psp, Tsp, and Ir Measurement Techniques for Flat Plate Film Cooling," HT2005: Proceedings of the ASME Summer Heat Transfer Conference 2005, Vol 3, pp. 37-46.

[21] Li, X. C., 2010, "Numerical Simulation on Fluid Flow and Heat Transfer of Film Cooling with Backward Injection," Proceedings of the Asme International Heat Transfer Conference - 2010, Vol 5, pp. 257-265.

[22] Baldauf, S., Scheurlen, M., Schulz, A., and Wittig, S., 2002, "Correlation of Film-Cooling Effectiveness from Thermographic Measurements at Enginelike Conditions," Journal of Turbomachinery-Transactions of the Asme, 124, pp. 686-698.

[23] Colban, W. F., Thole, K. A., and Bogard, D., 2010, "A Film-Cooling Correlation for Shaped Holes on a Flat-Plate Surface," Journal of Turbomachinery-Transactions of the Asme, 133, pp. 011002.

[24] Zhang, L. J., and Jaiswal, R. S., 2001, "Turbine Nozzle Endwall Film Cooling Study Using Pressure-Sensitive Paint," Journal of Turbomachinery-Transactions of the Asme, 123, pp. 730-738.

[25] Gao, Z. H., Wright, L. M., and Han, J. C., 2005, "Assessment of Steady State Psp and Transient Ir Measurement Techniques for Leading Edge Film Cooling," Proceedings of the ASME Heat Transfer Division 2005, Vol 1, 376-1, pp. 467-475.

[26] Han, J.-C., and Rallabandi, A., 2010, "Turbine Blade Film Cooling Using Psp Technique," Frontiers in Heat and Mass Transfer (FHMT), 1, pp. 013001.

[27] Kline, S. J., and Mcclintock, F. A., 1953, "Describing Uncertainties in a Single Sample Experiment," Mechanical Engineering (Am. Soc. Mech. Eng.), 75, pp. 3-8.

APPENDIX

All span-wise averaged effectiveness plots and corresponding contour plots for all different test cases are presented in the following pages. The sequence will follow the below table.

Case	**Figure Number**
Simple angled cylindrical holes	Fig. A 1 - Fig. A 3
Compound angled cylindrical holes	Fig. A 4 - Fig. A 6
Simple angled fan-shaped holes	Fig. A 7 - Fig. A 9
Compound angled fan-shaped holes	Fig. A 10 - Fig. A 12
Higher Turbulence Simple angled cylindrical holes	Fig. A 13 - Fig. A 14
Higher Turbulence Compound angled cylindrical holes	Fig. A 15 - Fig. A 16
Higher Turbulence Simple angled fan-shaped holes	Fig. A 17 - Fig. A 18
Higher Turbulence Compound angled fan-shaped holes	Fig. A 19 - Fig. A 20
Backward Injection Simple angled cylindrical holes	Fig. A 21 - Fig. A 23
Backward Injection Compound angled cylindrical holes	Fig. A 24 - Fig. A 26
Backward Injection Simple angled fan-shaped holes	Fig. A 27 - Fig. A 29
Backward Injection Compound angled fan-shaped holes	Fig. A 30 - Fig. A 32

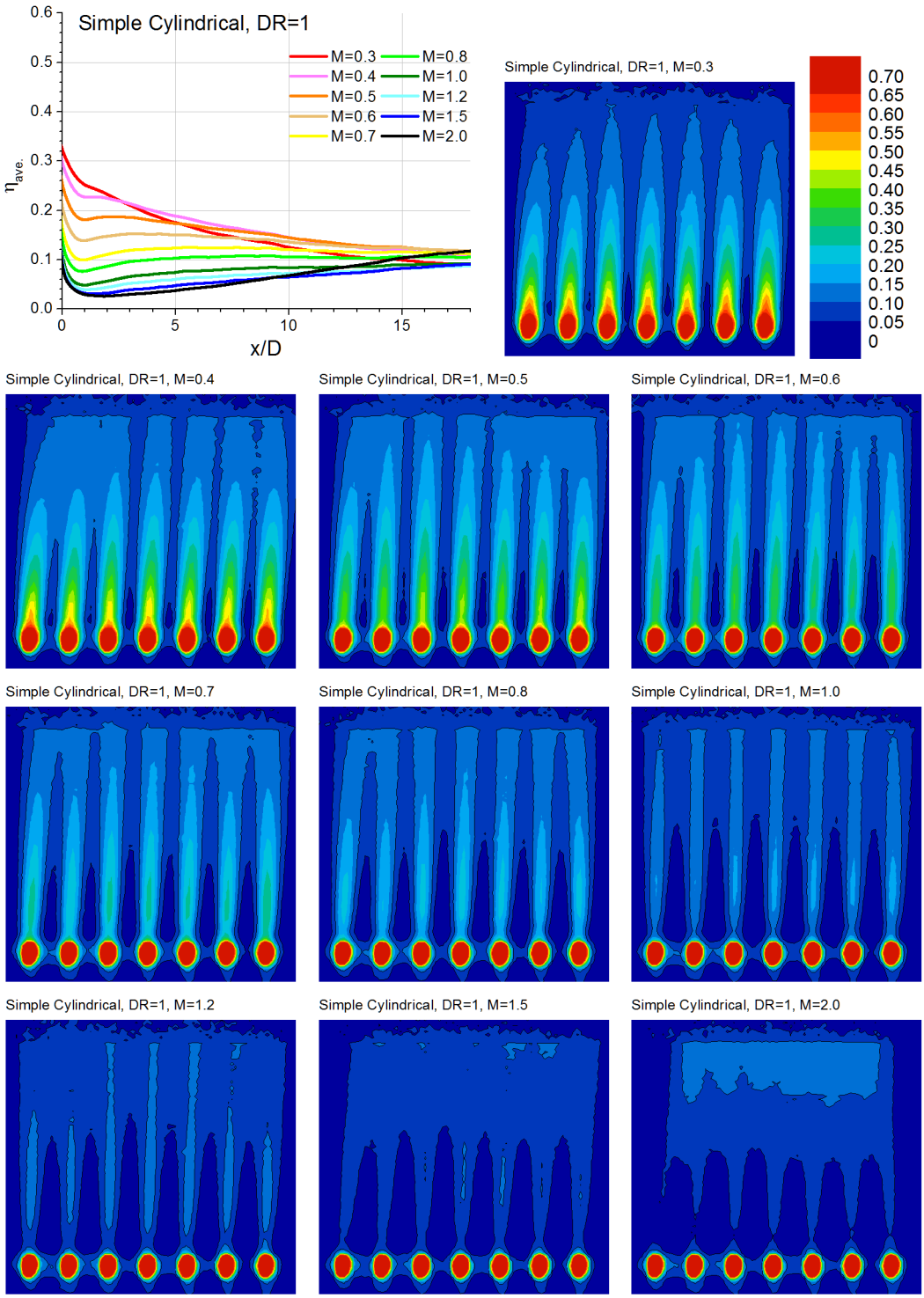

Fig. A 1 Laterally averaged effectiveness and contour plots for simple angled cylindrical holes at DR = 1

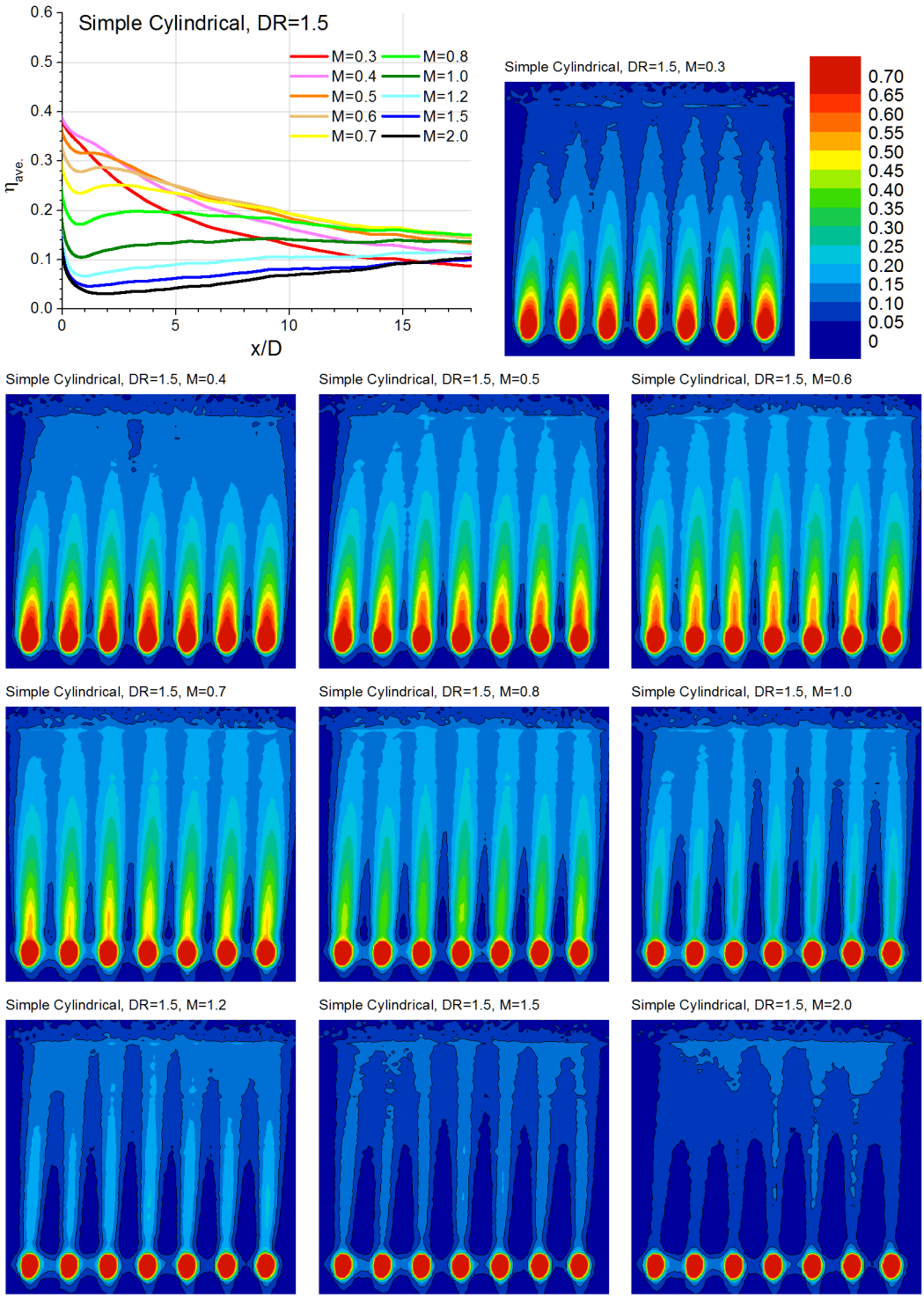

Fig. A 2 Laterally averaged effectiveness and contour plots for simple angled cylindrical holes at DR = 1.5

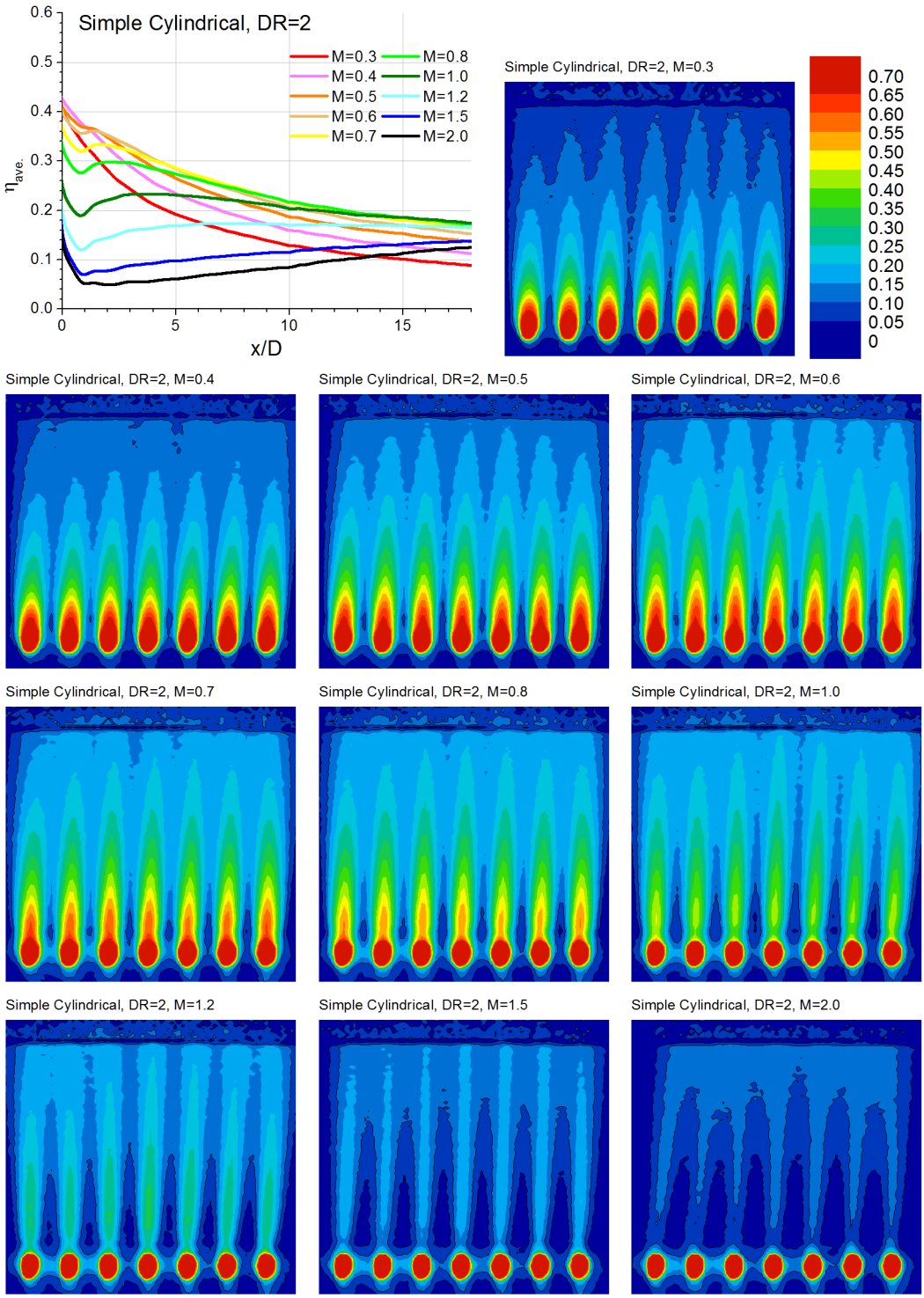

Fig. A 3 Laterally averaged effectiveness and contour plots for simple angled cylindrical holes at DR = 2

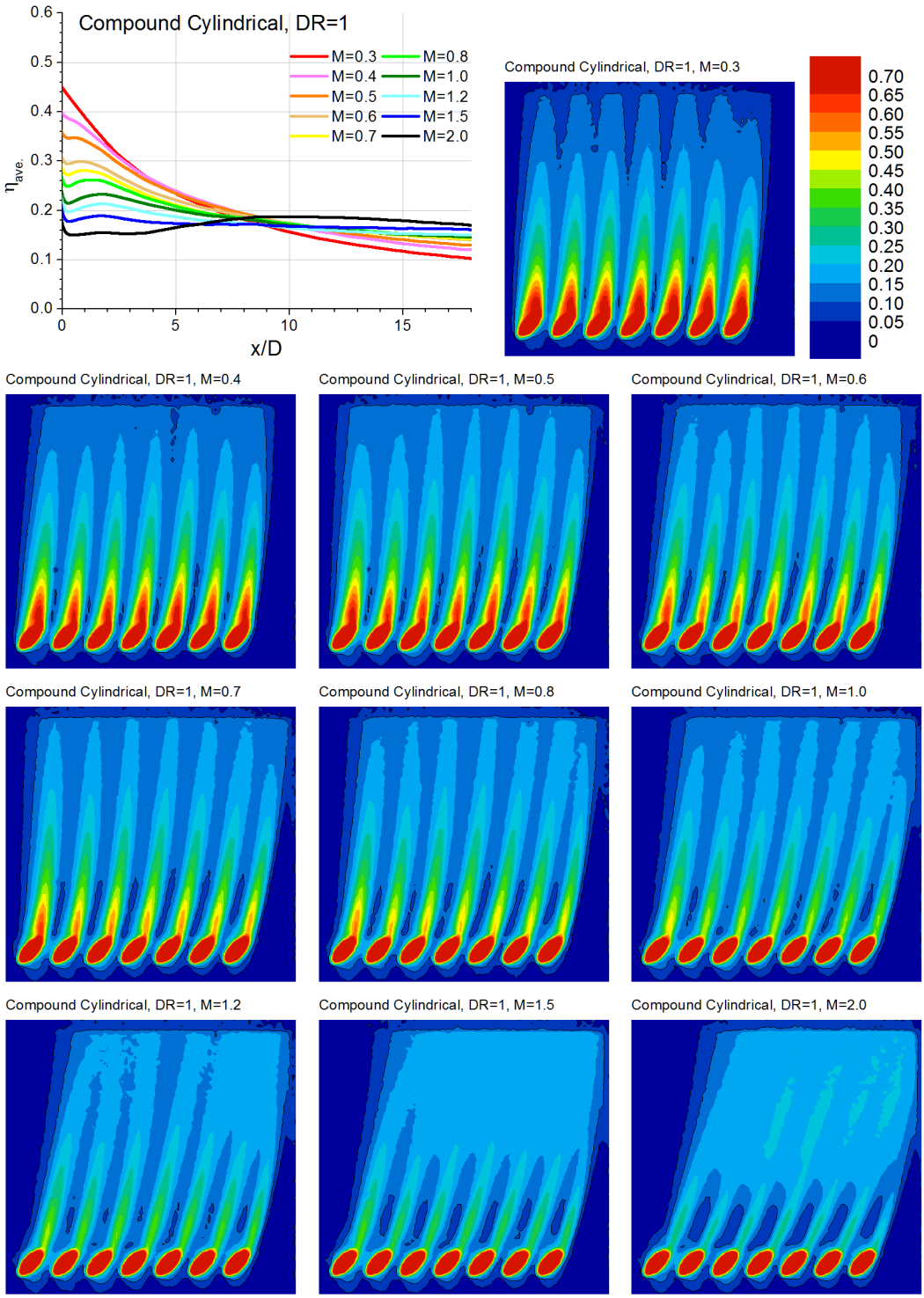

Fig. A 4 Laterally averaged effectiveness and contour plots for compound angled cylindrical holes at DR = 1

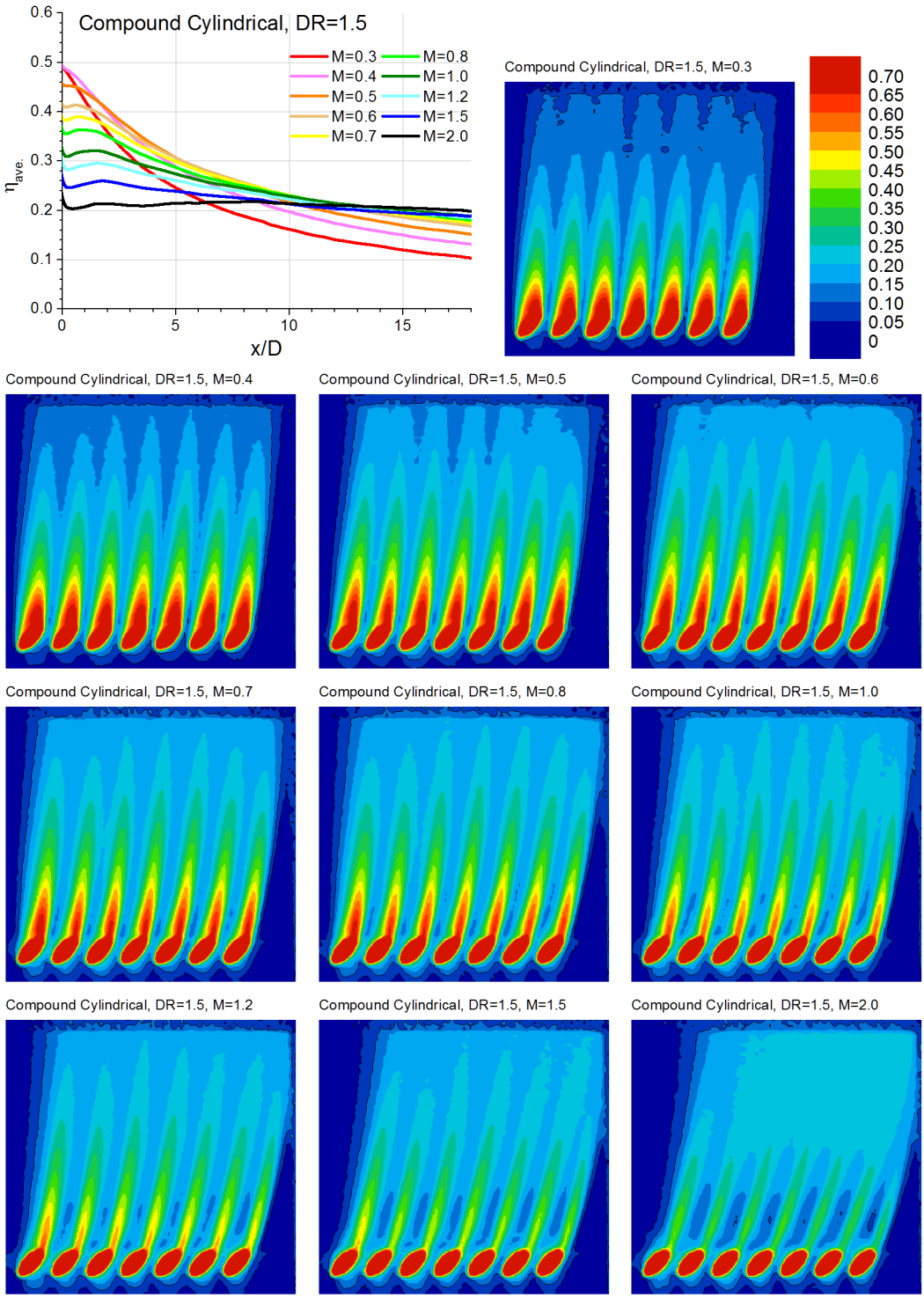

Fig. A 5 Laterally averaged effectiveness and contour plots for compound angled cylindrical holes at DR = 1.5

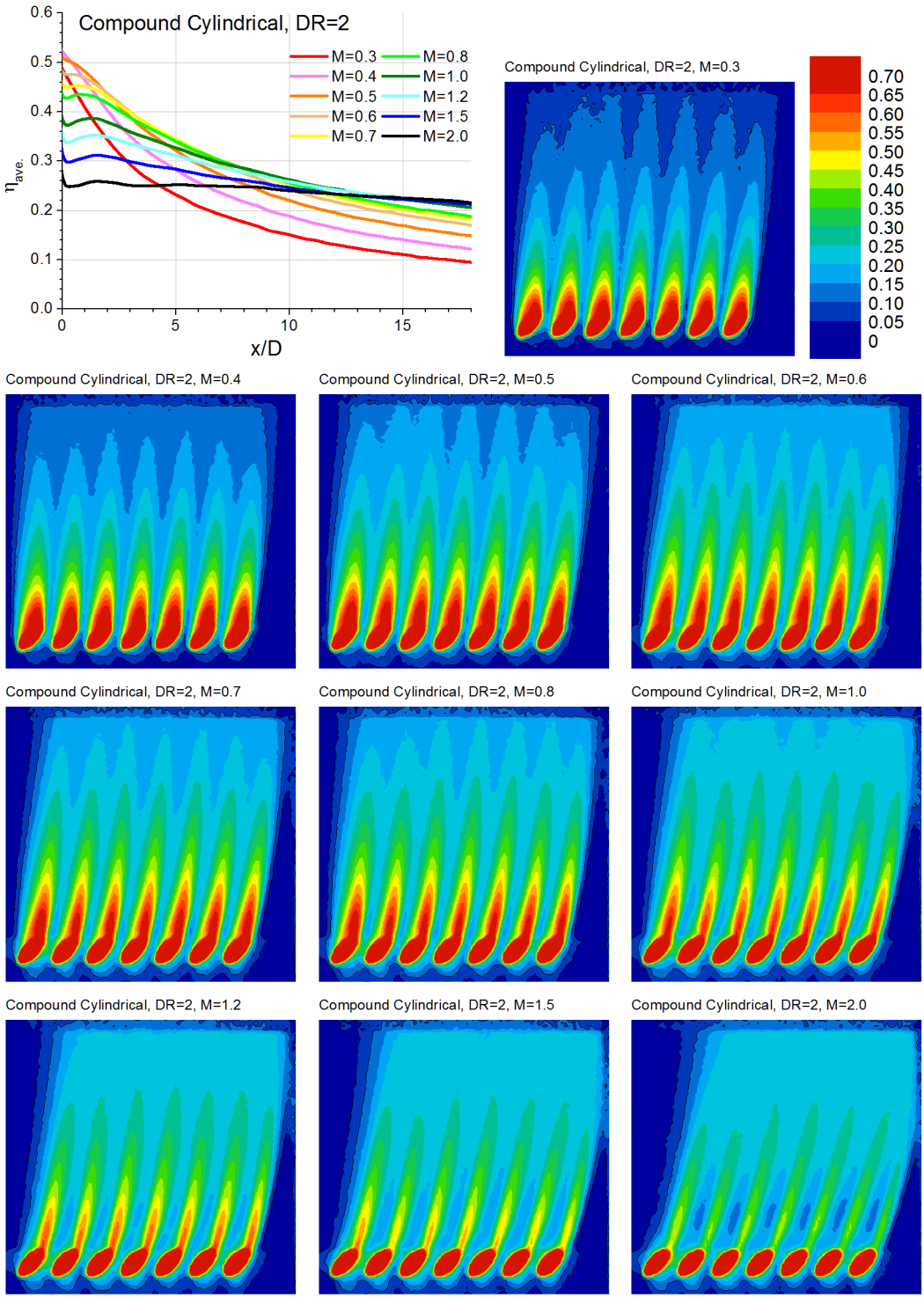

Fig. A 6 Laterally averaged effectiveness and contour plots for compound angled cylindrical holes at DR = 2

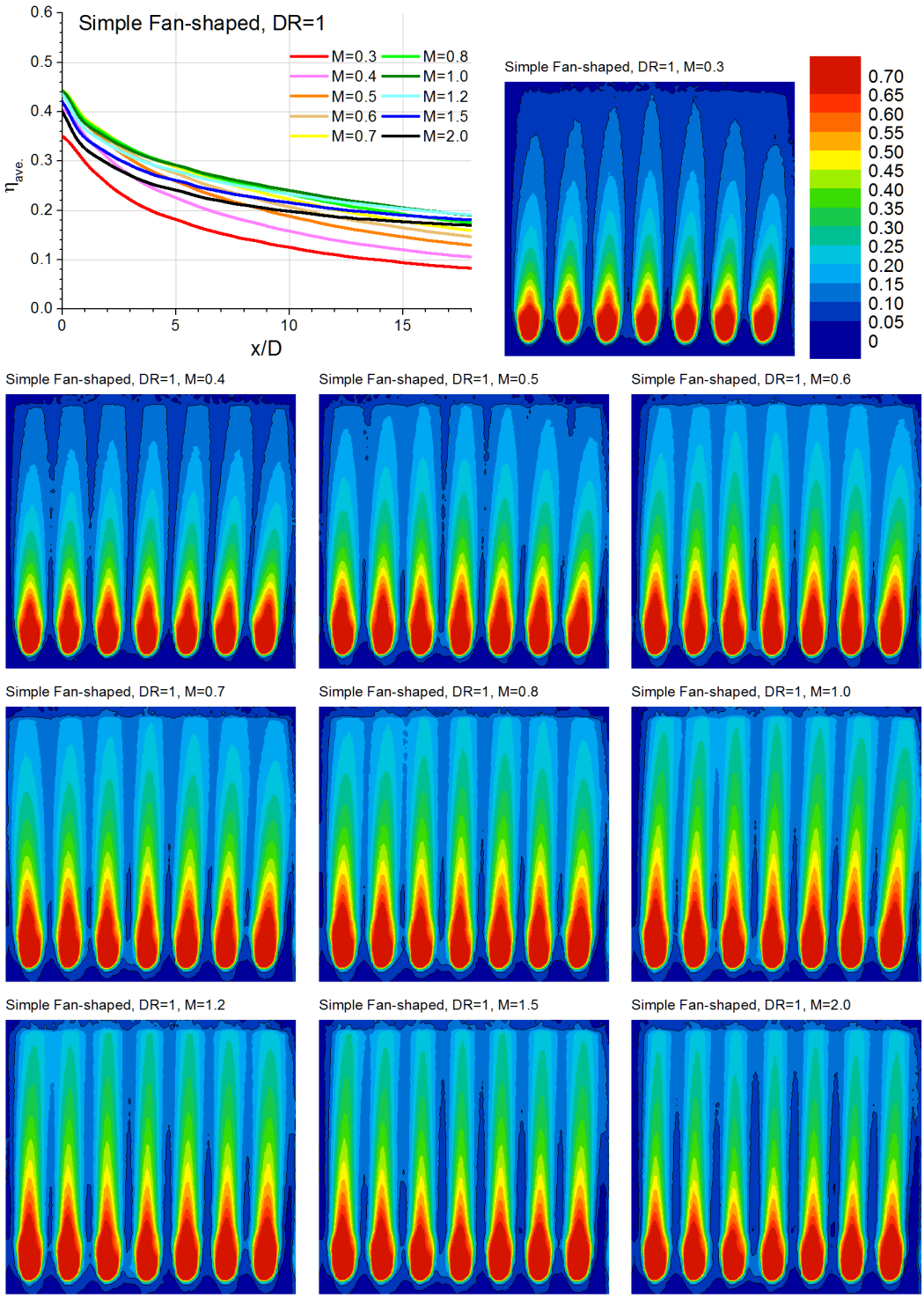

Fig. A 7 Laterally averaged effectiveness and contour plots for simple angled fan-shaped holes at DR = 1

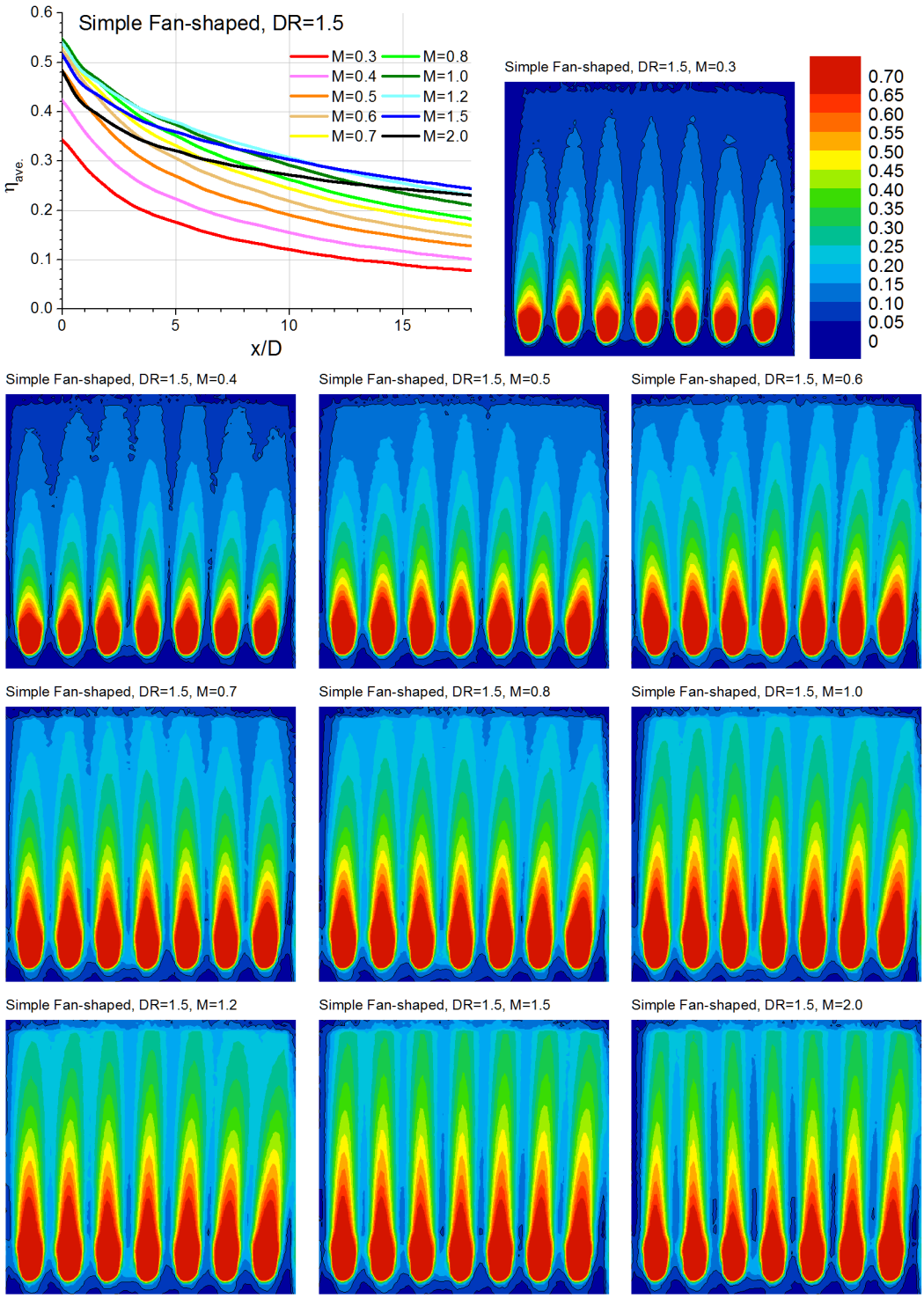

Fig. A 8 Laterally averaged effectiveness and contour plots for simple angled fan-shaped holes at DR = 1.5

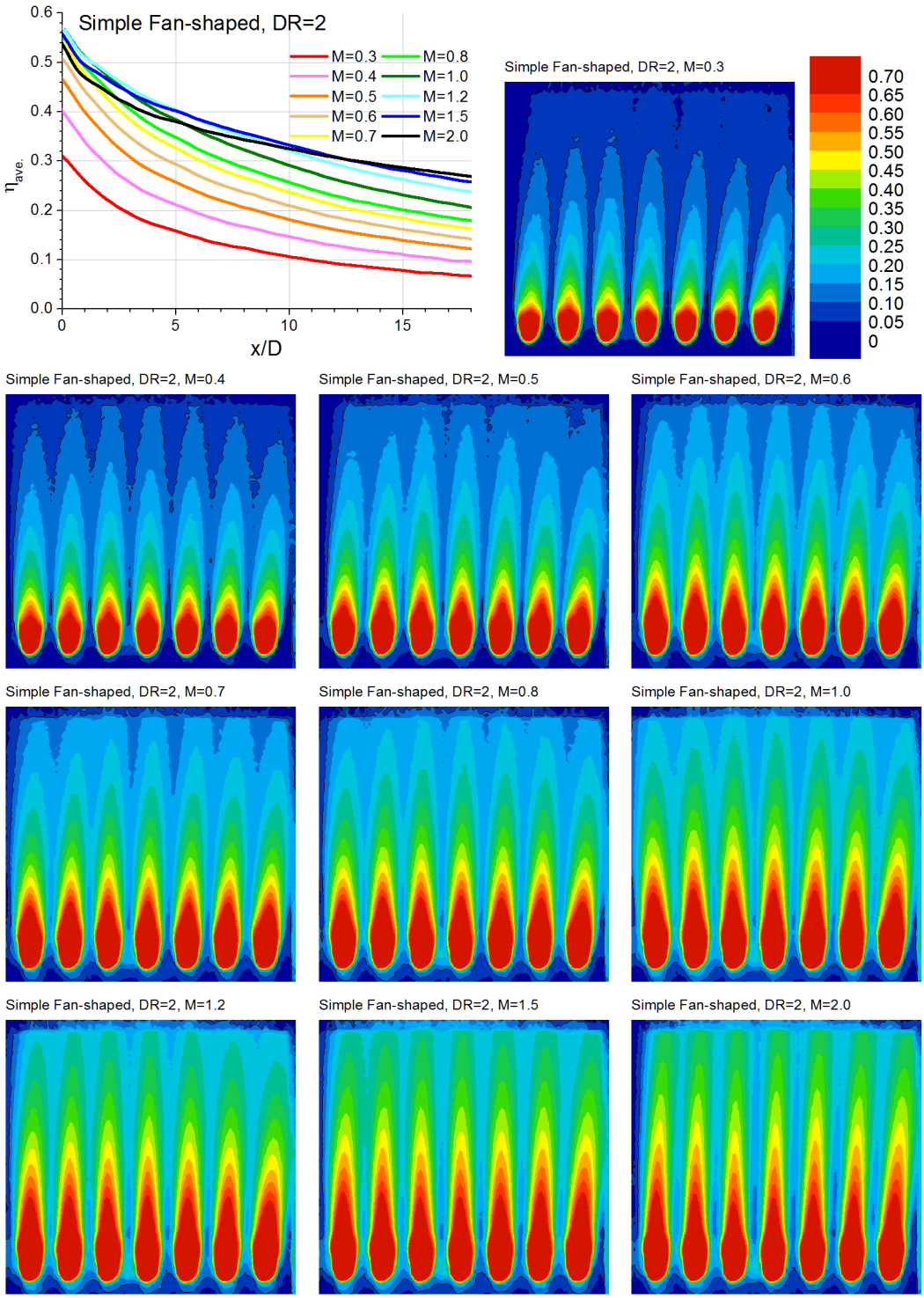

Fig. A 9 Laterally averaged effectiveness and contour plots for simple angled fan-shaped holes at DR = 2

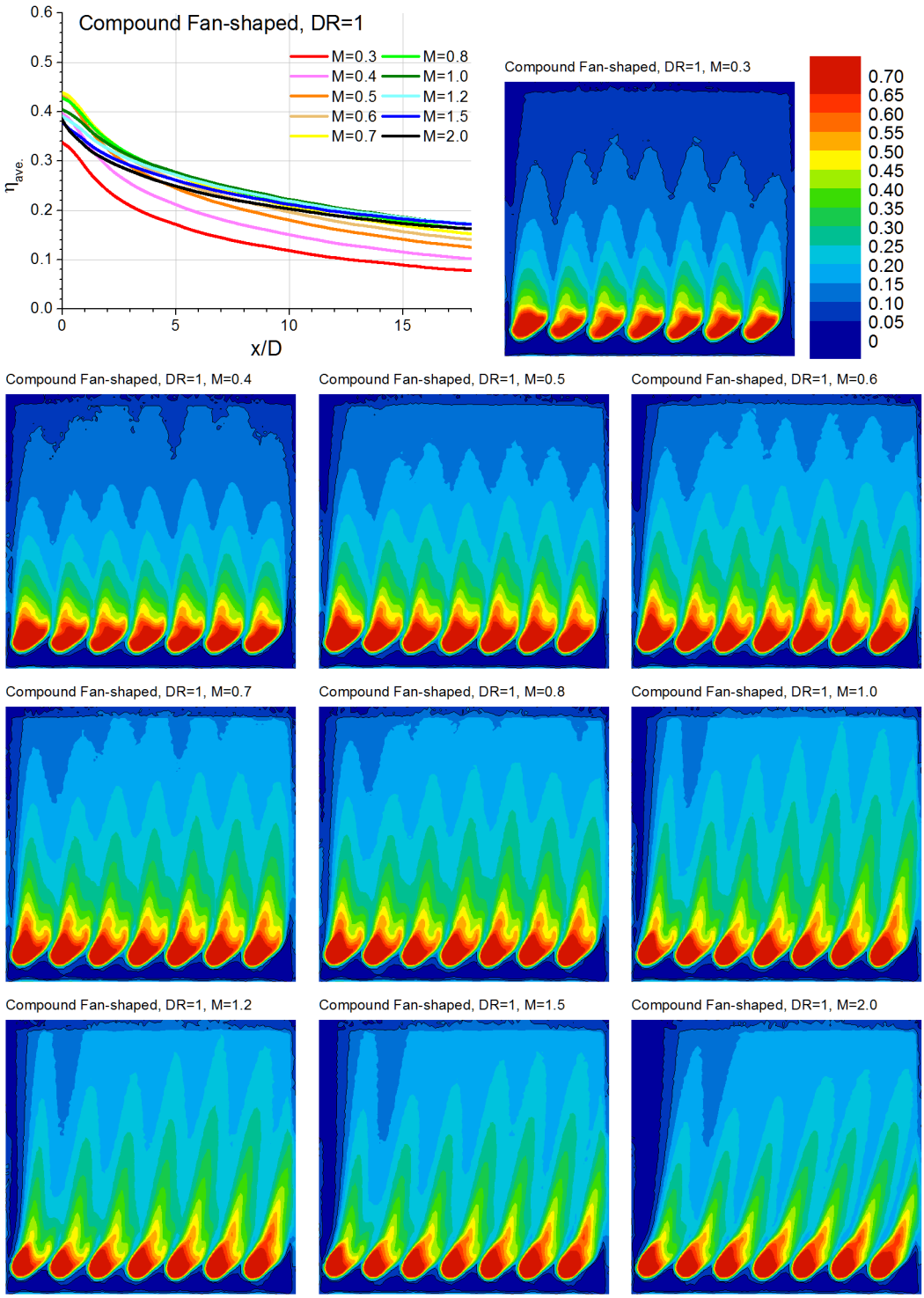

Fig. A 10 Laterally averaged effectiveness and contour plots for compound angled fan-shaped holes at DR = 1

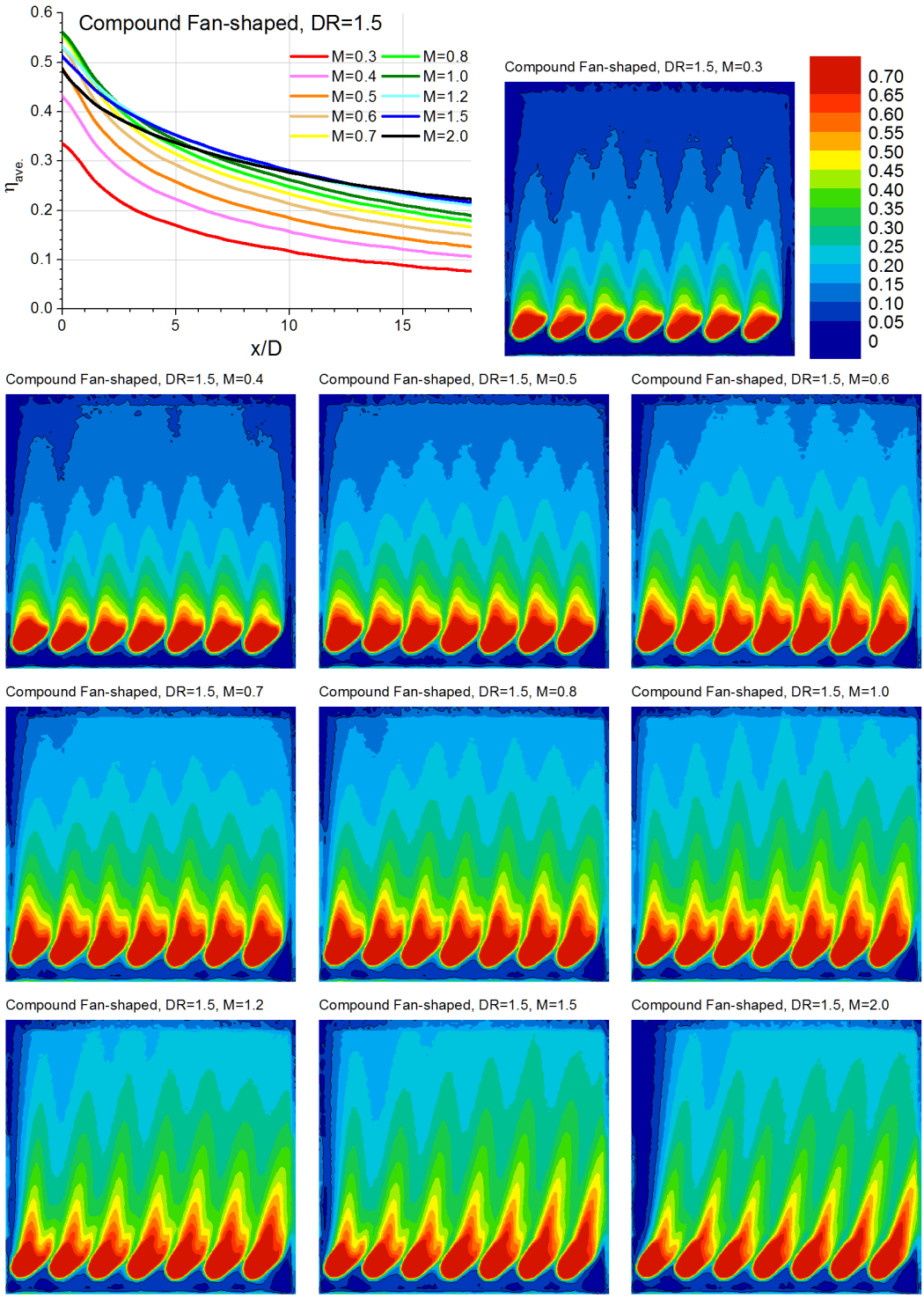

Fig. A 11 Laterally averaged effectiveness and contour plots for compound angled fan-shaped holes at DR = 1.5

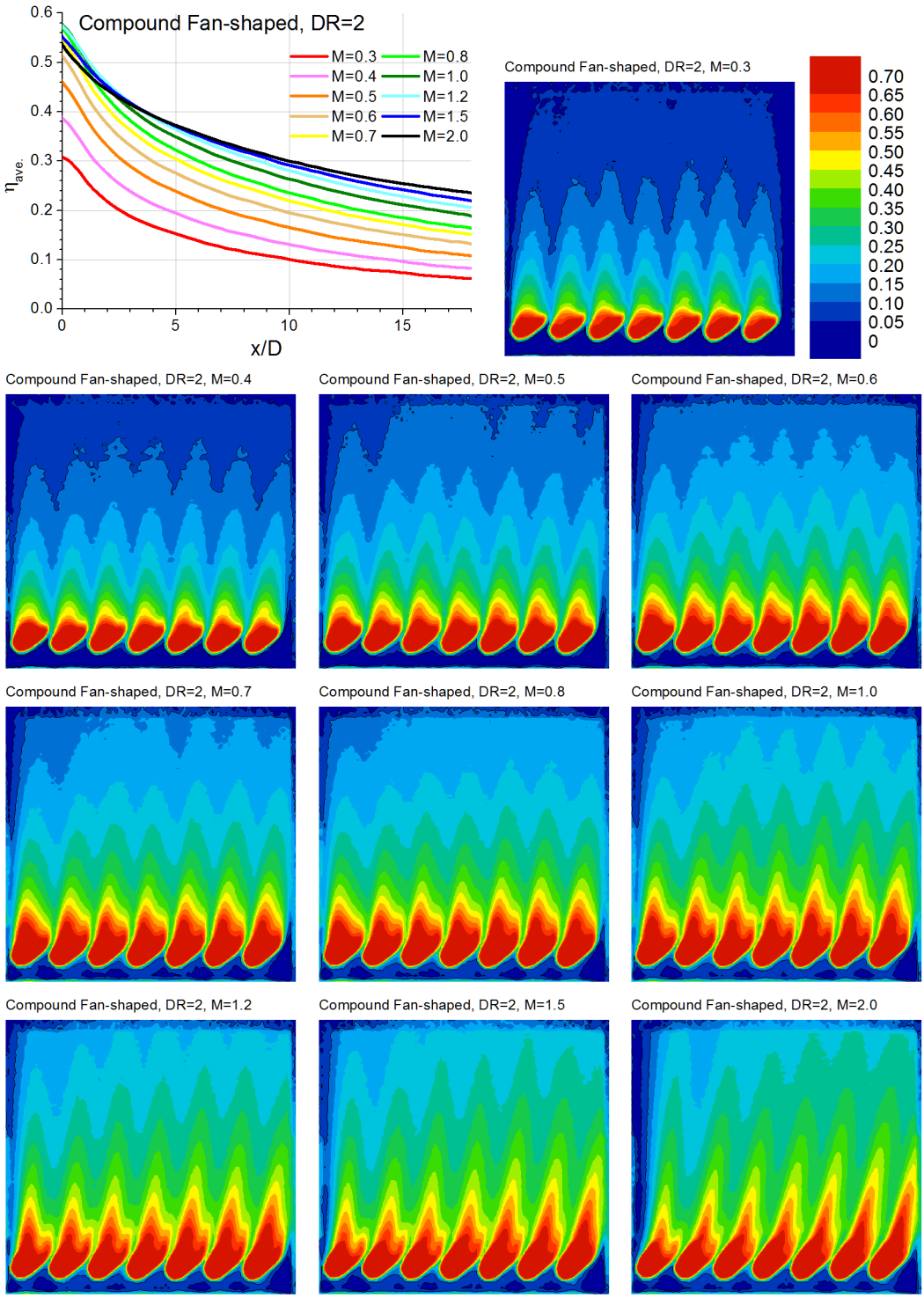

Fig. A 12 Laterally averaged effectiveness and contour plots for compound angled fan-shaped holes at DR = 2

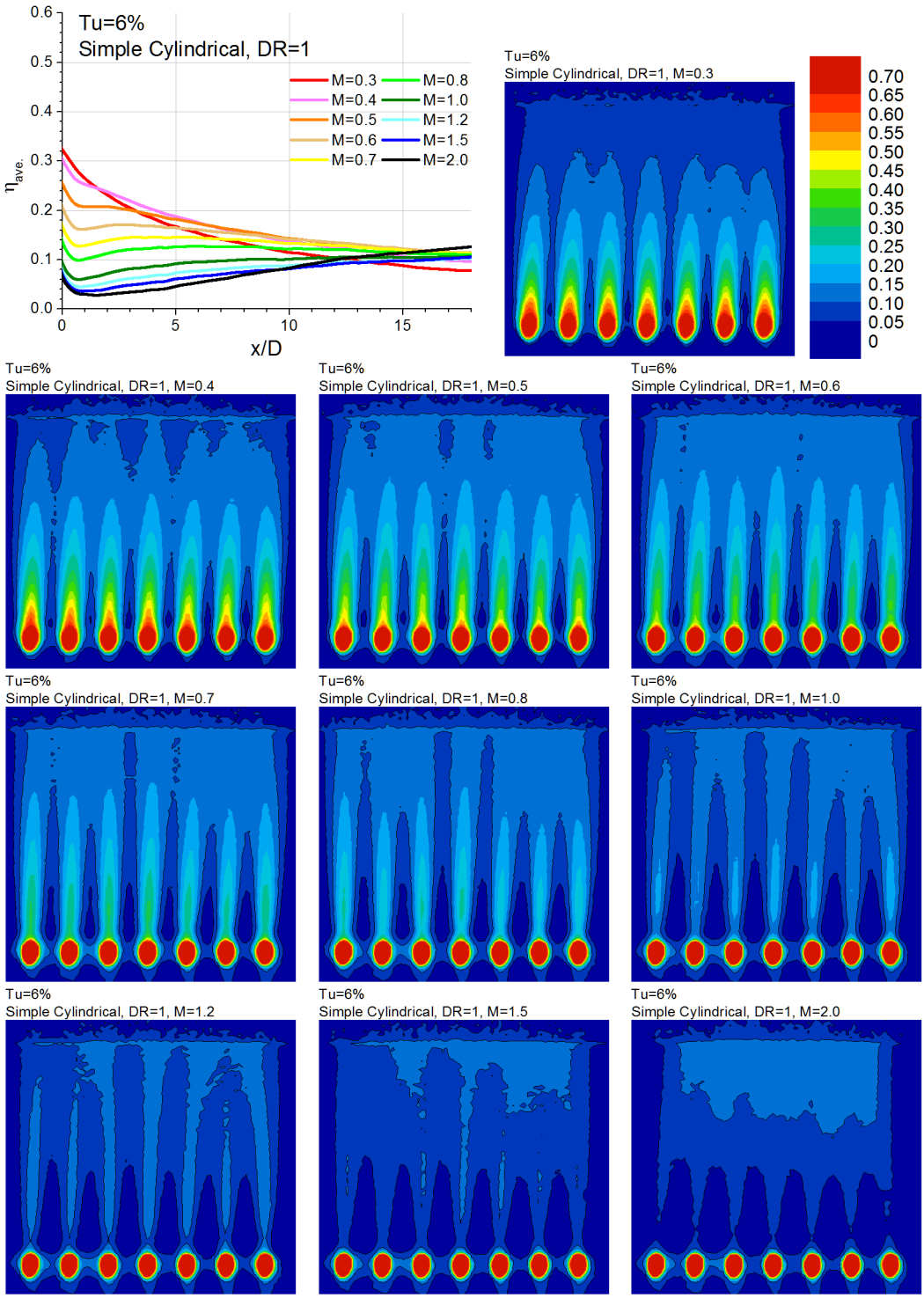

Fig. A 13 Laterally averaged effectiveness and contour plots for simple angled cylindrical holes at Tu = 6%, DR = 1

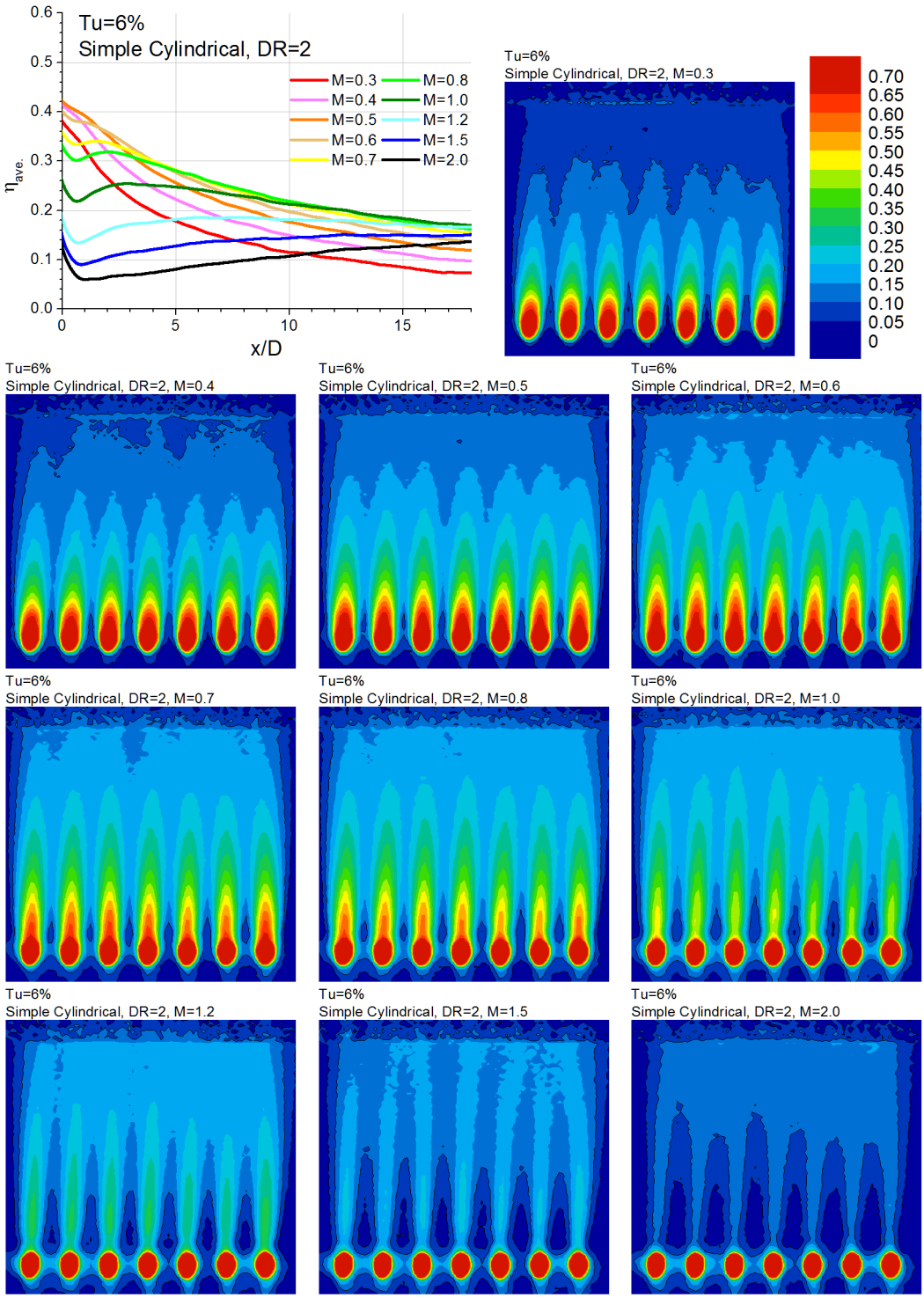

Fig. A 14 Laterally averaged effectiveness and contour plots for simple angled cylindrical holes at Tu = 6%, DR = 2

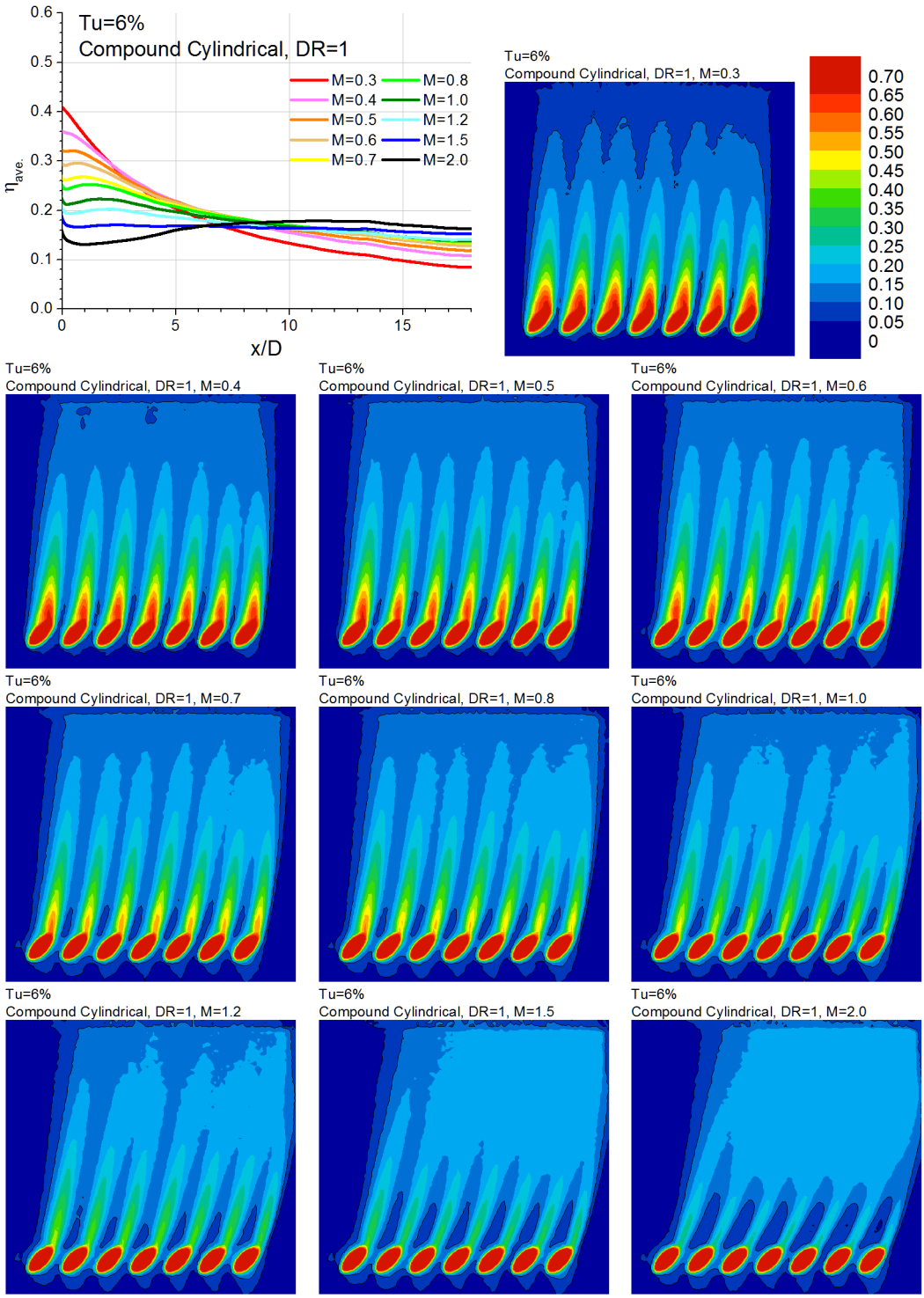

Fig. A 15 Laterally averaged effectiveness and contour plots for compound angled cylindrical holes at Tu = 6%, DR = 1

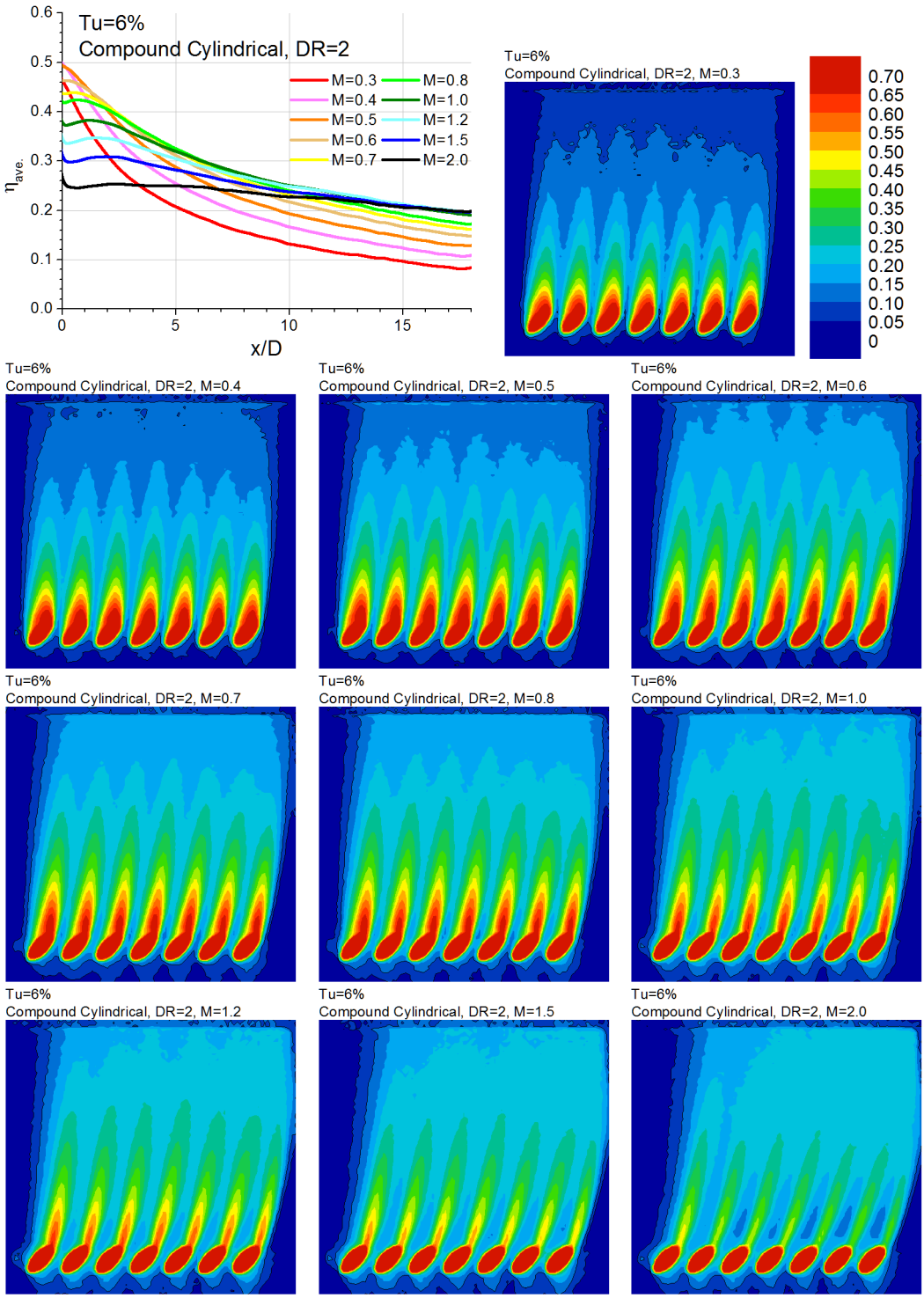

Fig. A 16 Laterally averaged effectiveness and contour plots for compound angled cylindrical holes at Tu = 6%, DR = 2

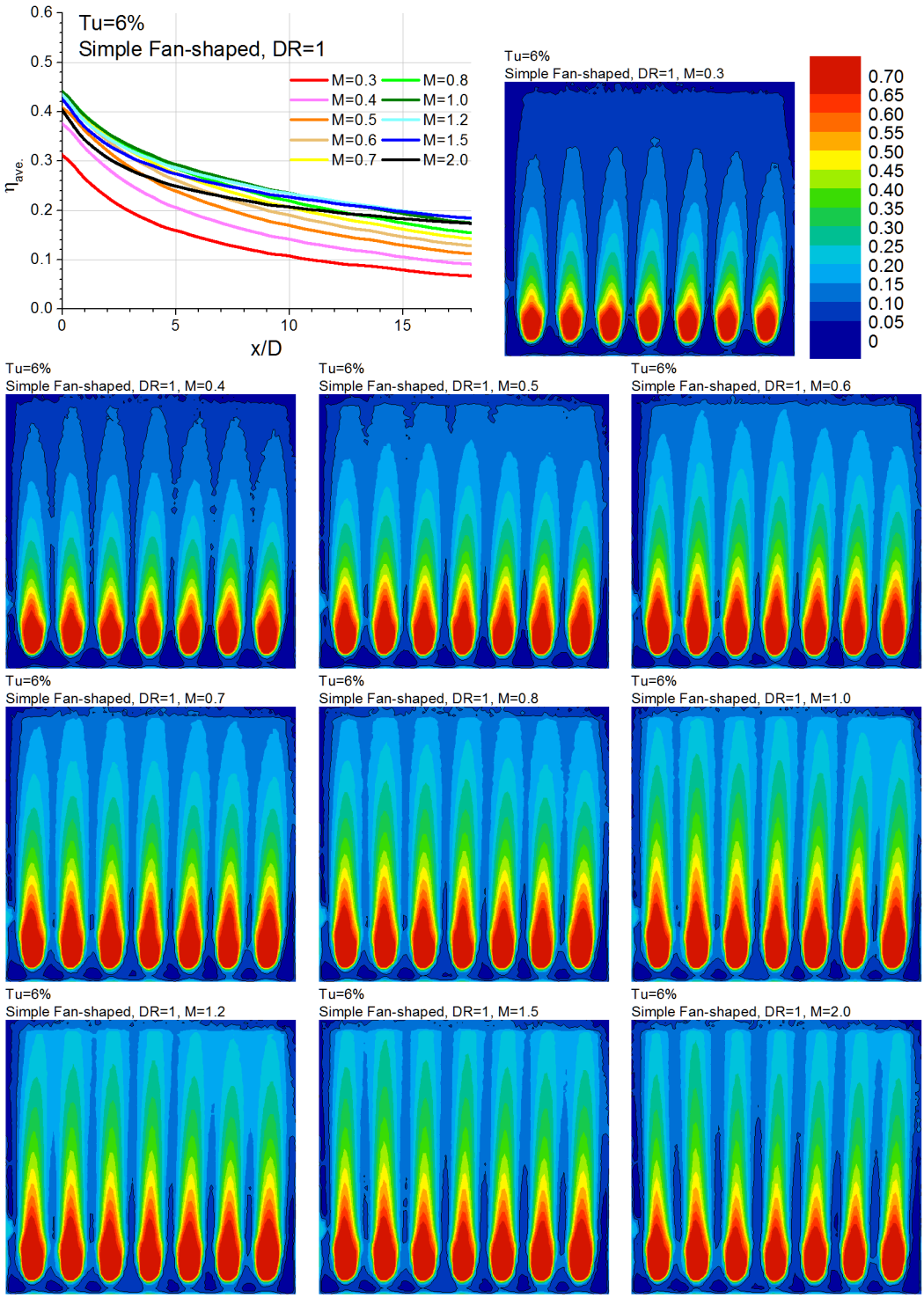

Fig. A 17 Laterally averaged effectiveness and contour plots for simple angled fan-shaped holes at Tu = 6%, DR = 1

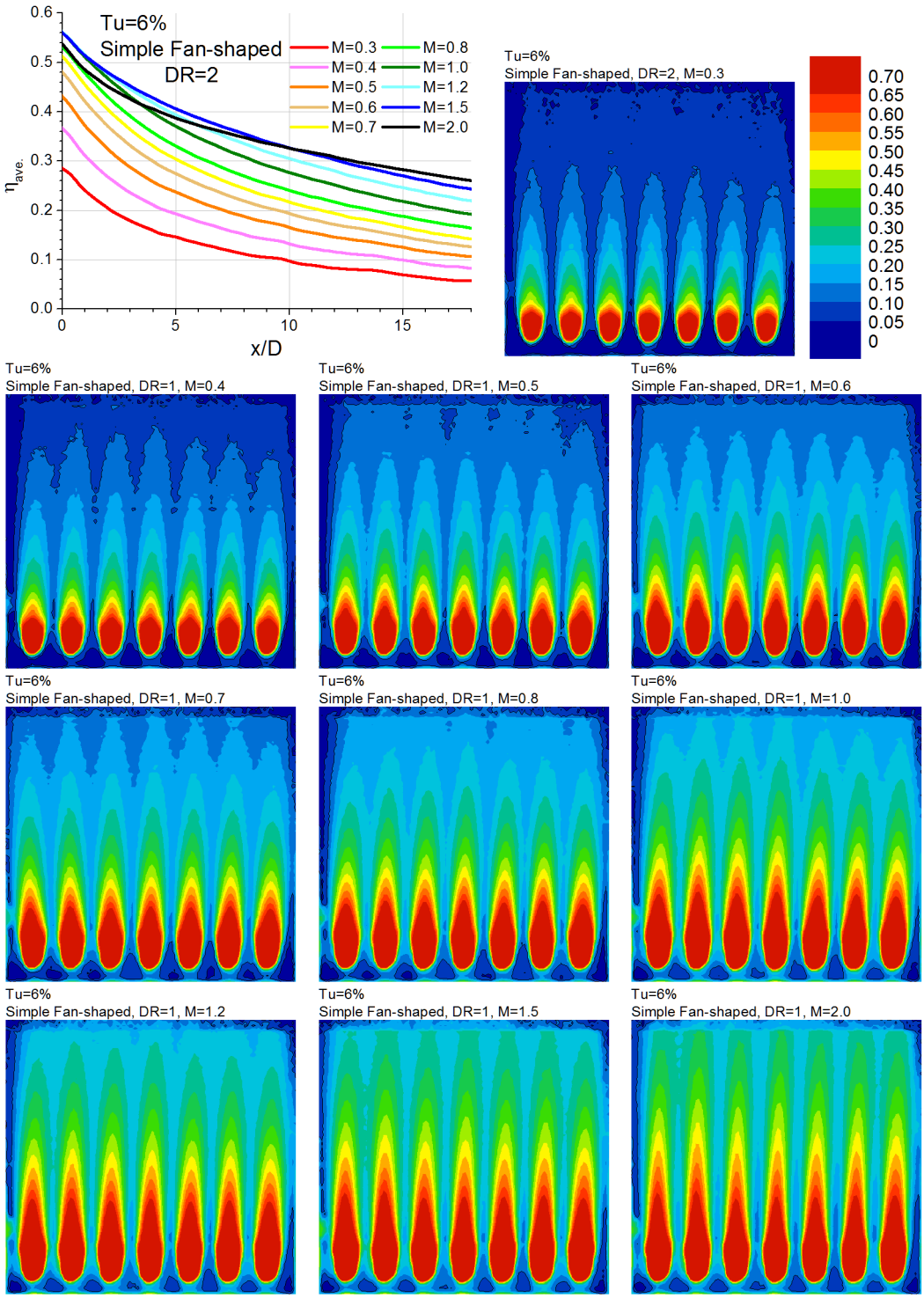

Fig. A 18 Laterally averaged effectiveness and contour plots for simple angled fan-shaped holes at Tu = 6%, DR = 2

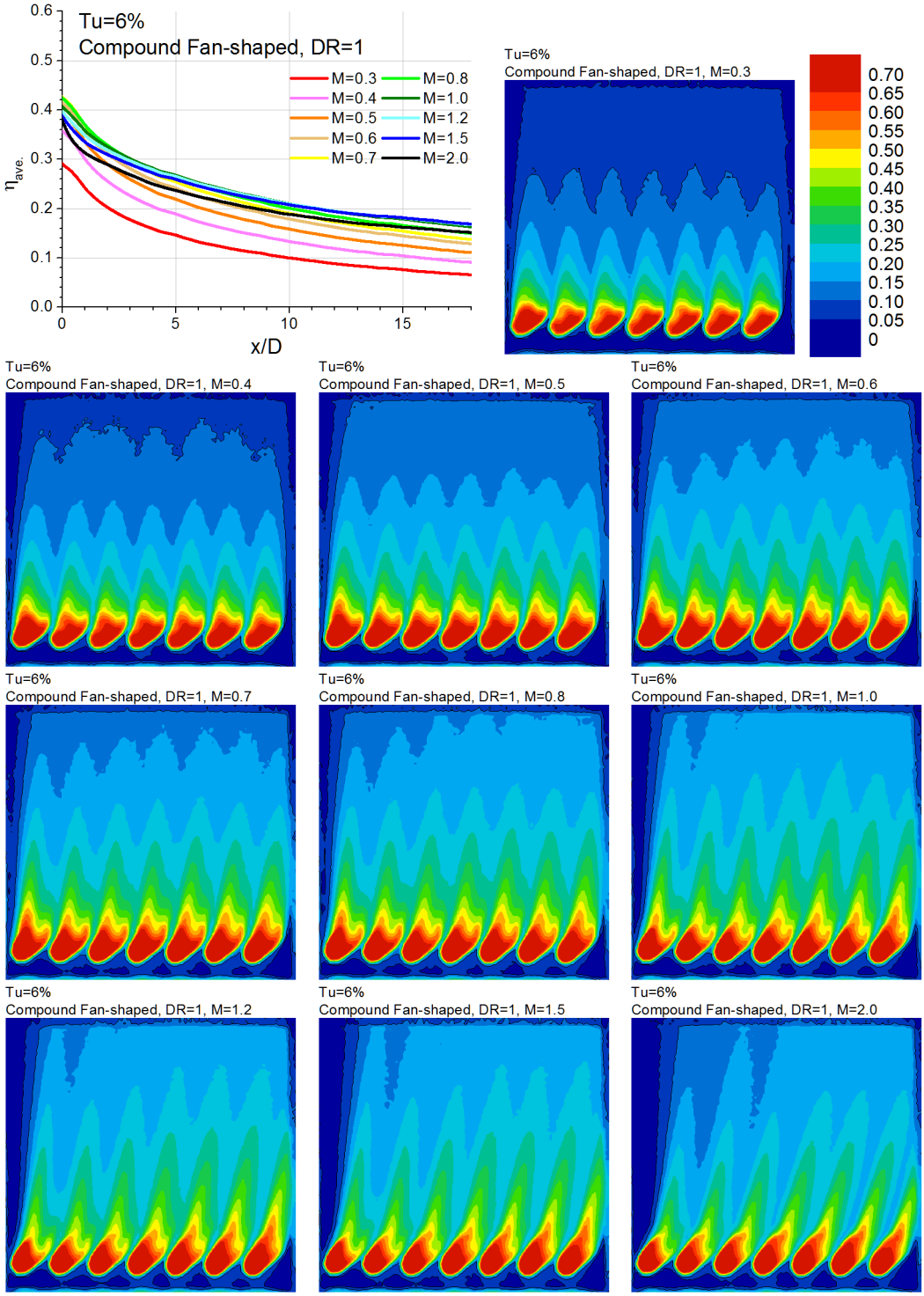

Fig. A 19 Laterally averaged effectiveness and contour plots for compound angled fan-shaped holes at Tu = 6%, DR = 1

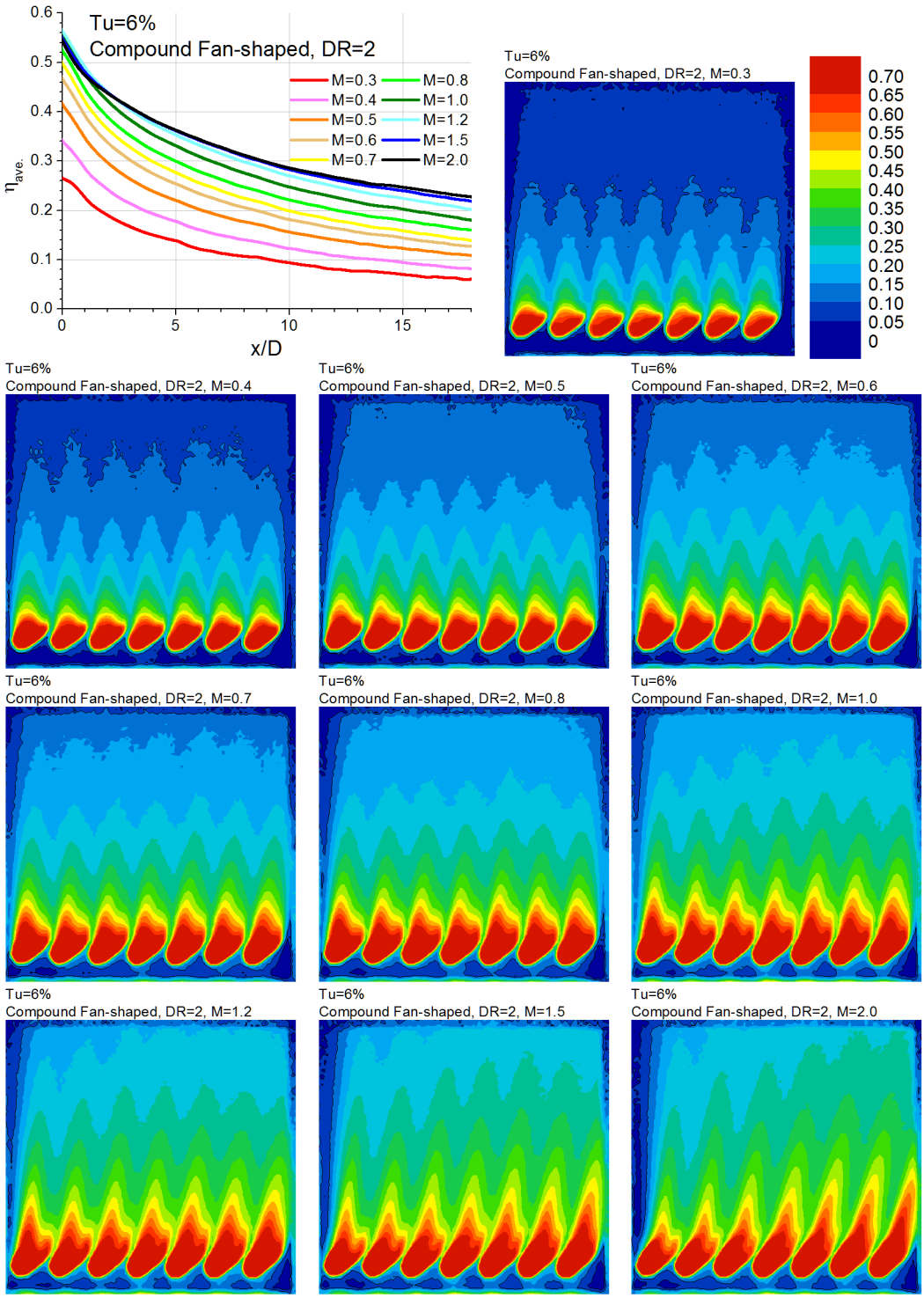

Fig. A 20 Laterally averaged effectiveness and contour plots for compound angled fan-shaped holes at Tu = 6%, DR = 2

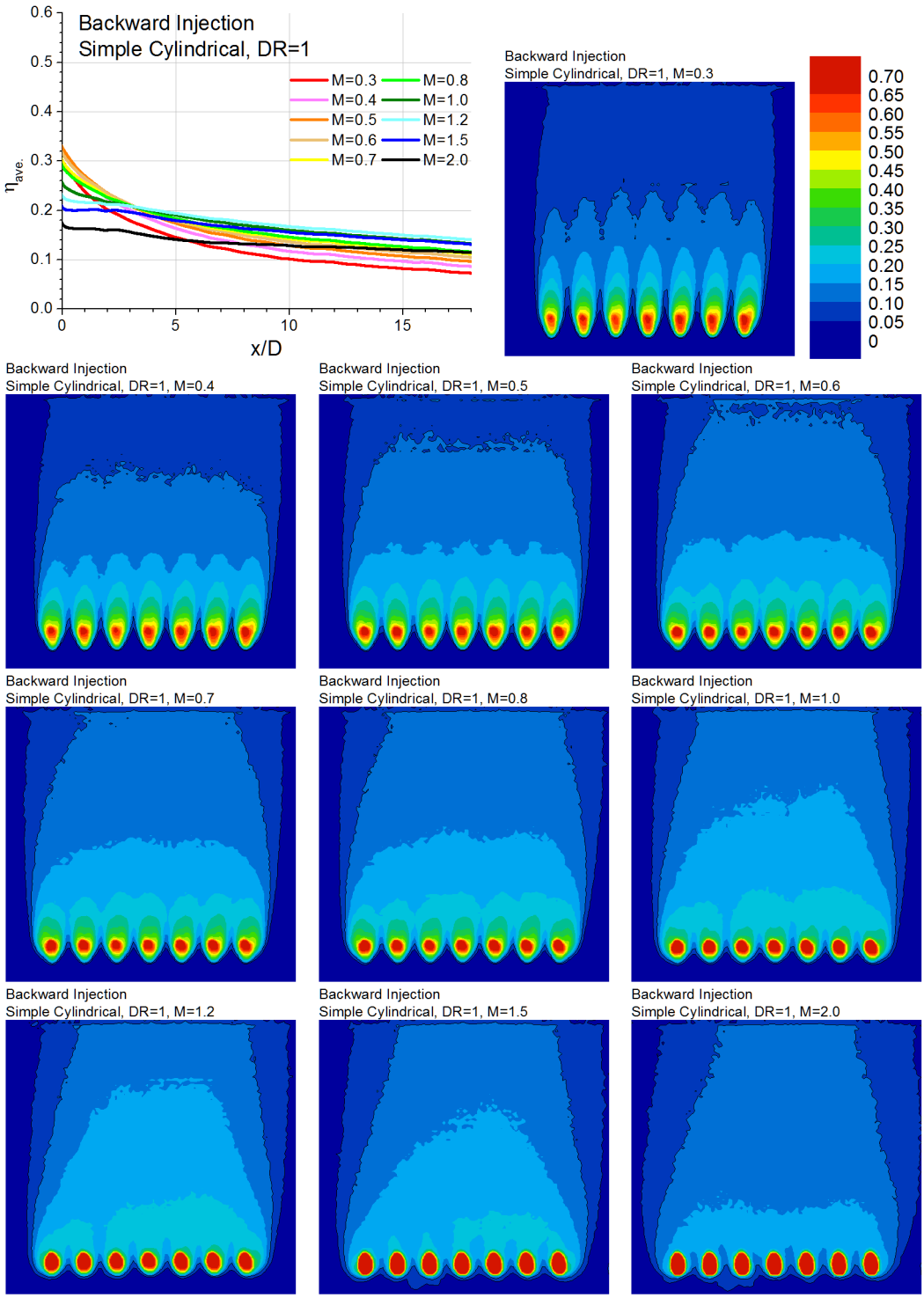

Fig. A 21 Laterally averaged effectiveness and contour plots for simple angled cylindrical holes backward injection at DR = 1

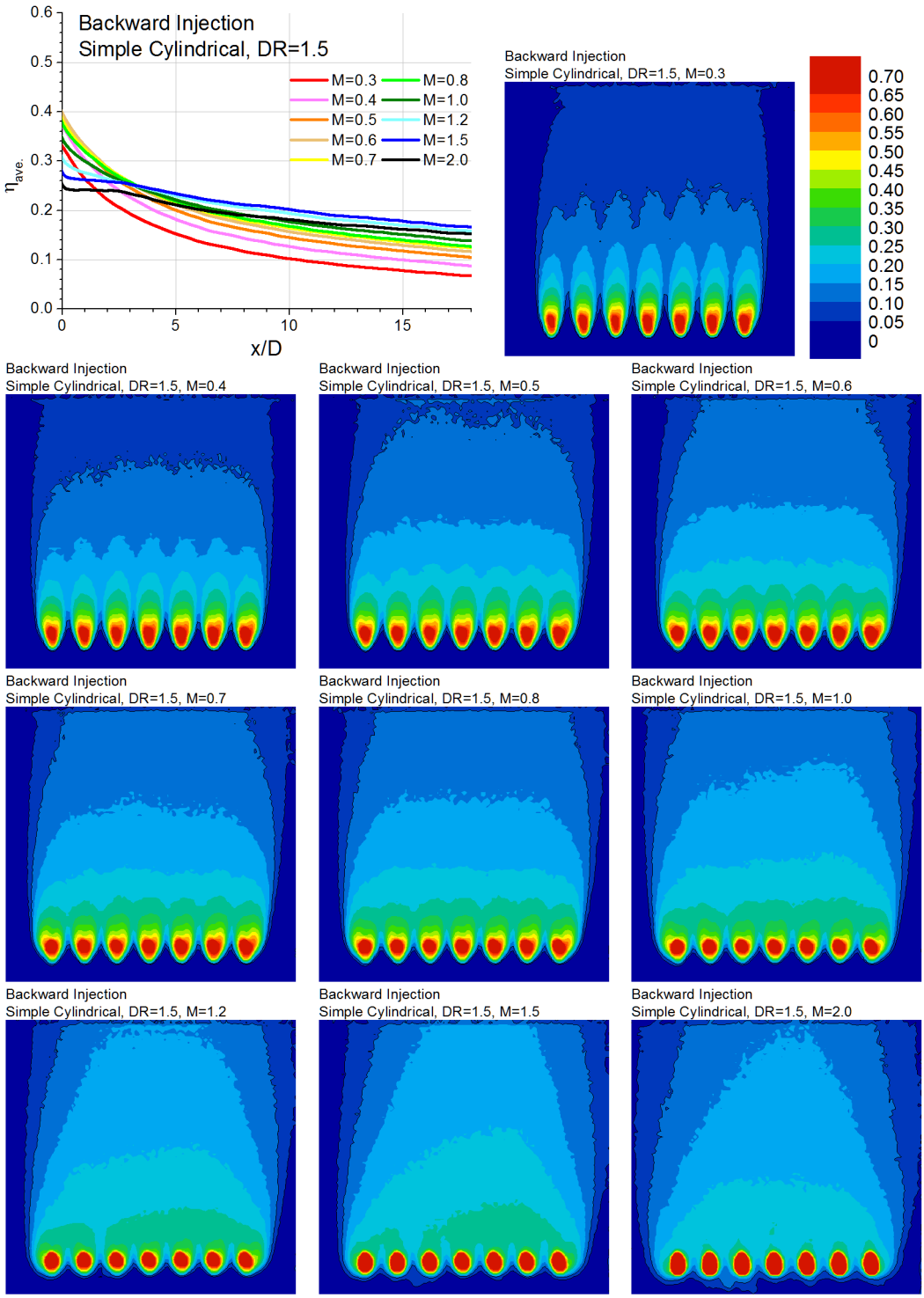

Fig. A 22 Laterally averaged effectiveness and contour plots for simple angled cylindrical holes backward injection at DR = 1.5

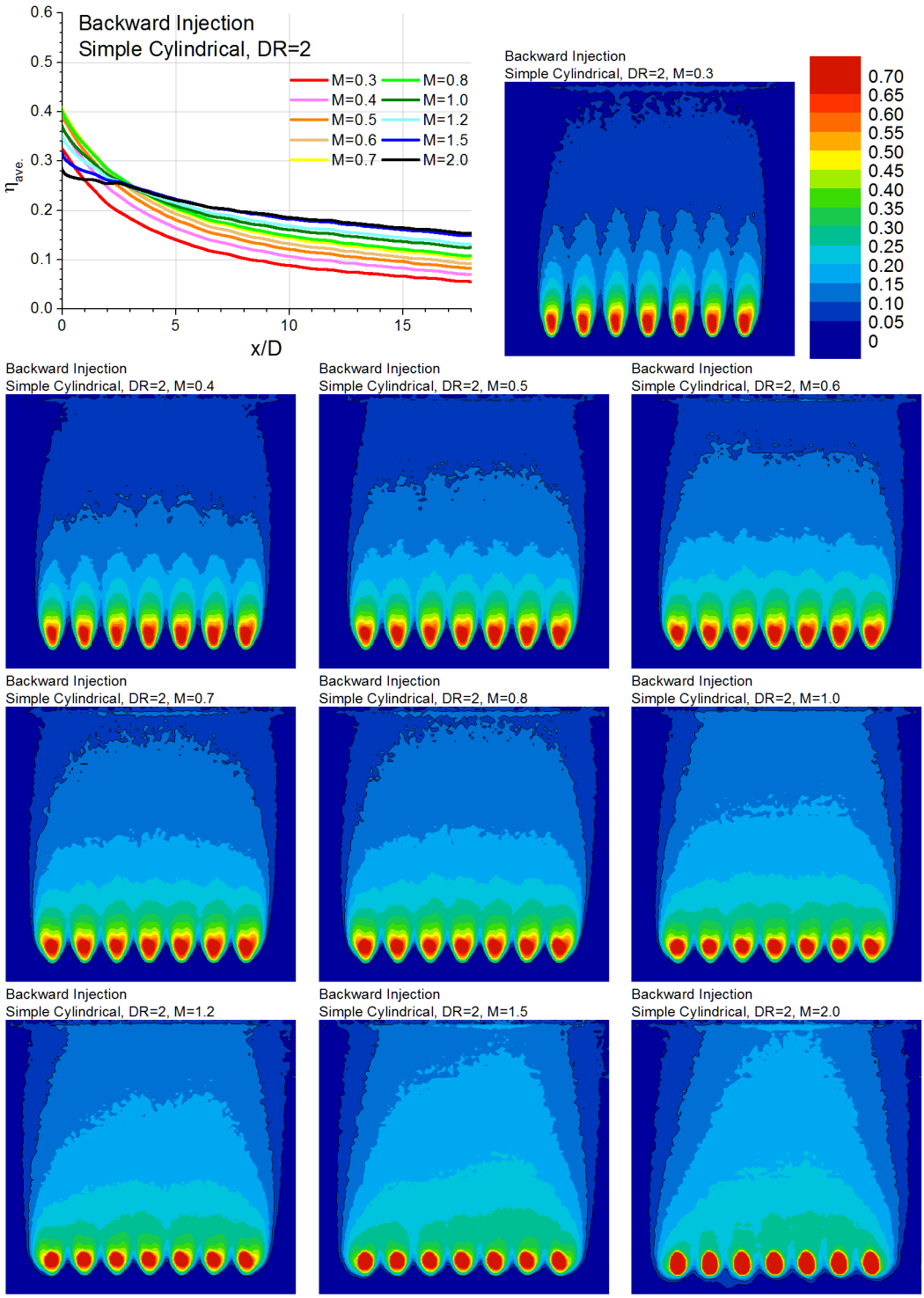

Fig. A 23 Laterally averaged effectiveness and contour plots for simple angled cylindrical holes backward injection at DR = 2

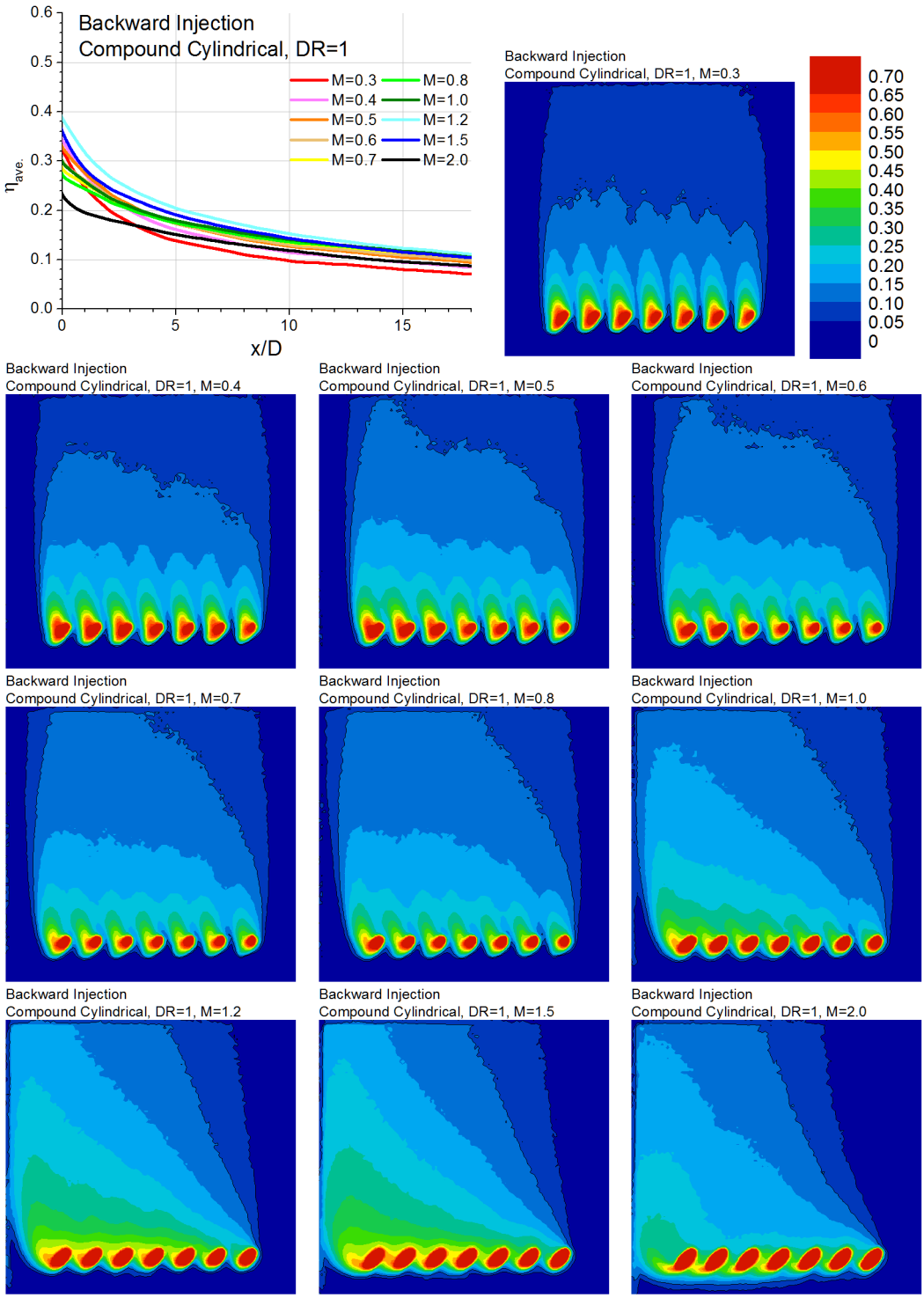

Fig. A 24 Laterally averaged effectiveness and contour plots for compound angled cylindrical holes backward injection at DR = 1

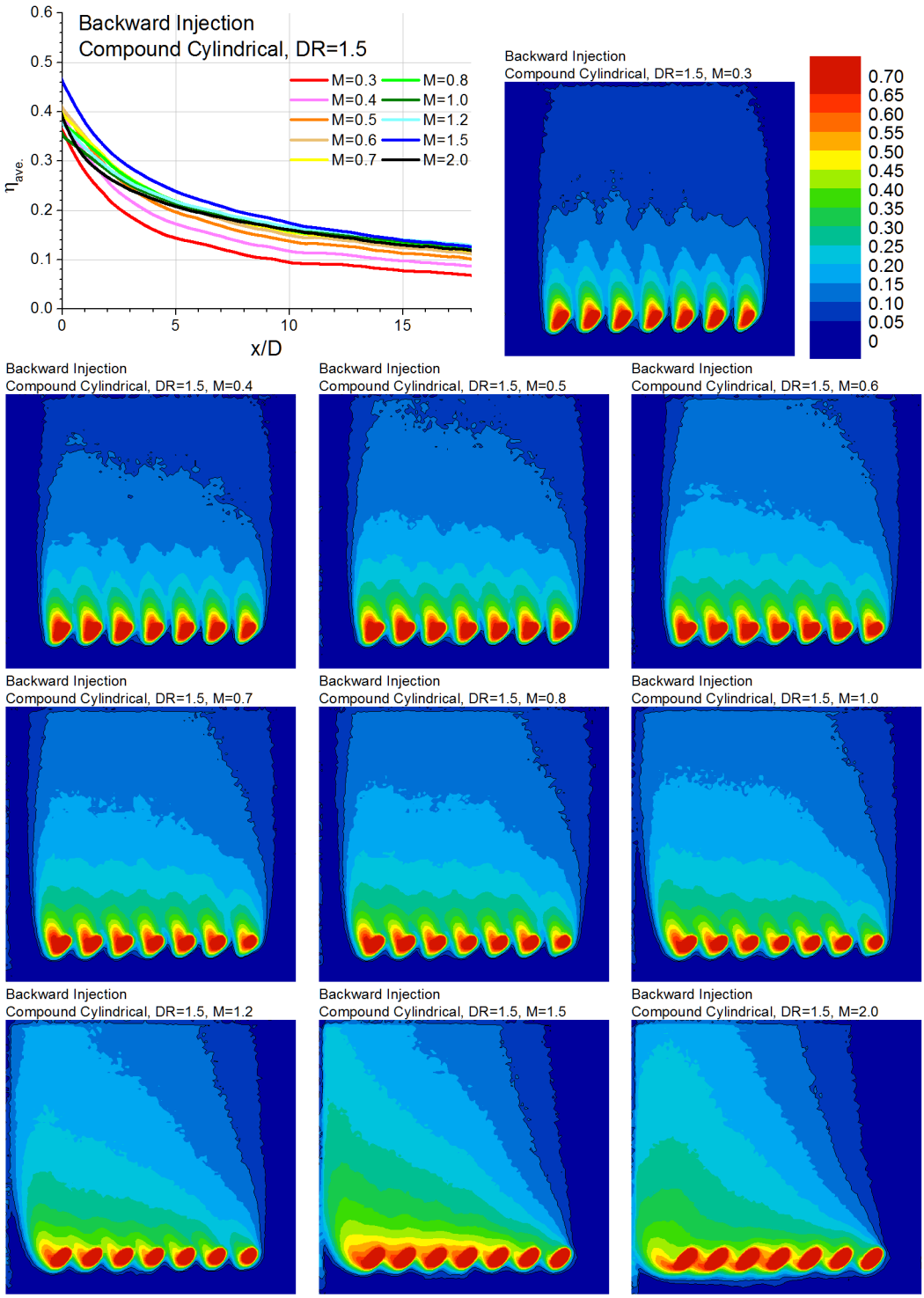

Fig. A 25 Laterally averaged effectiveness and contour plots for compound angled cylindrical holes backward injection at DR = 1.5

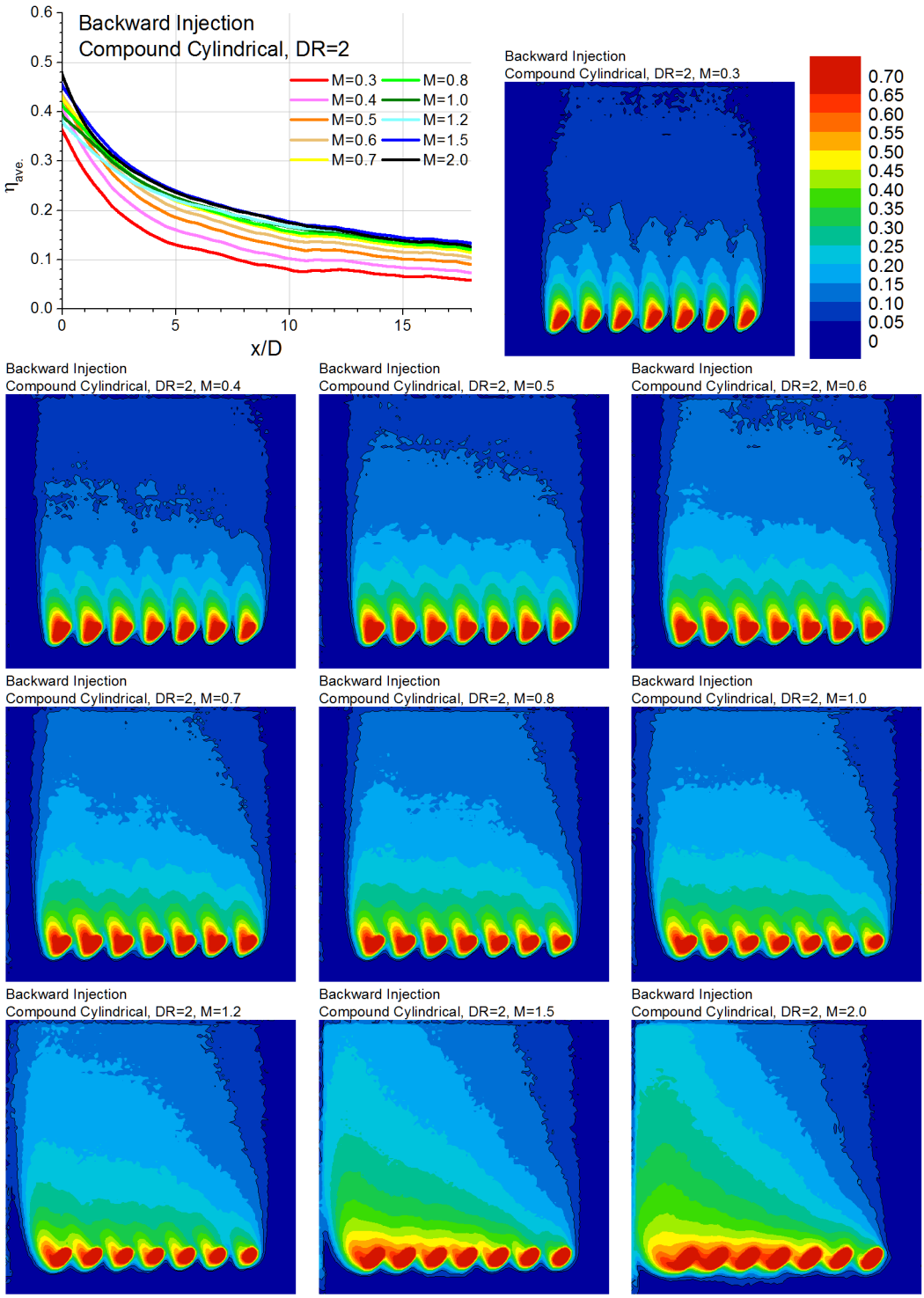

Fig. A 26 Laterally averaged effectiveness and contour plots for compound angled cylindrical holes backward injection at DR = 2

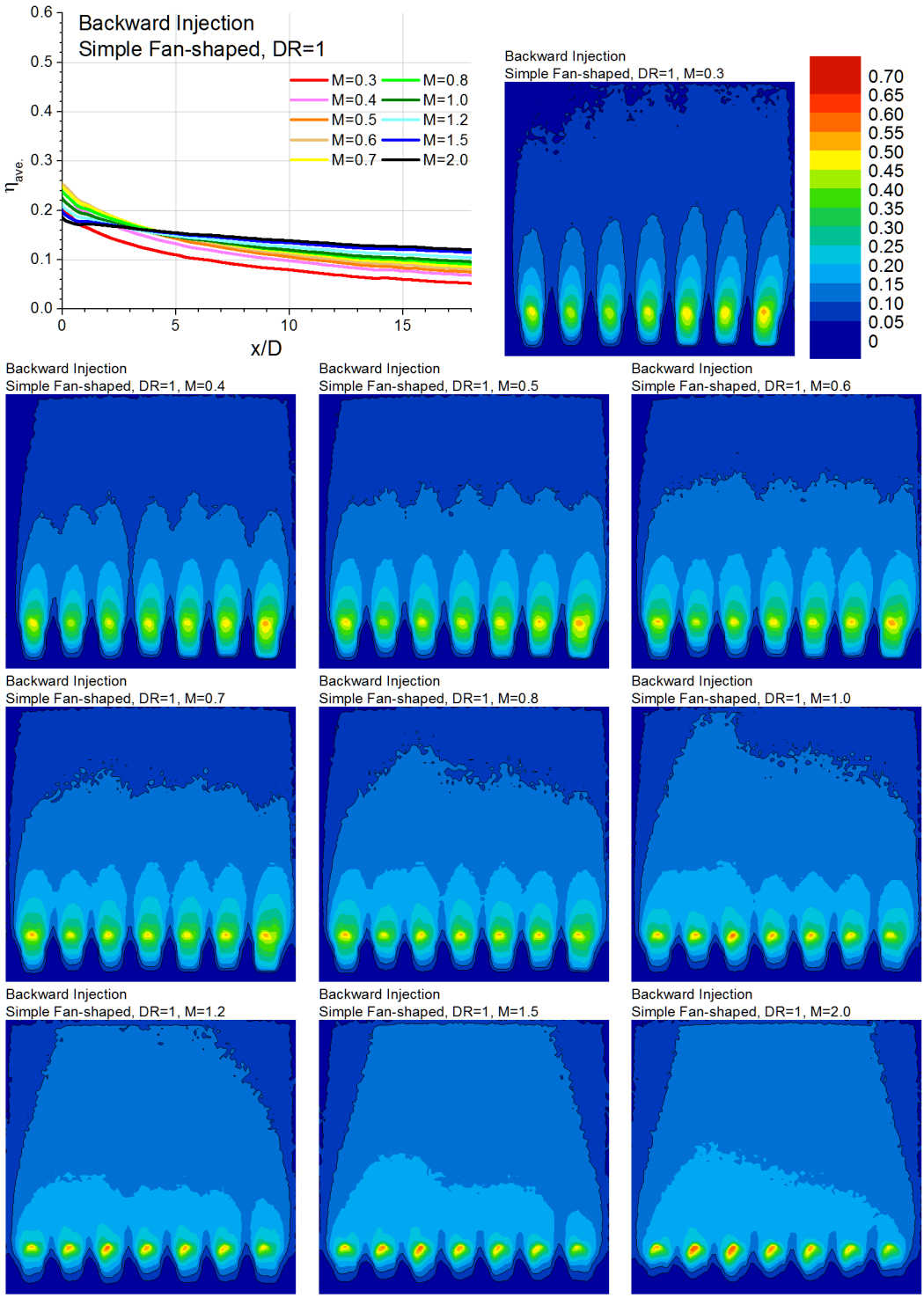

Fig. A 27 Laterally averaged effectiveness and contour plots for simple angled fan-shaped holes backward injection at DR = 1

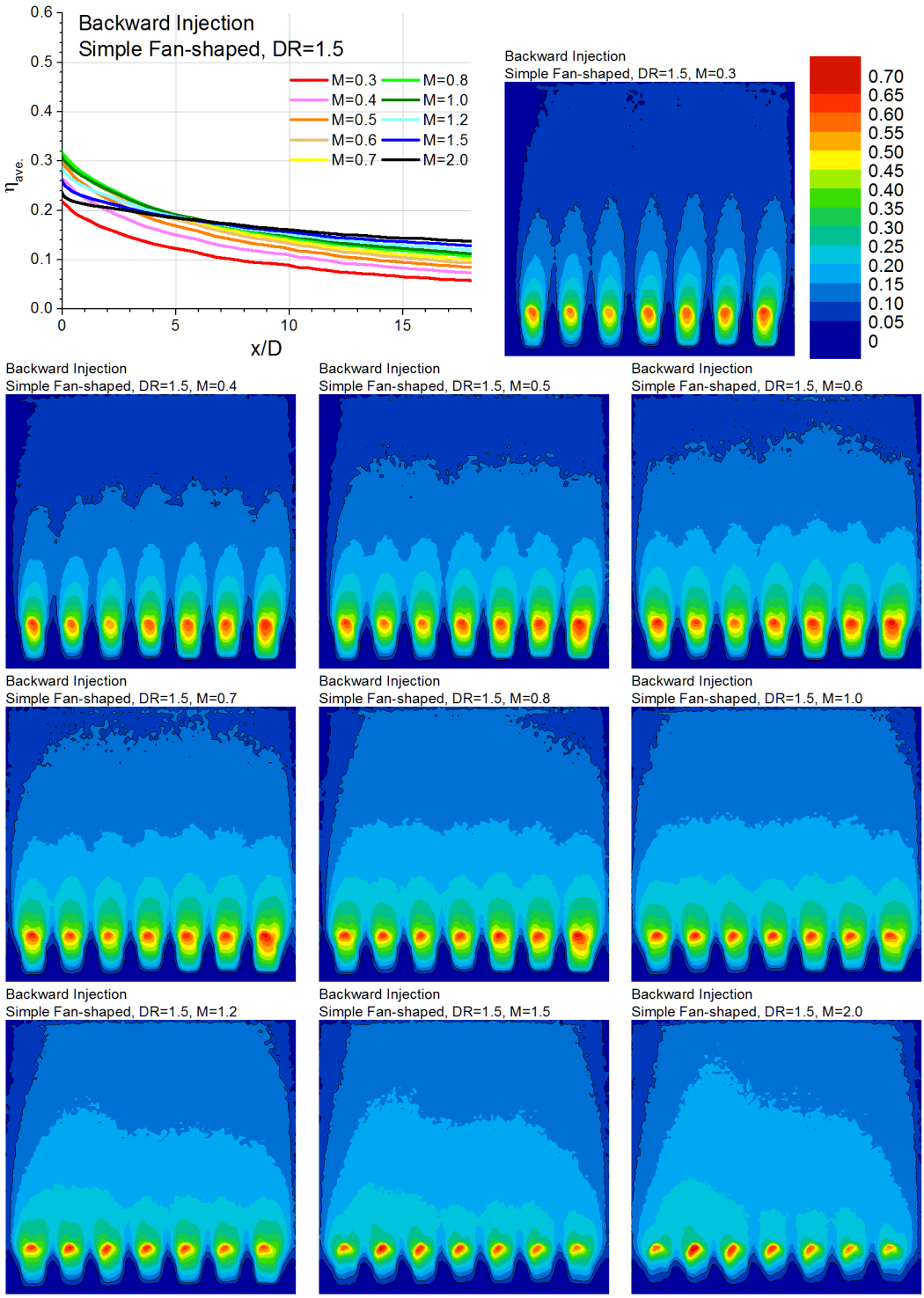

Fig. A 28 Laterally averaged effectiveness and contour plots for simple angled fan-shaped holes backward injection at DR = 1.5

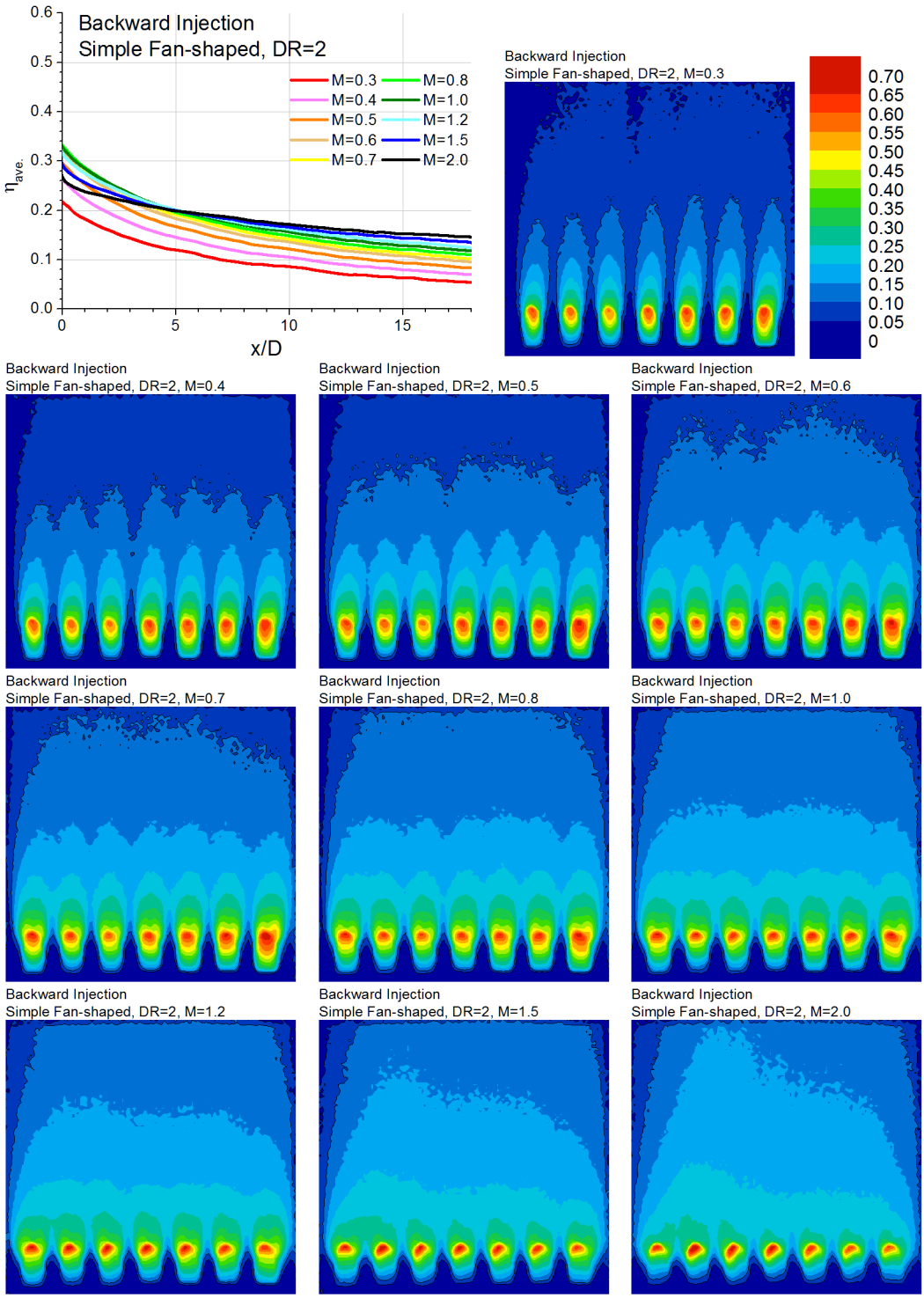

Fig. A 29 Laterally averaged effectiveness and contour plots for simple angled fan-shaped holes backward injection at DR = 2

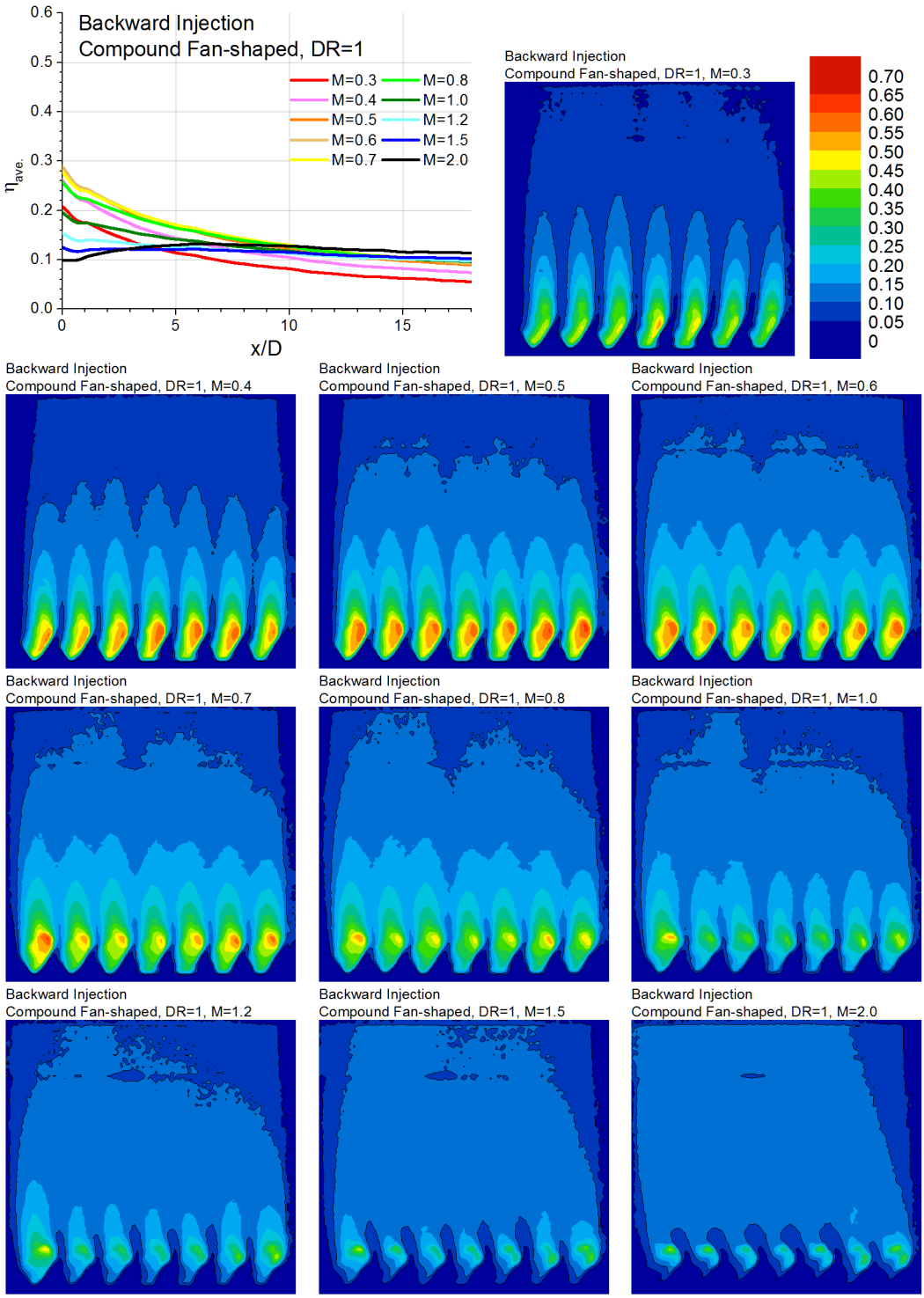

Fig. A 30 Laterally averaged effectiveness and contour plots for compound angled fan-shaped holes backward injection at DR = 1

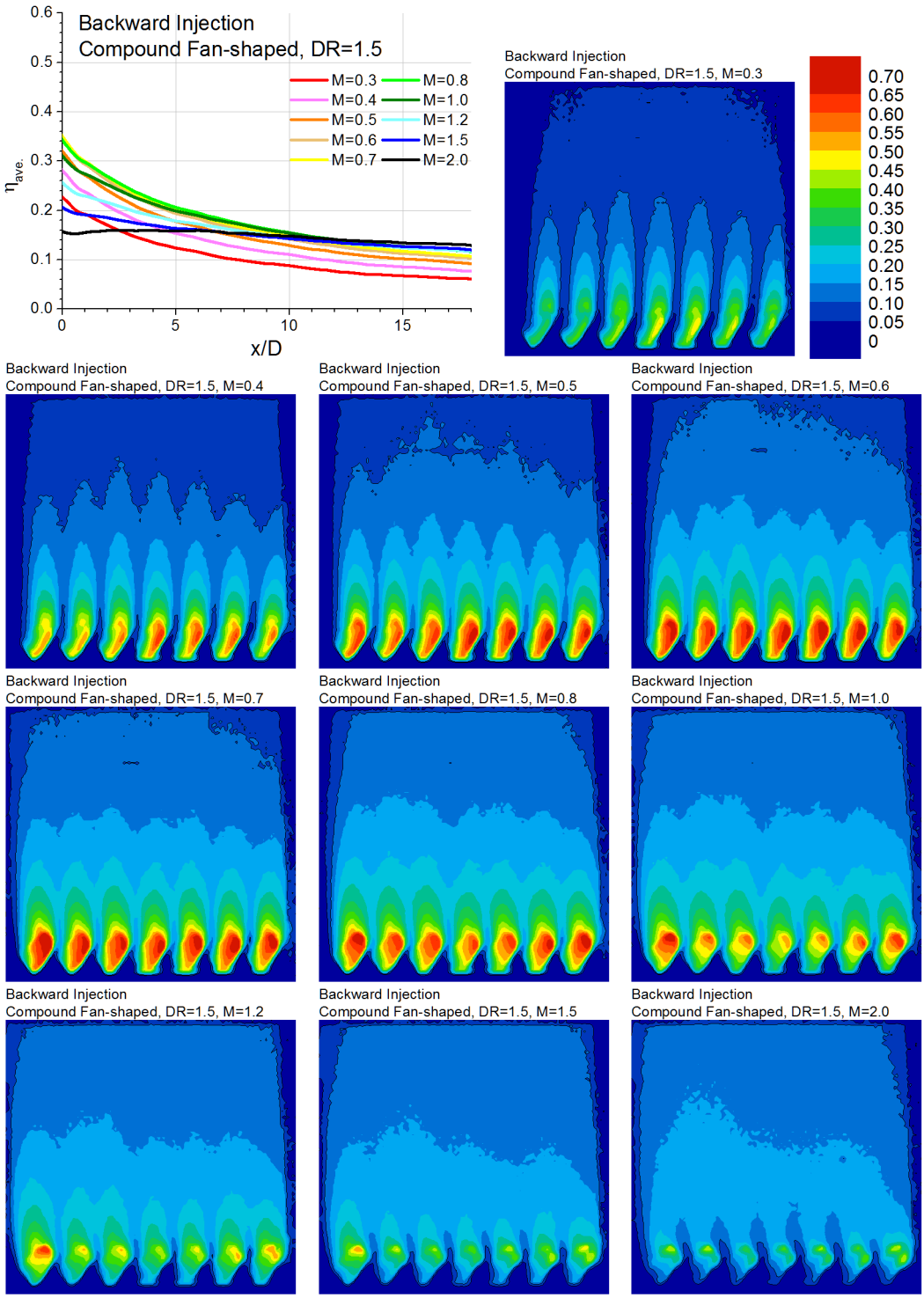

Fig. A 31 Laterally averaged effectiveness and contour plots for compound angled fan-shaped holes backward injection at DR = 1.5

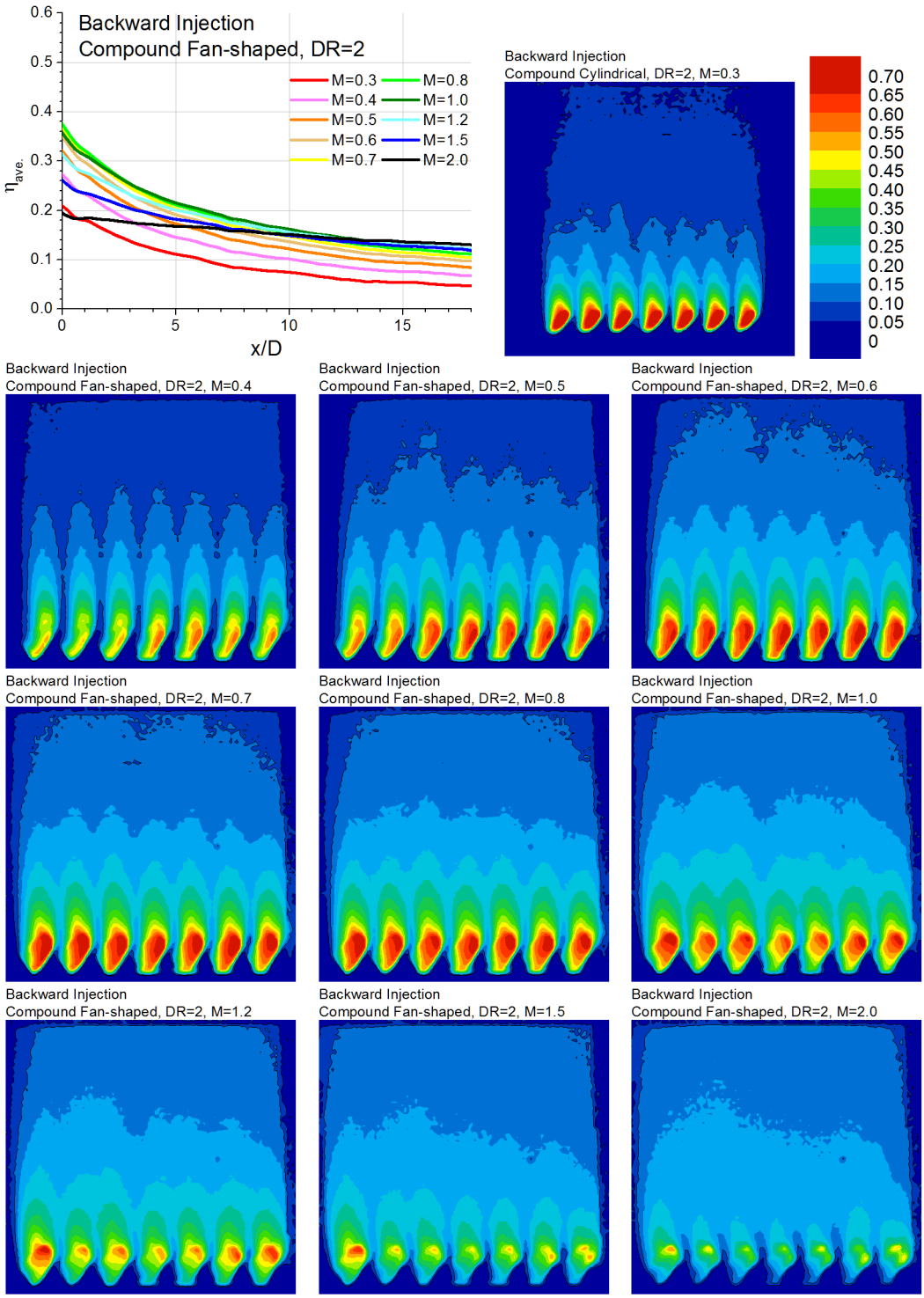

Fig. A 32 Laterally averaged effectiveness and contour plots for compound angled fan-shaped holes backward injection at DR = 2